Mechanistic Investigations of a Novel Flavin-dependent Enzyme Involved in Styrene Biosynthesis

By

Nattapol Arunrattanamook

A dissertation submitted in partial fulfillment
of the requirements for the degree of
Doctor of Philosophy
(Chemical Engineering)
in the University of Michigan
2018

Doctoral Committee:

Professor E. Neil G. Marsh, Chair
Professor Erdogan Gulari
Assistant Professor Kristin Koutmou
Associate Professor Nina Lin
Assistant Professor Fei Wen

Nattapol Arunrattanamook
arunratt@umich.edu
ORCID ID: 0000-0002-7832-7981

Dedication

I would like to dedicate this body of work to a Royal Thai Government Scholarship for funding my college education, to my parents for encouraging me in academic research.

Acknowledgement

First and foremost, I would like to thank my advisor, Prof. E. Neil G. Marsh, for his support and direction. I have learned an incredible amount from him about scientific writing, the practical application of the scientific method, and about how to conduct myself as a scientist and an independent researcher. In particular, I would like to thank him for his patient and understanding during the most difficult time of my research and enthusiastically push me forward. I would like to thank my committee members Prof. Koutmou, Prof. Wen, Prof. Nina Lin, and Prof. Gulari for their suggestions and guidance. I would like to thank Dr. Paul Lennon and Dr. James Windak for helping to teach me GC-MS and other analytical instruments. I would like to thank Prof. Ruotolo and Chunyi Zhao for their help and contribution on native mass spectrometry portion of this project. I would like to thank Prof. Palfey for gifting me valuable FMN analogs to study in my thesis. I would like to thank Dr. Hoarau for teaching me Molecular Docking simulation. I would like to thank Kyle Ferguson and Dr. Fengming Lin for their help and efforts on the project. I would like to thank my Dr. Ben Ellington, Dr. Tad Ogorzalek, Dr. Mckenna Schroeder, Dr. Matthew Waugh and my other lab mates for making lab environment fun and full of professional science to learn. I would like to thank other staff and faculty for their help and assistance. I would like to thank my family for all their love and support.

Table of Contents

Dedication ii

Acknowledgements iii

List of Figures ix

List of Tables xi

List of Abbreviations xii

Abstract xiv

Chapter 1 Introduction 1

1.1 Sustainability and biorenewable resources 1

1.1.1 Sustainability 1

1.1.2 Industrial/conventional manufacturing process of styrene 4

1.1.3 Biorenewable resources 5

1.1.4 Biosynthesis of aromatic compounds and styrene in nature 8

1.2 Phenylacrylic acid decarboxylase (PAD) and Ferulic acid decarboxylase (FDC) 10

1.2.1 Decarboxylase 10

1.2.2 Phenylacrylic acid decarboxylase (PAD) and Ferulic acid decarboxylase (FDC) 13

1.2.3 Decarboxylase 13

1.2.4 Crystal structure of FDC1 and UbiX 14

1.3 Goals 17

1.4 References 18

Chapter 2 ^{1}H NMR, Linear free energy analysis and isotope effects on decarboxylation catalyzed by FDC 22

2.1 Introduction 22

2.2 Materials and methods 26

2.2.1 Materials 26

2.2.2 ^{1}H NMR analysis 26

2.2.3 Enzyme Assay 27

2.2.4 pH Dependence and Solvent and Secondary Deuterium Isotope Effect Measurements 28

2.3 Results and discussion 29

2.3.1 ^{1}H NMR analysis 29

2.3.2 Linear free energy analysis (Hammett analysis) of FDC 31

2.3.3 pH Dependence and solvent isotope effects 33

2.3.3.1 Dependence of rate on pL 33

2.3.3.2 Proton inventory analysis 35

2.3.4 Secondary kinetic isotope effects 36

2.3.5 Interpretation of linear free energy analysis and isotope effect 37

2.4 Conclusions 39

2.5 References 41

Chapter 3 Kinetic Characterization of Prenyl-flavin Synthase from *Saccharomyces cerevisiae* 44

3.1 Introduction 44

3.2 Materials and methods 47

3.2.1 Materials 47

3.2.2 Malachite green phosphate assay 47

3.2.3 EnzChek phosphate Assay 48

3.2.4 Assay for prFMN formation by scPFS 48

3.2.5 GC-MS assay 49

3.2.6 HPLC assays 49

3.2.7 PiPer™ Pyrophosphate Assay 50

3.3 Results and discussion 50

3.3.1 Malachite green phosphate assay 51

3.3.2 EnzChek phosphate Assay 54

3.3.3 Development of a scPFS-FDC coupled assay 58

3.3.3.1 pH optimization 59

3.3.3.2 Investigation of the impact of each substrate with preliminary set up 60

3.3.3.3 Investigation of the cause of inconsistency 61

3.3.4 DMAPP vs DMAP 62

3.3.5 Steady state kinetic analysis of scPFS 64

3.3.6 Single turnover kinetics of FMN consumption 65

3.3.7 PiPer™ Pyrophosphate Assay 67

3.4 Conclusions 69

3.5 References 71

Chapter 4 Cofactor analogs 74

4.1 Introduction 74

4.2 Materials and methods 78

4.2.1 Materials 78

4.2.2 Assay for pr-FMN formation by scPFS 78

4.2.3 HPLC assays 79

4.2.4 GC-MS assay 80

4.2.5 Native mass spectrometry 80

4.2.6 Molecular docking 81

4.3 Results and discussion 82

4.3.1 HPLC Assay 82

4.3.2 GC-MS Assay 85

4.3.3 Native Mass Spectrometry 86

4.3.4 Molecular docking 88

4.4 Conclusions 90

4.5 References 92

Chapter 5 Conclusion and outlooks 95

5.1 Overview 95

5.1.1 Probe of decarboxylation mechanism 96

5.1.2 scPFS prenylation assay 97

5.1.3 Cofactor analogs 98

5.2 Future directions 100

5.2.1 Substrate analogs (aromatic and aliphatic) and active site mutagenesis to probe mechanism of FDC 100

5.2.2 Cofactor maturation 101

5.2.3 Linear free energy analysis, isotope effect and inhibitor complex to probe prenylation mechanism and application of cofactor analogs to probe decarboxylation mechanism 102

5.2.4 Active site and cofactor engineering of FDC1 for other functionality 102

5.3 References 104

List of Figures

Figure 1.1 – United Nations projected world population growth model. 2

Figure 1.2 – BP projected growth in energy demand. 2

Figure 1.3 – Observations of a changing global climate system. 3

Figure 1.4 – Biosynthesis of aromatic compounds through the Shikimate pathway 9

Figure 1.5 – Mechanistic models of decarboxylases without an exogenous cofactor. 11

Figure 1.6 – Schematic representation of the proposed UbiX mechanism. 14

Figure 1.7 – Isomers of prFMN in crystal structure of *A. niger* FDC1 15

Figure 1.8 – Proposed FDC decarboxylation mechanisms. 16

Figure 2.1 – Constructed styrene biosynthesis pathway in *Escherichia Coli* that successfully synthesizes styrene from renewable substrates such as glucose. 23

Figure 2.2 – Proposed mechanisms for the FDC-catalyzed decarboxylation of phenylacrylic acid 25

Figure 2.3 – ^{1}H NMR spectrum of deuterated styrene product. 30

Figure 2.4 – Hammett plot for the FDC-catalyzed decarboxylation 33

Figure 2.5 – pL-rate profile for the FDC-catalyzed decarboxylation 34

Figure 2.6 – Proton inventory for FDC 35

Figure 2.7 – Scheme showing the possible reaction products of the substrate mimic, 2-fluoro-2-nitrovinylbenzene and observed native mass spectrum m/z. 40

Figure 3.1 – Proposed mechanism for FMN prenylation 46

Figure 3.2 – Color-changed chemical reaction in malachite green assay 52

Figure 3.3 – Principle of the Enzcheck phosphate assay. 56

Figure 3.4 – Negative control reaction between DMAP and Enzchek phosphate reagent. 56

Figure 3.5 – Negative control reaction between sodium dithionite and Enzchek phosphate reagent. 57

Figure 3.6 – Spectra comparing reaction with scPFS and without scPFS. 57

Figure 3.7 – Catalytic activity of scPFS at different pH. 59

Figure 3.8 – Monitoring of catalytic FMN prenylation by FDC-coupled assay 63

Figure 3.9 – Steady state kinetic analysis utilizing FDC coupling assay. 64

Figure 3.10 – Single turnover kinetic analysis of prFMN production by scPFS. 66

Figure 3.11 – Principle of the PiPer™ Pyrophosphate Assay. 68

Figure 3.12 – Reaction between each components of scPFS prenylation with PiPer™ Pyrophosphate Assay working solution. 69

Figure 4.1 – Proposed mechanism for decarboxylation by FDC and proposed mechanism for prFMN synthesis 75

Figure 4.2 – Diagram describing the synthesis and the use of cofactor analogs to study phenylacrylic acid decarboxylation 78

Figure 4.3 – Structures of substrate analogs 83

Figure 4.4 – Single turnover kinetic of prenylation with substrate analogs. 84

Figure 4.5 – Decarboxylation activity of FDC utilized cofactor analogs 86

Figure 4.6 – Native MS spectrum of scPFS prenylation reaction 87

Figure 4.7 – Results from molecular docking simulation 89

Figure 4.8 – Overlay pictures between DMAP from the UbiX crystal structure (PDB: 4ZAF) and prenyl source simulated by molecular docking. 90

List of Tables

Table 1.1 – Catalytic strategies for biological decarboxylation. 12

Table 2.1 – Assay wavelengths and extinction coefficients for Hammett analysis. 27

Table 2.2 – k_{cat}/K_M values measured for FDC-catalyzed decarboxylation of various phenylacrylic acid derivatives. 31

Table 2.3 – Summary of secondary kinetic isotope effects. 36

Table 3.1 – Result from quenching experiment using malachite green assay kit. 54

Table 3.2 – Table verified that prenylation by scPFS under preliminary condition was at maximal velocity (V_{max}) 60

List of Abbreviations

3,4-DHBA	3,4-dihydroxybenzoic acid
AAD	Acetoacitate decarboxylase
DHAP	3-deoxy-Darabinos-heptulosonate-7-phosphate
DMAP	dimethylallyl phosphate
DMAPP	Dimethylallyl pyrophosphate
DMSO	dimethylsulfoxide
DTT	Dithiothreitol
E4P	Erythrose-4-phosphate
FAD	Flavin adenine dinucleotide
FDC	Ferulic acid decarboxylase
FMN	Flavin mononucleotide
GC-MS	Gas Chromatography Mass Spectrometry
GP	Geranyl phosphate
GPP	Geranyl pyrophosphate
H_2O_2	Hydrogen peroxide
HCl	Hydrochloric acid
HEPES	(4-(2-hydroxyethyl)-1-piperazineethanesulfonic acid
HMBP	(E)-4-Hydroxy-3-methyl-but-2-enyl phosphate
HMBPP	(E)-4-Hydroxy-3-methyl-but-2-enyl pyrophosphate
HOMO	Highest occupied molecular orbital
HPLC	High-performance liquid chromatography
HRP	Horseradish peroxidase
KIE	Kinetic isotope effect
LUMO	Lowest unoccupied molecular orbital
MESG	2-amino-6-mercapto-7-methylpurine ribonucleoside
MG	Malachite green
MMCD	Methylmalonyl CoA decarboxylase
MS	Mass Spectrometry
NADH	Nicotinamide adenine dinucleotide
$NADP^+$	Nicotinamide adenine dinucleotide phosphate
NMR	Nuclear magnetic resonance
OMPDC	Orotidine 5'-monophosphate decarboxylase
PAD	Phenylacrylic acid decarboxylase

PAL	Phenylalanine-ammonia lyase
pD	Negative log of deuterium ion concentration
PEP	Phosphoenol pyruvate
PFS	Prenyl FMN synthase
pH	Negative log of hydrogen ion concentration
Pi	Inorganic phosphate
pK_a	Acid dissociation constant
pL	Negative log of ligand concentration
PNP	Purine nucleoside phosphorylase
PPi	Inorganic pyrophosphate
prFMN	Prenylated flavin mononucleotide
scPFS	*Saccharomyces cerevisiae prenyl FMN synthase*
tCA	*trans*-cinnamic acid
toe	Tons of oil equivalent
Tris-HCl	2-Amino-2-(hydroxymethyl)-1,3-propanediol hydrochloride
UbiD	3-octaprenyl-4-hydroxybenzoate decarboxylase
UbiX	Flavin prenyltransferase
V_{max}	Maximum velocity
V_{max}/K_M	k_{cat}/K_M
WS	PiPer™ Pyrophosphate Assay working solution
ρ	Hammett reaction constant
σ	Hammett substituent constant
χ	mole fraction of D_2O

Abstract

The development of biorenewable resources to substitute for oil-based feedstocks in polymer manufacture is essential to address sustainability. Ethylene, propylene, and styrene together represent ~90% of the feedstocks used by the polymer industry. Some industries have attempted to utilize bio-based ethylene and propylene. However, there are very few known biosynthetic pathways to produce styrene and, generally, they are not well understood. The decarboxylation of cinnamic acid by ferulic acid decarboxylase (FDC) is one of the few biological pathways known that form styrene. The focus of this dissertation is to explore the recently proposed FDC decarboxylation mechanisms and cofactor specificity of the enzyme.

The initially proposed mechanisms for FDC decarboxylation of phenylacrylic acid postulated either Michael addition or 1,3-dipolar cycloaddition. ^{1}H NMR analysis, isotope effects and linear free-energy analysis were employed to further investigate the proposed mechanisms and determine the rate-determining step in the reaction. ^{1}H NMR experiments demonstrated that FDC decarboxylation was stereospecific and the source of proton that replaced the carboxylic group of phenylacrylic acid was the solvent. Proton inventory experiments suggested that a single proton was involved in the transition state. The negative Hammett reaction constant provided evidence that the 1,3-cycloelimination step in the 1,3-dipolar cycloaddition mechanism is likely to be rate-determining in the FDC decarboxylation. This was further supported by secondary kinetic isotope effect experiments.

To investigate the biosynthesis of the prFMN cofactor by prenyl flavin synthase (PFS), a scPFS-FDC coupled assay was developed and optimized to monitor scPFS prenylation through the activation of FDC. With scPFS-FDC coupling assay, we found that scPFS selectively uses dimethylallyl pyrophosphate as the substrate for FMN prenylation, in contrast to the bacterial enzyme for which dimethylallyl monophosphate was reported to be the substrate. By implementing this coupled assay, steady-state kinetic parameters of scPFS prenylation were obtained.

Commercially available substrate analogs, (E)-4-Hydroxy-3-methyl-but-2-enyl pyrophosphate (HMBPP) and geranyl pyrophosphate (GPP), were used to investigate the substrate specificity of scPFS prenylation. The apparent first-order rate constants of prenylation were $4.45 \pm 0.87\ h^{-1}$, and $3.80 \pm 0.34\ h^{-1}$ when HMBPP and GPP were respectively used as substrate under single turnover kinetics. Under steady state conditions, FDC was shown to utilize the cofactor synthesized from HMBPP to decarboxylate cinnamic acid at $V_{max} = 5.50 \pm 0.37\ min^{-1}$. However, in the case of GPP counterpart, no decarboxylation activity was observed.

The results presented in this thesis provide better understanding of styrene biosynthesis by FDC. In order to be implemented in bioindustry, this system would have to be further optimized, especially in terms of enzymatic efficiency. One proposed strategy is the use of cofactor analogs. Preliminary investigations here have enabled to establish the procedure that would ultimately lead to the discovery of cofactor analogs with enhanced decarboxylation activity.

Chapter 1 Introduction

1.1 Sustainability and biorenewable resources

1.1.1 Sustainability

As the global population continues to grow, perhaps one of the most challenging and imminent concerns facing the humanity is that of sustainability. The recent report on World Population Prospect by the United Nations (1) numbers the world's population nearly 7.6 billion. The report predicts this number to increase by almost 50% at the end of this century, reaching 11.2 billion (Figure 1.1). In the last century and a half, fossil fuels have become one of the most prominent resources shaping the innovation and revolution of our society. Billions of tons of oil equivalent (toe) of fossil fuel have been consumed every year with positive demand growth predicted over next few decades (Figure 1.2) (2). The fate of fossil fuels can be sectionalized into power supply, construction, industry, transportation, and non-combusted fuel use such as feedstock in petrochemicals. Not only are these resources finite and being depleted, but their increasing demand and price lead to international tension and conflict. Utilization of these fuels moves the underground reserve of carbon to the atmosphere and is a substantial source of the greenhouse gas carbon dioxide (CO_2). The large unnatural influx of carbon dioxide has gradually changed the biosphere causing serious concern about global warming and climate change. Even though a minority may disregard the existence of global warming and climate change, the change in global temperature and global sea level have been statistically recorded over the past century and the rising trends have been observed (Figure 1.3a,b) (3). Non-coincidentally, these trends are similar

to the rise in global greenhouse gas concentrations (Figure 1.3c). The political, economic, and environmental concerns have driven a need for sustainable solutions to reduce fuel prices, replace rapidly depleting fossil fuels, and counteract global warming and climate change. Toward this goal, many countries have invested in research and development for substitutes from a renewable source, such as biomass.

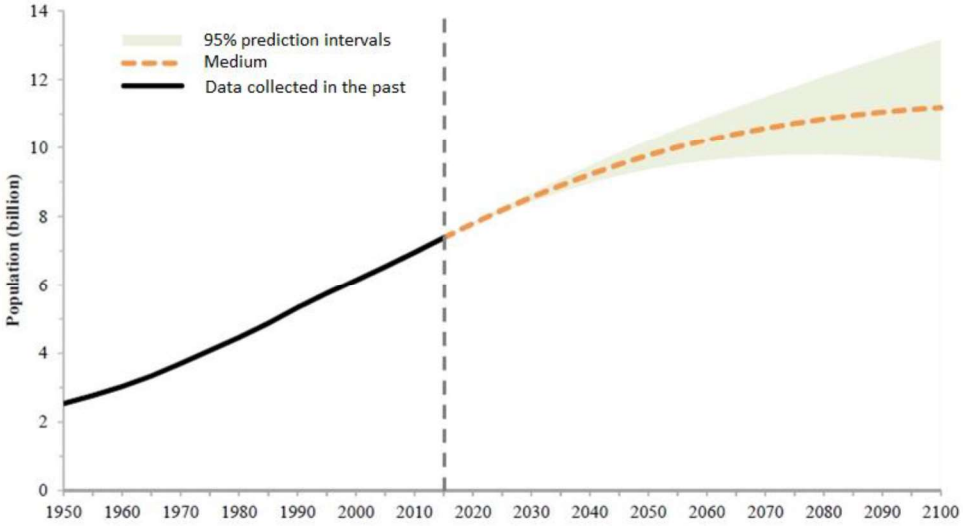

Figure 1.1: World population growth model projected by the United Nation. The black line shows observed population, the dash red line shows the median of 95% prediction intervals represented as grey area. Figure based on reference (1).

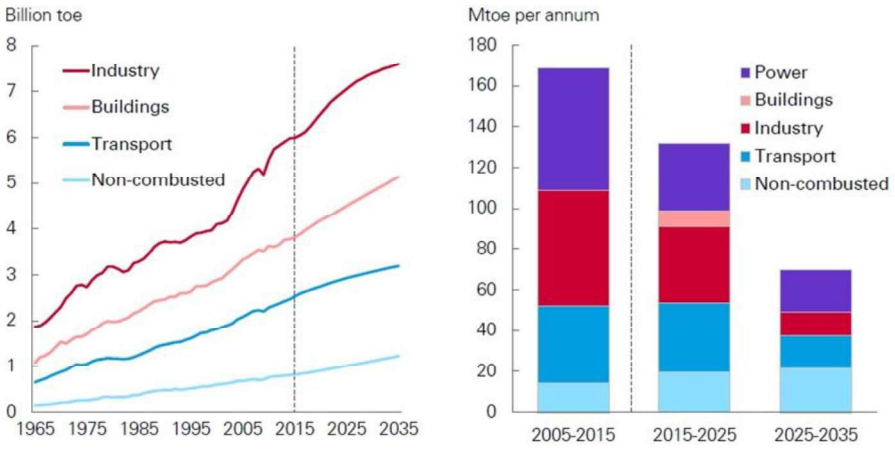

Figure 1.2: Projection of the growth in energy demand in industry based on electricity consumption (left) and fossil fuel (right). Figure based on reference (2).

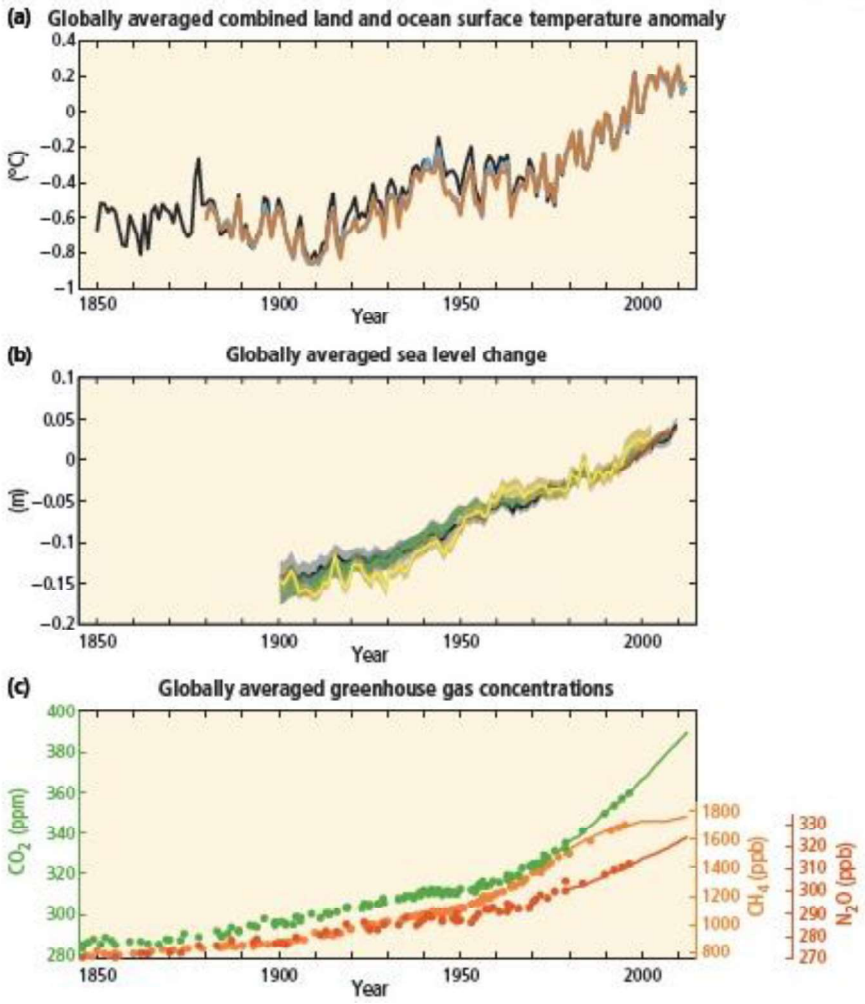

Figure 1.3: Observations of a changing global climate system. (a) Annually and globally averaged combined land and ocean surface temperature anomalies relative to the average over the period 1986 to 2005. Colors indicate different data sets. (b) Annually and globally averaged sea level change relative to the average over the period 1986 to 2005 in the longest-running dataset. Colors indicate different data sets. All datasets are aligned to have the same value in 1993, the first year of satellite altimetry data (red). Where assessed, uncertainties are indicated by colored shading. (c) Atmospheric concentrations of the greenhouse gases carbon dioxide (CO_2, green), methane (CH_4, orange) and nitrous oxide (N_2O, red) determined from ice core data (dots) and from direct atmospheric measurements (lines). Figure taken from reference (3)

1.1.2 Industrial/conventional manufacturing process of styrene

With the projected growth in demand as described previously (Figure 1.2), the use of fossil fuels as a feedstock for petrochemicals such as styrene is of high concern. While demand growth for fossil fuels in other sections gradually decreases over next few decades, the demand growth for non-combusted uses of fossil fuels remain consistent, if not increases. The main contributors of this sector comprise manufacturing of C2-C4 olefins and aromatics, which are the chemicals feedstocks for mass-produced polymers such as polyethylene, polypropylene and polystyrene.

Styrene production, in particular, has a global share of over 25 million metric tons per year with a small but consistent growth rate. The global market for styrene monomer is valued at approximately $30 billion and forecasted to grow by roughly an average of 3.6% per year (4,5). Despite consistently high demand and a large market for styrene, the current production process is unsustainable. Conventional styrene production is a two-step process consuming ethylene and benzene as feedstocks. The first step alkylates benzene with ethylene over an acid catalyst to form ethylbenzene. The second step converts ethylbenzene to styrene by dehydrogenation reaction over an iron oxide catalyst under vacuum at temperature in excess of 600°C (5,6). The conventional manufacturing process of styrene not only expends large amounts of energy and consumes unsustainable substrates, but also significantly contributes to emission of greenhouse gas such as carbon dioxide and methane.

1.1.3 Biorenewable resources

One of the most prominent responses to sustainability is the concept of biorenewable resources. Biorenewable resources, are organic materials with biological origins. Biorenewable resources are generally classified as waste or dedicated energy crops (7). Waste in this context not only includes discarded materials but also refers to low value co-products. Dedicated energy crops are plants grown for production of biobased products specifically. In the past decade, biomass research has been dedicated to the production of biofuels and the value enhancement of biomass.

Renewable biofuels are fuels that are produced through biological processes that convert biomass to useful fuels. The biomass conversion processes are divided into three different categories: thermal conversion; chemical conversion; and biochemical conversion. Biomass conversion can result in fuel in solid, liquid, or gaseous fuels. Bioethanol, biobutanol, and algae biodiesel have gained global interest as potential alternatives to transportation fuel. Bioethanol, in particular, has already been used as gasoline blend for automobiles (8,9). However, the drawback of bioethanol biofuel is its low energy content, roughly one-third lower energy content per unit of volume compared to gasoline. Therefore, bioethanol based vehicles will consume 30% more fuel volumetrically in comparison with petrol vehicle counterparts.

Biobutanol possesses several significant properties suitable for biofuel. These properties include high energy content, immiscibility with water, blending ability, compatibility to combustion engines, low corrosion and high octane rating (10,11). Despite these merits, current biobutanol production suffers from several problems such as selection of sustainable biomass, low yield, butanol inhibition of fermentation cultures and high product recovery costs (12). To make butanol biofuel economically feasible, wide spread research has been conducted both academically and industrially.

Biodiesel is produced from oils or fats using transesterification and is a liquid similar in composition to petroleum diesel. The common feedstock for biodiesel is plant oil. The major concerns with plant oil-derived biodiesel is its economic impact on food price and large area of cultivation land required to replace a significant amount of petroleum diesel. Microalgae, which are considered to be among the most efficient photosynthetic organisms on earth, become a potential source of biomass for second-generation biofuels. However, algal biodiesel economy is currently uneconomic due to high production cost. Production process for algal biodiesel includes algae cultivation, harvesting, biomass processing, oil extraction and biodiesel production. Biomass processing is an energy-intensive process while the oil extraction process can be done using either high energy or expensive solvent extraction (13,14). Various studies have been conducted to improve production of algae biodiesel in the past few decade. These studies range from optimization of algae strains to alternate approaches to process biomass and extract oil.

Although much smaller scale in comparison to transportation fuel, the polymer industry plays another important role shaping research in biorenewable resources. Biorenewable resources in the polymer industry are divided into monomers that replace existing counterparts from fossil sources and original monomers. Ethylene and propylene are well-known monomers belonging to the first group. Biorenewable ethylene is derived by dehydration of bioethanol. Industrial polyethylene production using bio-based ethylene was initiated by the Braskem Company starting in September 2010 with a plant production capacity of 200,000 tons per year. Even though bio-based propylene has not yet reached industrial capacity, the Braskem Company has been carrying out an extensive program of research and development aimed at optimizing synthesis of propylene from bioethanol (15).

Original monomers are unavailable from fossil resources. They are derived specifically from biomass and their polymers are intended to substitute fossil-based polymers. Citric acid and tartaric acid are common examples of the monomers in this group. Citric acid is a cheap commodity with a yearly industrial production over a million tons. The roles of citric acid in polymer industry include the synthesis of biodegradable polyesters and a co-monomer in preparation of isosorbide-based polyesters to enhance chemical and mechanical stability of bio-based coating polyester (16). Tartaric acid is an equally widespread and cheap natural compound. Novel polymers based on tartaric acid include the synthesis of biodegradable polycarbonates with anhydroalditols (17), optically-active hydrophilic aliphatic polyamides capable of producing supramolecular stereocomplexes (18), polyesters with controlled hydrophilicity (19), and polyurethane with a unique proneness to degrade hydrolytically upon incubation at low heat (80ºC) (20). Aside from these two groups of biorenewable monomers, lignin-based polymers have gained increasing interest. Appreciable proportions of aliphatic and phenolic OH groups in lignin make lignins useful as macromonomers for the synthesis of polyurethanes and polyesters. However, the major challenge with regard to lignin is its intrinsic irreproducibility. Rather than using lignin as macromonomers, a number of researchers have focused on the preparation of individual monomer structures, which can be purified to an adequate level before polymerization (15).

1.1.4 Biosynthesis of aromatic compounds and styrene in nature

Nature employs several strategies to synthesize aromatic compounds. One of the most common biosynthesis pathways is the shikimate pathway. The shikimate pathway is the biosynthetic route to the aromatic amino acids phenylalanine, tyrosine, and tryptophan. The roles of these compounds in biological systems are not limited to protein building blocks, but also serve as precursors for a large number of secondary metabolites. The shikimate pathway converts the glycolytic intermediate phosphoenol pyruvate (PEP) and the pentose phosphate pathway intermediate erythrose-4-phosphate (E4P) to chorismate. Chorismate is a precursor to various primary and secondary metabolites such as phenylalanine, tyrosine, tryptophan, quinones, and folates. The Shikimate pathway is composed of seven different steps (Figure 4) (21,22). PEP and E4P are first condensed to form 3-deoxy-Darabinos-heptulosonate-7-phosphate (DHAP) by DAHP synthase. Then the ring oxygen is exchanged for the exocyclic C7 of DHAP to form 3-dehydroquinate. The remaining steps introduce a side chain and two double bonds that convert the cyclohexene ring into the benzene ring.

In the context of styrene biosynthesis, the occurrence of styrene in a wide variety of food has been reported since the late nineteen century. Several possible origins of styrene had been proposed. Through several scientific efforts, the pathway in which certain plants and yeast species synthesize styrene from excess L-phenylalanine through the series of reactions has been elucidated (23,24). Biosynthesis of styrene is a two-step process. In the first step, phenylalanine-ammonia lyase (PAL) deaminates phenylalanine to cinnamic acid. Then, ferulic acid decarboxylase (FDC) performs decarboxylation yielding styrene. In yeast this process also serves as detoxification mechanism against various aromatic carboxylic acids that are inhibitory to growth.

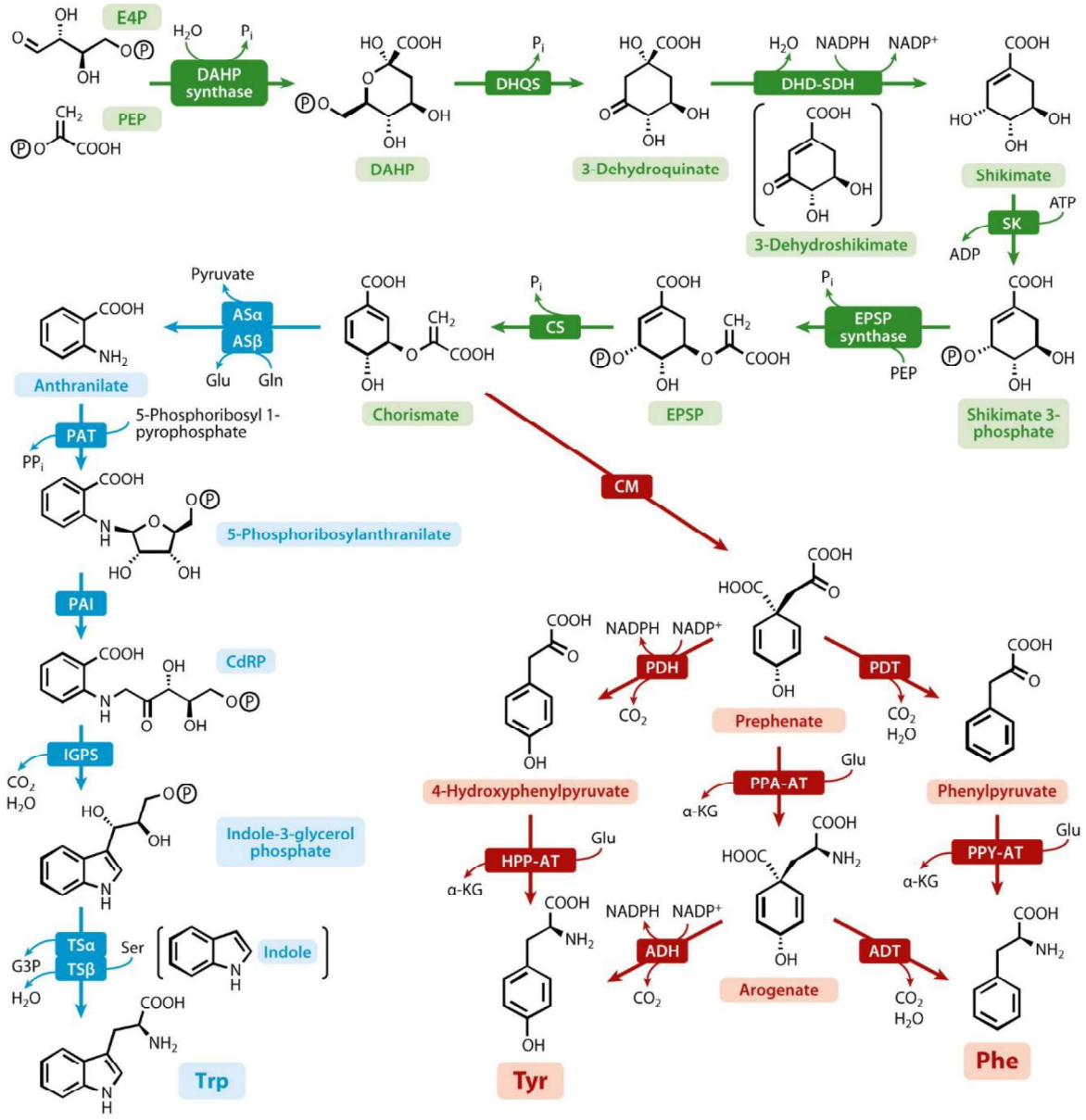

Figure 1.4: The diagram describes biosynthesis of aromatic compounds through the Shikimate pathway. Figure taken from reference (22).

1.2 Phenylacrylic acid decarboxylase (PAD) and Ferulic acid decarboxylase (FDC)

1.2.1 Decarboxylase

Decarboxylation is one of the most fundamental processes in biological systems. Decarboxylases are involved with a wide variety of anabolic and catabolic pathways. More than 90 different decarboxylases has been identified within the IUPAC classification (25). Enzymatic decarboxylation usually utilizes an exogenous cofactor to stabilize the carbanion that transiently develops during the elimination of carbon dioxide from the substrate and catalyze the reaction. However, a few decarboxylases such as orotidine 5'-monophosphate decarboxylase (OMPDC), methylmalonyl CoA decarboxylase (MMCD), and acetoacitate decarboxylase (AAD) develop different strategies to decarboxylate their substrates without a cofactor. OMPDC catalyzed decarboxylation proceeds by a concerted mechanism with the help of conserved aspartic acid and lysine residues; and thus avoids the development of a high energy carbanion intermediate (26). In the case of MMCD, a conserved tyrosine orients the substrate in a plane with thioester carbonyl group. Then, the extremely hydrophobic characteristic of MMCD active site thermodynamically promotes decarboxylation yielding favorable neutral carbon dioxide molecule (27). In the case of AAD, the pKa of the lysine residue in the active site is perturbed from 10.5 to 6. This deprotonated lysine serves as a nucleophile in active site of AAD. The lysine bond is further oxidized to form Schiff base intermediate. The formation of Schiff base and repulsive force between the substrate's carboxylate group and nearby glutamate residue facilitate the decarboxylation reaction (28).

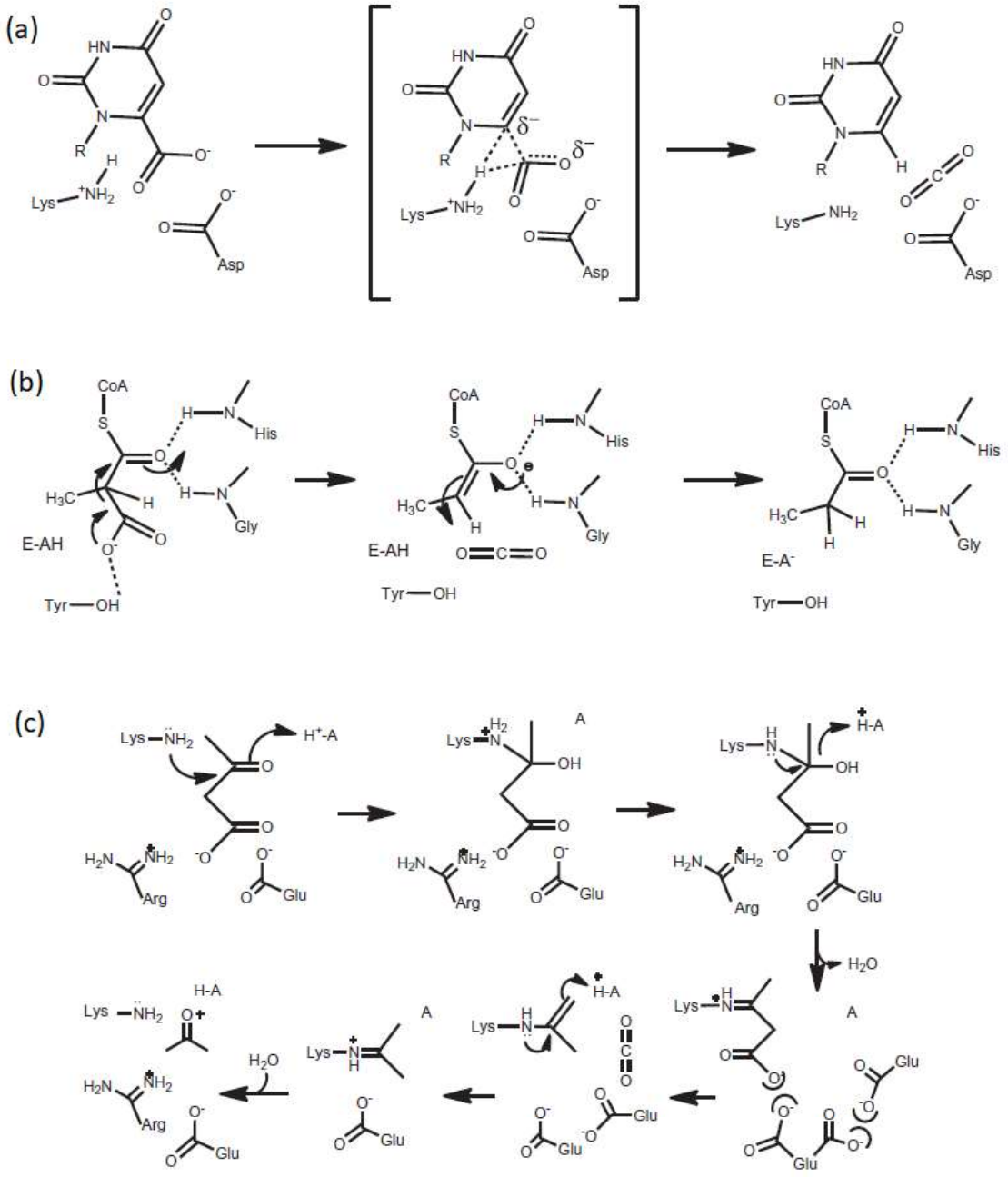

Figure 1.5: Representive mechanistic models of decarboxylases without an exogenous cofactor: (a) OMPDC, (b) MMCD and (c) AAD. Figure adapted from reference (25).

Cofactors for decarboxylases can be either inorganic or organic. Ferrous iron, manganese (II) and magnesium are cofactors for inorganic cofactor-based decarboxylases. These metals serve as electron sinks and Lewis acid centers. Coordination between substrate and the metal center stabilizes the buildup of negative charge during decarboxylation, and therefore reduces the energy barrier to reaction. Organic cofactor-based decarboxylations often proceed through an oxidation-reduction mechanism. In this mechanism, the decarboxylation is initiated in the oxidative step, and followed by the reduction of the intermediate. Organic cofactors for decarboxylation include electron carriers such as flavin, and $NAD(P)^+$ as well as pyridoxal phosphate and thiamin pyrophosphate that serve to delocalize electron density through system of conjugated π-bonds (25).

Table 1.1: Table summarizes catalytic strategies for biological decarboxylation and their examples.

Catalytic cofactor		Representative enzyme
none		Orotidine monophosphate decarboxylase
		Methylmalonyl CoA decarboxylase
		Acetoacitate decarboxylase
Inorganic	Fe^{2+}/O_2 (oxidative)	Gallic acid decarboxylase
		CloR decarboxylase
	Mn^{2+}/O_2	Oxalate decarboxylase
	Mg^{2+}	3-Keto-L-gulonate 6-phosphate decarboxylase
Organic	Flavin	4-Phosphopantethenoyl cysteine decarboxylase
	$NAD^+/NADP^+$	Methylmalonyl CoA decarboxylase
	Pyridoxal 5'-phosphate	Glycine decarboxylase
		Ornithine decarboxylase
		DOPA decarboxylase
	Thiamin diphosphate	Phosphonopyruvate decarboxylase

1.2.2 Phenylacrylic acid decarboxylase (PAD) and Ferulic acid decarboxylase (FDC)

Phenolic compounds such as coumaric acid and ferulic acid are important components of the plant cell wall material, lignocellulose. Breakdown of lignocellulose releases phenolic acids from their natural esterified forms. The resulting free phenolic acids are toxic to most microorganisms. However, some yeasts and other organisms such as *Bacillus Pumilus* and *Lactobacillus plantarum* have evolved metabolic pathways capable of transporting and decarboxylating these compounds. The enzyme responsible for ferulic acid decarboxylation was first purified from *Bacillus Pumilus* in the late twentieth century (29). The potential of phenylacrylic acid decarboxylases (PAD)/ferulic acid decarboxylases (FDC) for styrene biosynthesis has been one driving force for research into these enzymes. Since then, PAD/FDCs from different microorganisms such as *Lactobacillus plantarum, Pediococcus pentosaceus, Brettanomyces bruxellensis, Mycobacterium colombiense, Methylobacterium* sp., *Enterobacter* sp., and *Saccharomyces cerevisiae* have been purified and studied (30–35). In order to construct a styrene biosynthesis pathway from glucose, various isoenzymes of phenylalanine ammonia lyase (PAL) and PAD/FDC have been screened and tested for decarboxylation activity (24). While bacterial PAD can convert coumaric acid to p-hydroxystyrene, only yeast FDC can catalyze the decarboxylation of cinnamic acid yielding styrene.

1.2.3 Yeast FDC1 and PAD1

Decarboxylation of phenolic acid in yeast involves with two proteins, early identified as ferulic acid decarboxylase1 (FDC1) and phenylacrylic acid decarboxylase1 (PAD1). Subsequent studies (36) have found that decarboxylation reaction in yeast requires co-expression of both FDC1 and PAD1. However, purified PAD1 does not exhibit decarboxylase activity, while purified FDC1 alone can convert cinnamic acid and coumaric acid to styrene and hydroxystyrene (24). The result

suggests that FDC1 is the actual decarboxylase while PAD1 assists FDC1 in some way. The role of PAD1 has been proposed to produce flavin-based cofactor that is required by FDC for decarboxylase activity (37). Evidence for this comes from an experiment in which active FDC1 loses its activity after dialyzing against buffer (membrane cutoff = 3,500 Da) for 24 hours. The result indicates that FDC1 binds to a small cofactor rather than directly binds to PAD1 enzyme.

1.2.4 Crystal structure of FDC1 and UbiX

Recently, the cofactor of FDC1 has been successfully identified through crystal structures of *Aspergillus niger* FDC1 and *Pseudomonas aeruginosa* UbiX (38–40). The studies have identified flavin cofactor to be a novel cofactor derived from prenylation of FMN by UbiX to form additional ring between C5 and N6 position of isoalloxazine moiety. Based on crystal structure if UbiX, prenylation mechanism has been proposed with FMN and dimethyl allylmonophosphate as substrates (Figure 1.6).

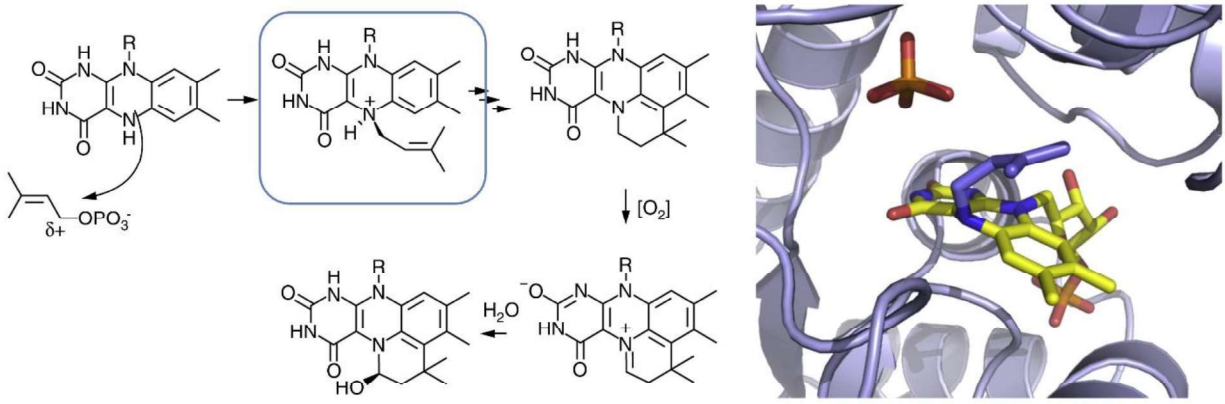

Figure 1.6: Schematic representation of the proposed UbiX mechanism. The first intermediate was identified as a sp^3 N5-prenyl adduct (PDB: 4ZAV). Figure taken from reference (40).

Two forms of oxidized prFMN isomers were observed from the crystal structure of *A. niger* FDC1: ketamine form and iminium form (Figure 1.7) (38). The enoic acid double bond of phenylacrylic acid substrate is found to position directly above the C4 of both oxidized prFMN. The position of the substrate α,β-unsaturated carbonyl directly above the C4 of prFMN suggests the possibility of transient formation of a bond between C4 of prFMN and β carbon of substrate reminiscent of Michael addition-like chemistry and other flavin-catalysed reactions (41). In the proposed mechanism through Michael addition, the N5 secondary ketimine of prFMN could act as a probable acid-base catalyst, providing a rationale for both FMN modification and rearrangement.

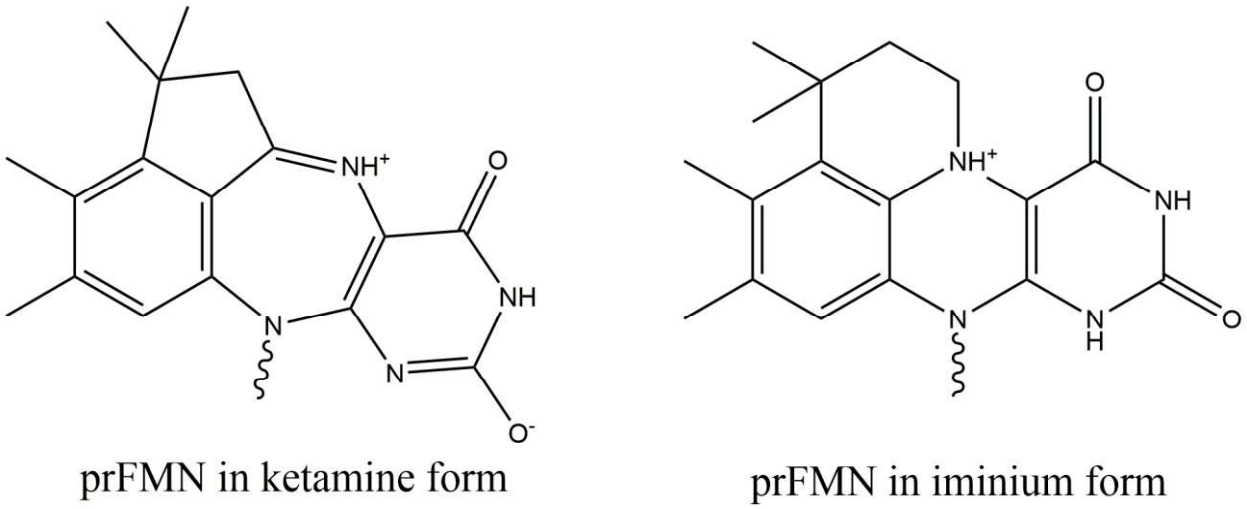

Figure 1.7: Isomers of prFMN observed in the crystal structure of *A. niger* FDC1 (Left) ketamine form (right) iminium form.

However, the subsequent studies using phenylpyruvate as substrate reveals a covalent adduct formed between the prenyl-C1' of the prFMN cofactor in iminium form and substrate. The results imply that iminium form of prFMN is the catalytically relevant species. Iminium form of prFMN contain distinct azomethine ylide character (a well-known 1,3-dipole) that is positioned directly adjacent to the substrate α,β-unsaturated carbonyl (a dipolarophile) by the enzyme. Therefore, a

1,3-dipolar cycloaddition mechanism has been proposed as an alternative decarboxylation mechanism using iminium form of prFMN cofactor.

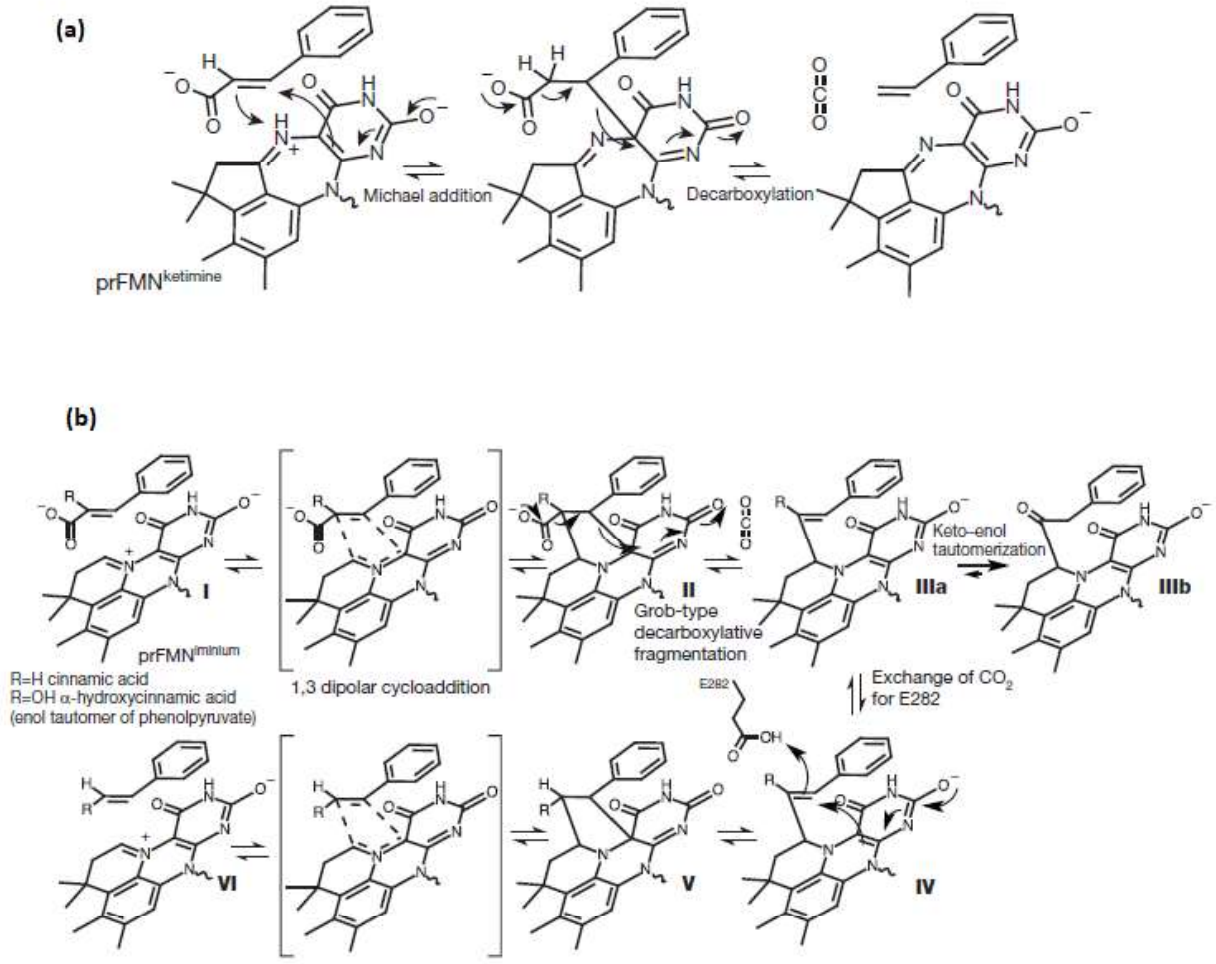

Figure 1.8: Insight into FDC1 decarboxylation mechanism. (a) Proposed mechanism based on Michael addition-like chemistry using ketamine form of prFMN as cofactor. (b) Proposed mechanism based on 1,3-dipolar cycloaddition using iminium form of prFMN as cofactor. Figure adapted from reference (38).

1.3 Goals

Over the last decade, previous studies by our lab and others have established a firm foundation from which we can investigate the mechanism of FDC1 and PAD1 as well as the interaction between the two enzymes. We know that FDC1 serves as decarboxylase while PAD1 generates the flavin based cofactor. However, the mechanisms by which the cofactor is generated by PAD1 and the decarboxylation reaction by FDC1 utilizing this cofactor were unknown. In order to utilize FDC1-PAD1 toward sustainable production of styrene, understanding of the unusual chemistry employed by FDC1 and PAD1 are necessary.

The research in this thesis seeks to provide further understanding of catalytic mechanism employed by FDC1 and PAD1 with regard to yeast phenylacrylic acid decarboxylation. First, in chapter 2, linear free energy analysis and isotope effects were employed to explore dearboxylation mechanism. Results from Hammett analysis and isotope effects provided evidence supporting a 1,3-dipolar cycloaddition mechanism as well as identify probable rate limiting step of the reaction. Next, several approaches to assay biosynthesis of prFMN cofactor were investigated in chapter 3. Dual enzyme assay and HPLC assay were developed in this chapter and utilized to study prFMN cofactor analogs in chapter 4. These work serve to expand our mechanistic understanding of styrene biosynthesis and provide insight to the identification of non-natural cofactors for FDC that exhibit superior decarboxylase activity.

1.4 References

1. World Population Prospects: The 2017 Revision, Key Findings and Advance Tables. United Nations, Department of Economic and Social Affairs, Population Division; 2017.

2. BP Energy Outlook 2017 Edition [Internet]. British Petroleum; 2017. Available from: https://www.bp.com/content/dam/bp/pdf/energy-economics/energy-outlook-2017/bp-energy-outlook-2017.pdf

3. Pachauri RK, Mayer L, Intergovernmental Panel on Climate Change, editors. Climate change 2014: synthesis report. Geneva, Switzerland: Intergovernmental Panel on Climate Change; 2015. 151 p.

4. New Processes for Producing Styrene Cuts Costs, Saves Energy, and Reduces Greenhouse Gas Emissions. U.S. Department of Energy; 2012.

5. Global Styrene Market Key Factors Influencing the Future Landscape. Styrolution; 2013.

6. Tossavainen A. Styrene use and occupational exposure in the plastics industry. Scand J Work Environ Health. 1978;4 Suppl 2:7–13.

7. Brown RC, Brown TR. Biorenewable resources: engineering new products from agriculture. Second edition. Chichester, West Sussex, UK: Wiley Blackwell; 2014. 375 p.

8. Kim S, Dale BE. Global potential bioethanol production from wasted crops and crop residues. Biomass Bioenergy. 2004 Apr;26(4):361–75.

9. Balat M, Balat H. Recent trends in global production and utilization of bio-ethanol fuel. Appl Energy. 2009 Nov;86(11):2273–82.

10. Dürre P. Biobutanol: an attractive biofuel. Biotechnol J. 2007 Dec;2(12):1525–34.

11. Pfromm PH, Amanor-Boadu V, Nelson R, Vadlani P, Madl R. Bio-butanol vs. bio-ethanol: A technical and economic assessment for corn and switchgrass fermented by yeast or Clostridium acetobutylicum. Biomass Bioenergy. 2010 Apr 1;34(4):515–24.

12. Kumar M, Gayen K. Developments in biobutanol production: New insights. Appl Energy. 2011 Jun 1;88(6):1999–2012.

13. Jena U, Vaidyanathan N, Chinnasamy S, Das KC. Evaluation of microalgae cultivation using recovered aqueous co-product from thermochemical liquefaction of algal biomass. Bioresour Technol. 2011 Feb;102(3):3380–7.

14. Mata TM, Martins AA, Caetano NS. Microalgae for biodiesel production and other applications: A review. Renew Sustain Energy Rev. 2010 Jan 1;14(1):217–32.

15. Gandini A, Lacerda TM. From monomers to polymers from renewable resources: Recent advances. Prog Polym Sci. 2015 Sep 1;48(Supplement C):1–39.

16. Noordover BAJ, Duchateau R, Benthem RATM van, Ming W, Koning CE. Enhancing the Functionality of Biobased Polyester Coating Resins through Modification with Citric Acid. Biomacromolecules. 2007;12(8):3860–70.

17. Yokoe M, Aoi K, Okada M. Biodegradable polymers based on renewable resources. IX. Synthesis and degradation behavior of polycarbonates based on 1,4:3,6-dianhydrohexitols and tartaric acid derivatives with pendant functional groups. J Polym Sci Part Polym Chem. 2005 Sep 1;43(17):3909–19.

18. Marín R, de Ilarduya AM, Romero P, Sarasua JR, Meaurio E, Zuza E, et al. Spectroscopic Evidence for Stereocomplex Formation by Enantiomeric Polyamides Derived from Tartaric Acid. Macromolecules. 2008 May;41(10):3734–8.

19. Dhamaniya S, Jacob J. Synthesis and characterization of polyesters based on tartaric acid derivatives. Polymer. 2010 Oct 29;51(23):5392–9.

20. Marín R, Martínez de Ilarduya A, Muñoz-Guerra S. Linear polyurethanes made from naturally occurring tartaric acid. J Polym Sci Part Polym Chem. 2009 May 1;47(9):2391–407.

21. Herrmann KM. The Shikimate Pathway: Early Steps in the Biosynthesis of Aromatic Compounds. Plant Cell. 1995 Jul;7(7):907–19.

22. Maeda H, Dudareva N. The shikimate pathway and aromatic amino Acid biosynthesis in plants. Annu Rev Plant Biol. 2012;63:73–105.

23. Pagot Y, Belin J-M, Husson F, Spinnler H-E. Metabolism of phenylalanine and biosynthesis of styrene in Penicillium camemberti. J Dairy Res. 2007 May;74(02):180.

24. McKenna R, Nielsen DR. Styrene biosynthesis from glucose by engineered E. coli. Metab Eng. 2011 Sep;13(5):544–54.

25. Li T, Huo L, Pulley C, Liu A. Decarboxylation mechanisms in biological system. Bioorganic Chem. 2012 Aug;43:2–14.

26. Begley TP, Ealick SE. Enzymatic reactions involving novel mechanisms of carbanion stabilization. Curr Opin Chem Biol. 2004 Oct;8(5):508–15.

27. Benning MM, Haller T, Gerlt JA, Holden HM. New reactions in the crotonase superfamily: Structure of methylmalonyl CoA decarboxylase from Escherichia coli. Biochemistry (Mosc). 2000 Apr 25;39(16):4630–9.

28. Ho M-C, Ménétret J-F, Tsuruta H, Allen KN. The origin of the electrostatic perturbation in acetoacetate decarboxylase. Nature. 2009 May 21;459(7245):393–7.

29. Rosazza JP, Huang Z, Dostal L, Volm T, Rousseau B. Review: biocatalytic transformations of ferulic acid: an abundant aromatic natural product. J Ind Microbiol. 1995 Dec;15(6):457–71.

30. Rodríguez H, Landete JM, Curiel JA, de las Rivas B, Mancheño JM, Muñoz R. Characterization of the p-Coumaric Acid Decarboxylase from Lactobacillus plantarum CECT 748T. J Agric Food Chem. 2008 May 1;56(9):3068–72.

31. Barthelmebs L, Lecomte B, Divies C, Cavin JF. Inducible metabolism of phenolic acids in Pediococcus pentosaceus is encoded by an autoregulated operon which involves a new class of negative transcriptional regulator. J Bacteriol. 2000 Dec;182(23):6724–31.

32. Godoy L, Martínez C, Carrasco N, Ganga MA. Purification and characterization of a p-coumarate decarboxylase and a vinylphenol reductase from Brettanomyces bruxellensis. Int J Food Microbiol. 2008 Sep 30;127(1–2):6–11.

33. Wuensch C, Pavkov-Keller T, Steinkellner G, Gross J, Fuchs M, Hromic A, et al. Regioselective Enzymatic β-Carboxylation of para-Hydroxy- styrene Derivatives Catalyzed by Phenolic Acid Decarboxylases. Adv Synth Catal. 2015 May 26;357(8):1909–18.

34. Clausen M, Lamb CJ, Megnet R, Doerner PW. PAD1 encodes phenylacrylic acid decarboxylase which confers resistance to cinnamic acid in Saccharomyces cerevisiae. Gene. 1994 May;142(1):107–12.

35. Cavin JF, Barthelmebs L, Diviès C. Molecular characterization of an inducible p-coumaric acid decarboxylase from Lactobacillus plantarum: gene cloning, transcriptional analysis, overexpression in Escherichia coli, purification, and characterization. Appl Environ Microbiol. 1997 May;63(5):1939–44.

36. Mukai N, Masaki K, Fujii T, Kawamukai M, Iefuji H. PAD1 and FDC1 are essential for the decarboxylation of phenylacrylic acids in Saccharomyces cerevisiae. J Biosci Bioeng. 2010 Jun;109(6):564–9.

37. Lin F, Ferguson KL, Boyer DR, Lin XN, Marsh ENG. Isofunctional enzymes PAD1 and UbiX catalyze formation of a novel cofactor required by ferulic acid decarboxylase and 4-hydroxy-3-polyprenylbenzoic acid decarboxylase. ACS Chem Biol. 2015 Apr 17;10(4):1137–44.

38. Payne KAP, White MD, Fisher K, Khara B, Bailey SS, Parker D, et al. New cofactor supports α,β-unsaturated acid decarboxylation via 1,3-dipolar cycloaddition. Nature. 2015 Jun 25;522(7557):497–501.

39. White MD, Payne KAP, Fisher K, Marshall SA, Parker D, Rattray NJW, et al. UbiX is a flavin prenyltransferase required for bacterial ubiquinone biosynthesis. Nature. 2015 Jun 25;522(7557):502–6.

40. Leys D, Scrutton NS. Sweating the assets of flavin cofactors: new insight of chemical versatility from knowledge of structure and mechanism. Curr Opin Struct Biol. 2016 Dec 1;41(Supplement C):19–26.

41. Xu S, Li W, Zhu J, Wang R, Li Z, Xu G-L, et al. Crystal structures of isoorotate decarboxylases reveal a novel catalytic mechanism of 5-carboxyl-uracil decarboxylation and shed light on the search for DNA decarboxylase. Cell Res. 2013 Nov;23(11):1296–309.

Chapter 2 ^{1}H NMR, Linear free energy analysis and isotope effects on decarboxylation catalyzed by FDC

The work described in this chapter has been published as: Ferguson KL, Arunrattanamook N, Marsh ENG. Mechanism of the Novel Prenylated Flavin-Containing Enzyme Ferulic Acid Decarboxylase Probed by Isotope Effects and Linear Free-Energy Relationships. Biochemistry (Mosc). 2016 May 24;55(20):2857–63.;

2.1 Introduction

Decarboxylation reactions constitute an important class of biological reactions that are ubiquitous in both primary and secondary metabolism in living organisms. However, decarboxylation reactions usually have very high energy barriers that require enzymes to catalyze the reaction on a biologically feasible timescale. Therefore, nature employs a wide variety of catalytic strategies to facilitate decarboxylation utilizing an array of prosthetic groups; such as metal ions, pyridoxal phosphate and thiamin pyrophosphate (1–4).

The enzyme that is subject of this thesis is ferulic acid decarboxylase (FDC). This enzyme, and several of its analogs are found in yeast strains and a variety of different microbes (5–10). The major functions of these enzymes include: detoxifying antimicrobial compounds such as sorbic acid and phenylacrylic acid by decarboxylating them to give carbon dioxide and volatile a byproduct, and decarboxylation of aromatic carboxylic acid intermediates in the ubiquinone biosynthesis pathway (11). Unlike other enzyme-catalyzed decarboxylation reactions, FDC does

not require the substrate to have an additional activating group such as carbonyl (benzoylformate decarboxylase), carboxylate (isocitrate dehydrogenase), hydroxy (bacterial phenylacrylic acid decarboxylase), and amino (amino acid decarboxylase). As such, FDC can decarboxylate trans-phenylacrylic acid derivatives and sorbic acid yielding hydrocarbon products free of heteroatom functional groups, in this case styrene and 1, 3-pentadiene, respectively. Thus, it is of great interest to use FDC as a model enzyme for biosynthesis of styrene and other valuable monomer feedstocks for mass-produced polymers.

An attempt to construct a styrene biosynthesis pathway in an industrially viable microorganism such as *Escherichia coli* has recently been reported (12). The pathway is composed of two-steps: the deamination of phenylalanine by phenylalanine lyase, followed by the decarboxylation of the corresponding product, *trans*-cinnamic acid (tCA), with ferulic acid decarboxylase from *Saccharomyces cerevisiae* (Figure 2.1).

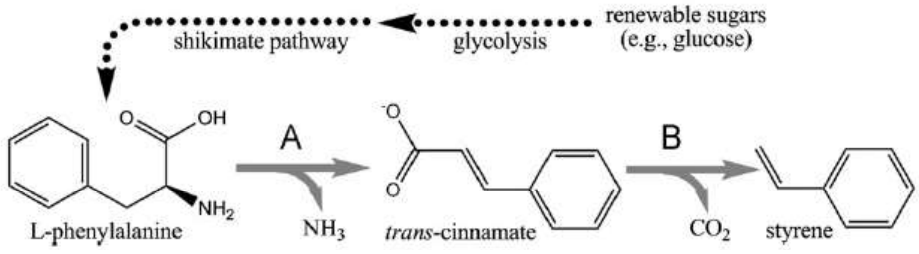

Figure 2.1: Constructed styrene biosynthesis pathway in *Escherichia Coli* that successfully synthesizes styrene from renewable substrates such as glucose. A is phenylalanine lyase and B is ferulic acid decarboxylase. Figure taken from reference (12).

The successful construction of this pathway served as a starting point for biosynthesis of styrene; however, the mechanism of the enzyme catalyzing the decarboxylation step, FDC, remained largely unknown at the time. Subsequent studies on FDC have identified a new flavin-derived cofactor involved in the decarboxylation of phenylacrylic acids (11,13,14). This cofactor, which

has been termed as prenylated flavin, is a modified form of FMN (prFMN) containing an extra 6-membered ring formed by the addition of an isopentyl group between the N5 and C6 positions of the isoalloxazine moiety. In the same subsequent study, prFMN was shown to be synthesized from dimethylallyl phosphate (DMAP) and FMN by UbiX.

On the basis of crystallographic evidence (15), a mechanism has been proposed for FDC that involves an initial 1,3-dipolar cycloaddition between prFMN and the double bond of phenylacrylic acid, which is followed by a Grob-type elimination of carbon dioxide (Figure 2.2a). Protonation of the substrate by an active site glutamate and finally cyclo-elimination to yield styrene and prFMN complete the catalytic cycle. The mechanism of FDC is of considerable interest because true thermal pericyclic reactions are extremely rare in enzymes, and 1,3-dipolar cycloadditions are unprecedented. A simpler mechanism involving a Michael addition of prFMN to the double bond of phenylacrylic acid followed by decarboxylation and elimination of the cofactor was also proposed as alternate mechanism (Figure 2.2b). However, this mechanism was disfavored on the basis of an X-ray structure of a covalent inhibitor−prFMN adduct that appeared inconsistent with prFMN reacting in this way.

This chapter describes a combination of ^{1}H NMR analysis, isotope effects and linear free-energy analysis studies, which my colleague Kyle Ferguson and I undertook in order to further investigate the proposed mechanisms for phenylacrylic decarboxylation. Isotope effects and linear free-energy analysis are informative in identifying intermediate bond formation and bond breakage during the chemical limiting step. The presence of these effects may inform on the nature of the rate-determining step.

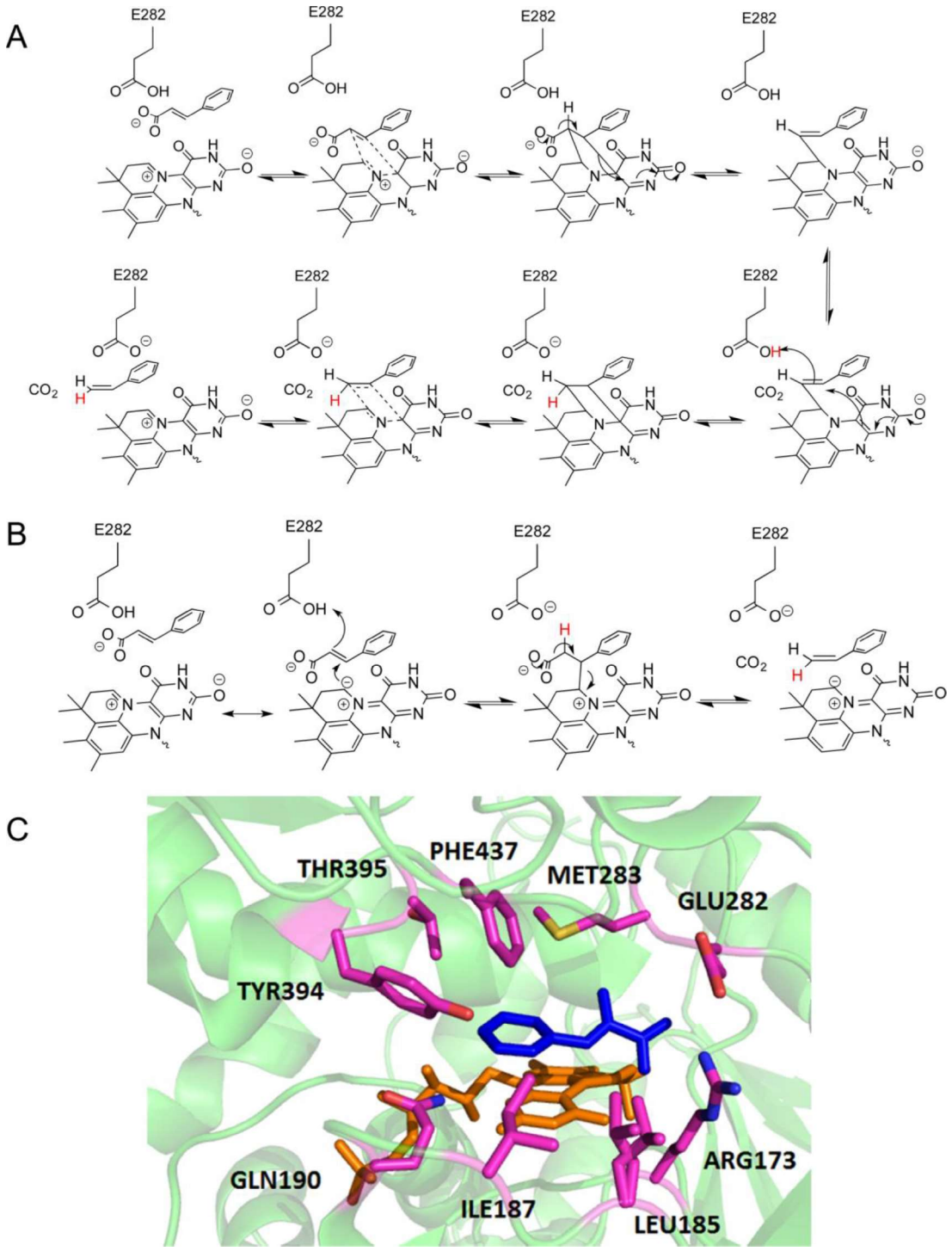

Figure 2.2. Proposed mechanisms for the FDC-catalyzed decarboxylation of phenylacrylic acid proceeding through (A) 1,3-dipolar cyclo-addition to the prFMN cofactor and (B) Michael addition/elimination of prFMN to the substrate. (C) Details of the active site: active site residues are shown in magenta with the prFMN cofactor in orange. The substrate analogue α-methylphenylacrylic acid (blue) is shown bound in the active site (PDB ID: 4ZA7).

2.2 Materials and methods

2.2.1 Materials

trans-cinnamic acid, styrene, *p*-coumaric acid, 4-methoxycinnamic acid, 4-fluorocinnamic acid, 4-formylcinnamic acid, 4-bromocinnamic acid, 4-chlorocinnamic acid, and 4-methylcinnamic acid were purchased from Acros Organic. *trans*-cinnamic acid, 3-nitrocinnamic acid, and 3-methoxycinnamic acid were purchased from Sigma-Aldrich. 4-Cyanocinnamic acid was purchased from Matrix Scientific. 4-Aminocinnamic acid and 4-nitrocinnamic acid were purchased from Tokyo Chemical Industries. 4-(2-Carboxy-vinyl)-benzoic acid methyl ester was purchased from Santa Cruz Biotechnology. All other chemicals were purchased from Sigma-Aldrich. d7-trans-Cinnamic acid and 3-d1-trans-cinnamic acid were purchased from Sigma-Aldrich; 2-d1-trans-cinnamic acid was synthesized by reaction of benzaldehyde with d6-acetic anhydride using standard literature procedures (16). Holo-FDC was recombinantly expressed in Escherichia coli and purified as described previously (14).

2.2.2 ^{1}H NMR analysis

Decarboxylated products of trans-cinnamic acid were prepared by the reaction between 4 mM of tran-cinnamic acid and 1 μM of FDC1 enzyme in 3 mL of (a) 100 mM phosphate buffer pH 7 (b) pH 7 of deuterated HEPES buffer (typical HEPES buffer prepared with deuterated water and NaOD). After 30 minutes of reaction, decarboxylated products were collected and centrifuged at 7000 rpm for 30 minutes to separate FDC enzyme from the solution. Then, the solutions were extracted with 400 μL of $CDCl_3$ three times. Molecular sieves were added into combined $CDCl_3$ phase to absorb traces of water in the organic phase. The ^{1}H NMR experiments and data acquisitions were carried out using Varian MR400 NMR spectrometer.

2.2.3 Enzyme Assay

Assays of FDC activity were routinely performed in 100 mM phosphate buffer (pH 7.4) at 25°C. Stock solutions of substrates were prepared in DMSO. Assays contained substrates at various initial concentrations between 10 and 50 μM. Reactions were initiated by addition of FDC to a final concentration between 50 and 500 nM depending on the activity of the enzyme with a particular substrate. We followed the activity spectrophotometrically by monitoring depletion of the substrates. The wavelengths used to monitor the enzyme activity and extinction coefficients of the various substrates are given in Table 2.1. Care was taken to ensure that the assay remained linear at the concentrations of substrate and enzyme used.

Table 2.1: Assay wavelengths and extinction coefficients for phenylacylic acid derivatives used in this study

substituent	Assay wavelength (nm)	$\varepsilon_{substrate}$ ($M^{-1}.cm^{-1}$)	$\varepsilon_{product}$ ($M^{-1}.cm^{-1}$)
p-NH_2–	292	17900	1840
p-HO–	294	16900	7930
p-CH_3O–	290	18900	5410
p-CH_3–	280	19000	Negligible
p-H–	276	17900	Negligible
p-F–	276	14300	948
m-CH_3O–	276	14300	Negligible
p-Cl–	280	21200	1810
p-Br–	278	22000	2630
p-CH_3OOC–	300	19000	Negligible
m-NO_2–	280	14800	7240
p-CN–	284	26600	7230
p-CHO–	304	24800	Negligible
p-NO_2–	314	18000	9760

2.2.4 pH Dependence and Solvent and Secondary Deuterium Isotope Effect Measurements

The pH dependence of FDC activity was studied with the following buffers: pH 4.0−6.5, 100 mM sodium citrate; pH 6.5−8.0, 100 mM sodium phosphate; pH 8.0−9.0, 100 mM Tris chloride. For measurements in deuterated solvents, the buffer components were dissolved in D_2O (99.9%) and repeatedly lyophilized to exchange protium. pD was corrected using eq 2.1, where χ is the mole fraction of D_2O.

$$pD = pH + 0.076\chi^2 + 0.3314\chi + 0.00009 \qquad \text{(Equation 2.1)}$$

To measure the solvent deuterium kinetic isotope effect on styrene formation, the reactions were performed in buffers containing various mole fractions of D_2O, and the deuterium content of the styrene produced was analyzed by GC-MS as described previously (17,18).

Secondary KIEs were measured at substrate concentrations of 50 μM and enzyme concentrations of 50 nM so that the measurements represent the KIE on V_{max}/K_M. Experiments were performed at a pD and pH of 6.5, where the activity of the enzyme is independent of pH.

2.3 Results and discussion

At the time research experiments in this chapter started, there was no studies regarding the reaction mechanism by which phenylacrylic acid is decarboxylated by FDC. Thus, the first aim of my research thesis was to gain a better understanding on the decarboxylation mechanism. The analytical tools used in the experiments to elucidate the mechanism include ^{1}H NMR and linear free energy correlations (Hammett analysis), along with solvent isotope effect and secondary kinetic isotope effect measurements made in collaboration with my colleague, Kyle Ferguson.

With the release of the crystal structure which allowed proposed mechanisms to be proposed, the results in this chapter have been exploited to verify the decarboxylation mechanism used by FDC, and describe the nature of this mechanism, as well its rate determining step.

2.3.1 ^{1}H NMR analysis

The ^{1}H NMR spectrum of styrene product obtained from the reaction performed in deuterated HEPES buffer is shown in Figure 2.3a. The ^{1}H NMR spectrum of styrene from reaction in phosphate buffer match with the reference spectrum (reference from WinChembase) of styrene described in Figure 2.3b. Deuterated styrene product displays two signals from proton on the double bond with equal intensity. The signal at chemical shift (horizontal axis) around 5.2 ppm is missing, indicating that FDC stereospecifically protonates at hydrogen position D (trans-terminal position), which is also the position of carboxylic group of *trans*-cinnamic acid (Figure 2.3c). Without hydrogen at position D, the signal of hydrogen at position B changes from doublet of doublets into doublet. The chemical shifts of the remaining signals of deuterated styrene product are consistent with the reference styrene spectrum. The result also implies that the source of hydrogen used for protonation comes from solvent; and thus, solvent diffusion could play an

important role in enzymatic activity. Furthermore, substituents on hydrogen position B or C are not likely to be steric effects that could alter substrate binding.

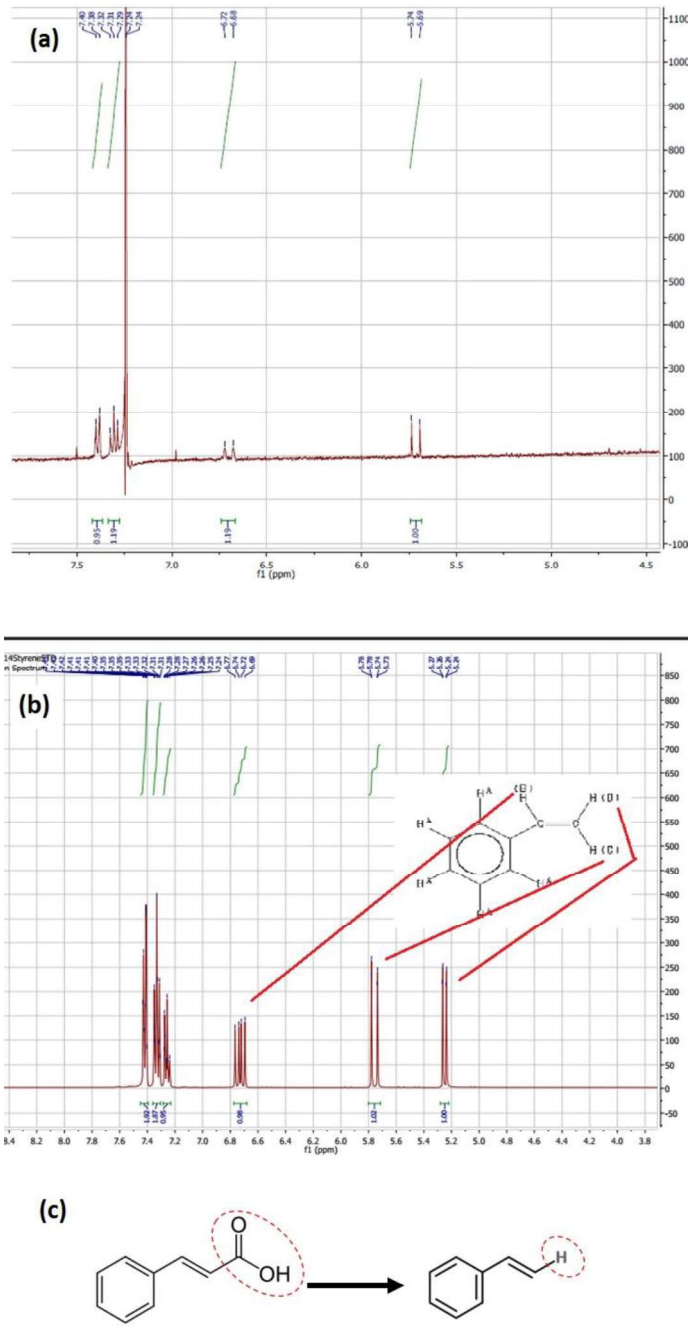

Figure 2.3. (a) ^{1}H NMR spectrum of deuterated styrene product. Two doublet signals corresponding to acrylate protons are observed at 6.7 and 5.7 ppm (b) ^{1}H NMR spectrum of styrene with assigned signal. Three acrylate protons are observed at 6.7, 5.7 and 5.2 ppm. (c) Decarboxylation reaction of *trans*-cinnamic acid. The protonation to form styrene product is specific at the same position as carboxyl group of *trans*-cinnamic acid.

2.3.2 Linear free energy analysis (Hammett analysis) of FDC

Linear free-energy relationships provide a powerful tool with which to interrogate reaction mechanisms (19–21). The narrow substrate range of most enzymes limits the utility of this approach for the investigation of enzyme reactions, although for more promiscuous enzymes, linear free energy analyses have proved to be highly informative. The broad substrate range of FDC made it an excellent candidate to conduct a Hammett analysis of the decarboxylation reaction. The linear free energy kinetic analysis was studied for a series of 14 para- and meta-substituted phenylacrylic acids covering the range of substituent constants σ^- of -0.66 to +1.25, which are listed in Table 2.2.

Table 2.2: k_{cat}/K_M Values Measured for FDC-catalyzed decarboxylation of various phenylacrylic acid derivatives

substituent	σ^-	k_{cat}/K_M (M^{-1} s^{-1})	log (k_{cat}/K_m)
p-NH_2-	-0.66	12400 ± 670	4.09 ± 0.023
p-HO-	-0.37	4550 ± 250	3.66 ± 0.023
p-CH_3O–	-0.27	28100 ± 1800	4.45 ± 0.027
p-CH_3–	-0.17	27000 ± 1600	4.43 ± 0.025
p-H–	0	24500 ± 1400	4.39 ± 0.023
p-F–	0.02	27500 ± 1800	4.44 ± 0.027
m-CH_3O–	0.12	27000 ± 2000	4.44 ± 0.031
p-Cl–	0.23	19600 ± 1200	4.29 ± 0.026
p-Br–	0.26	21400 ± 1300	4.33 ± 0.026
p-CH_3OOC–	0.66	11500 ± 320	4.06 ± 0.012
m-NO_2–	0.71	14300 ± 1000	4.16 ± 0.030
p-CN–	0.88	12800 ± 880	4.11 ± 0.029
p-CHO–	1.13	7600 ± 300	3.88 ± 0.015
p-NO_2–	1.25	8690 ± 160	3.94 ± 0.008

The resulting Hammett plot for a series of 12 of the substituted phenylacrylic acids listed in Table 2 is shown in Figure 2.4. The data poorly correlated with the standard Hammett parameter σ ($\rho = -0.5$; $r^2 = 0.65$) but showed a strong correlation with the Hammett parameter σ^- ($\rho = -0.39 \pm 0.03$; $r^2 = 0.93$). Two substrates, 4-amino- and 4-hydroxyphenylacrylic acid, reacted much slower than expected based on their highly negative σ^- values. These substrates are the only compounds that contain hydrogen bond-donating functional groups. Although it is unclear why they react so slowly, the large deviation of these compounds from the trend line suggests they may react by a different mechanism. For this reason, they were excluded from the calculation of ρ in our analysis.

The apparent linearity of the Hammett analysis provides strong evidence that a chemical step is rate-determining in the reaction. The negative reaction constant (ρ), which is caused by electron-releasing groups that increase the rate of reaction, is very unusual. With the exception of some metal catalyzed decarboxylations (21,22), decarboxylation reactions (both enzymatic and nonenzymatic) involve a buildup of negative charges in the transition state and are therefore associated with large positive ρ values. The strong correlation with σ^- indicates that, in addition to inductive effects, delocalization of electrons through the extended π-system associated with the aromatic ring is important in stabilization of the transition state in a step that contributes significantly to the overall rate of the reaction.

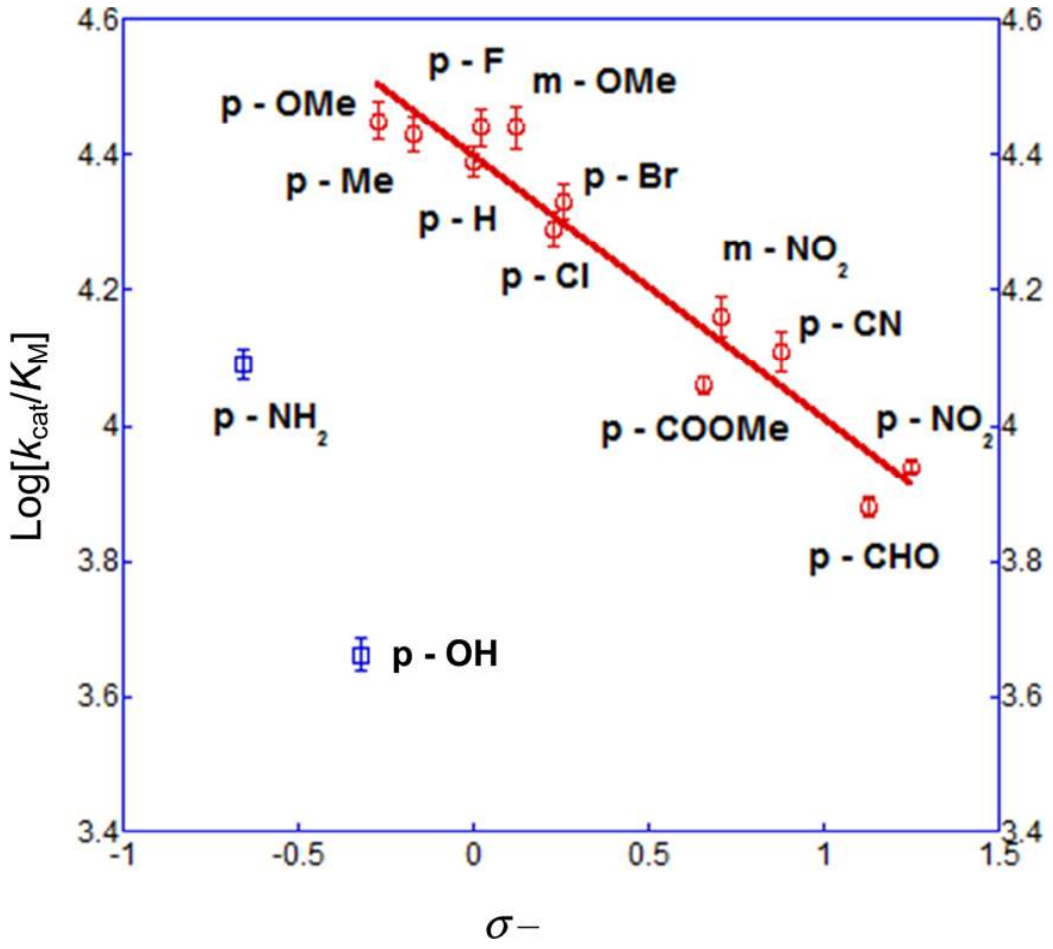

Figure 2.4: Hammett plot for the FDC-catalyzed decarboxylation of 14 different para- and meta-substituted phenylacrylic acids. Data points in red were used to determine ρ; the two outliers in blue were excluded from the analysis.

2.3.3 pH Dependence and solvent isotope effects

2.3.3.1 Dependence of rate on pL

Initial characterization by ^{1}H NMR of the styrene produced in the FDC reaction established that the solvent proton is incorporated *trans* to the phenyl ring of styrene, as described earlier. Therefore, decarboxylation occurs with the retention of the configuration at Cα, which is in accord with the geometry of the active site and the proposed role of Glu282 acting as the proton donor.

Because solvent isotope effects may be influenced by pH, we first investigated the activity of FDC as a function of pH and pD. Under V_{max} conditions, the enzyme exhibits a typical bell-shaped pH dependence curve with an activity maximum at pH 6.5. The acidic limb is characterized by pK_a = 5.3 ± 0.1, and the basic limb is characterized by pK_a = 8.0 ± 0.1. The enzyme activity in deuterated buffers was very similar, although the pKa of the acidic limb was shifted to a slightly lower value (pK_a = 5.0 ±0.1) (Figure 2.5). On the basis of the pL curves, the solvent KIE on Vmax ($^DV_{solvent}$) was measured at pL = 6.5. The value is close to unity ($^DV_{solvent}$ = 0.95 ± 0.05; n = 5), indicating that proton transfer to the product is not a kinetically significant step in the overall reaction.

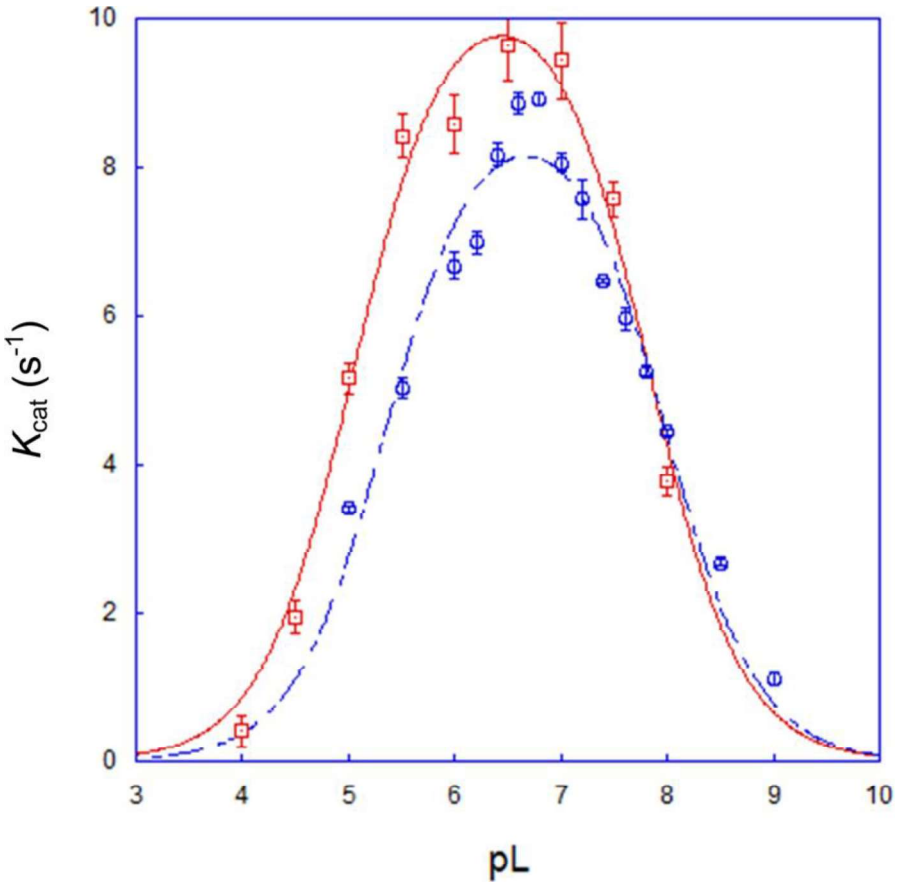

Figure 2.5: pL-rate profile for decarboxylation of phenylacylic acid by FDC in H_2O (blue) and D_2O (red) buffers.

2.3.3.2 Proton inventory analysis

To investigate the protonation step in more detail, we conducted a proton inventory analysis, which allowed us to measure the solvent KIE on V_{max}/K_M ($^{D}V/K_{solvent}$). Reaction mixtures were set up at pL 6.5 in buffers containing 0.1 mole fraction increments of deuterium (χ_{D2O}). The styrene produced by the reaction was isolated, and the mole fraction of deuterium ($\chi_{styrene}$) was determined by GC-MS. While $^{D}V/K_{solvent}$ may be estimated by the determination of $\chi_{styrene}$ at $\chi_{D2O} = 0.5$, for which $^{D}V/K_{solvent} = \sim 3.3$, we can determine it more accurately by fitting the full proton inventory data, shown in Figure 2.6, to eq 2.2.

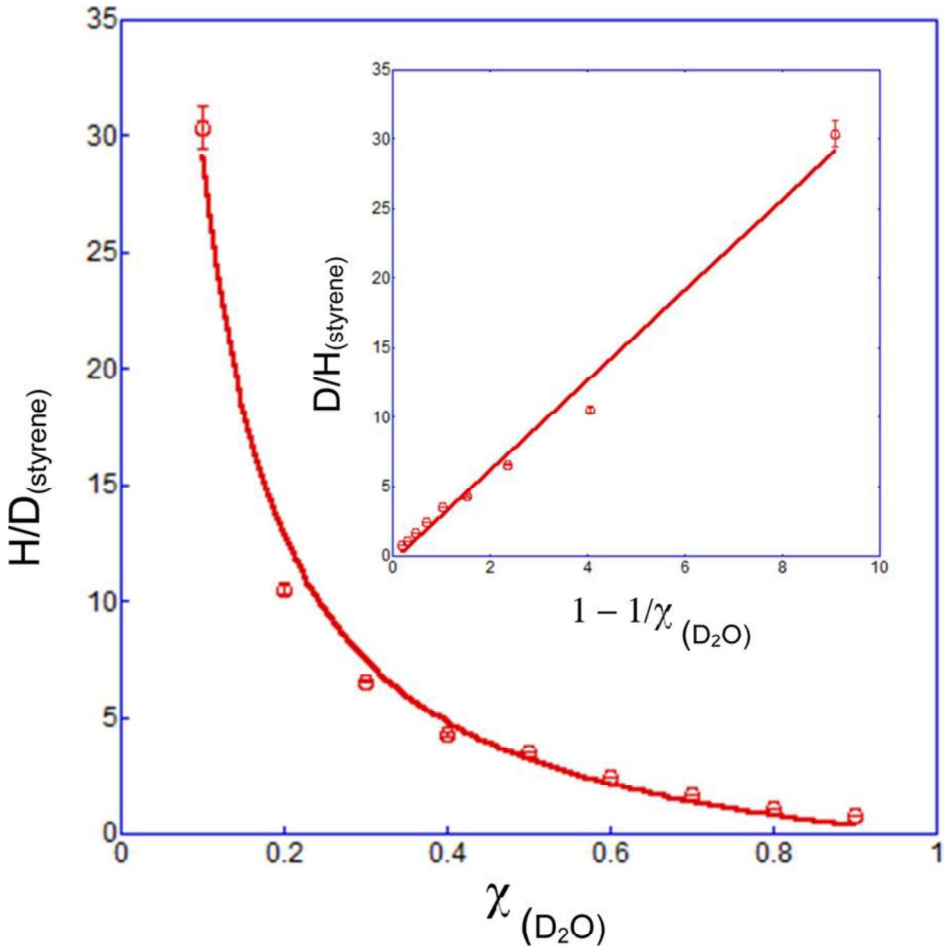

Figure 2.6. Proton inventory for FDC. The mole fraction of D_2O in the solvent is plotted against the ratio of protonated to deuterated styrene. The solid line represents the best fit to eq 2.2. A linearized plot of the data is shown in the inset.

$$\chi_{\text{product}} = {}^{D_2O}\text{SIE}_{\text{obs}} \left(\frac{1}{\chi_{\text{solvent}}} - 1\right) \qquad \text{(Equation 2.2)}$$

2.3.4 Secondary kinetic isotope effects

Secondary kinetic isotope effects report on changes in the stiffness of bonds adjacent to the site of the reaction. They are particularly informative for an examination of changes in the geometry of carbon atoms: the transition from tetrahedral to planar geometry is associated with a normal secondary KIE, whereas the transition from planar to tetrahedral geometry is associated with an inverse secondary KIE (23–26). To investigate the mechanism of the FDC reaction, we measured secondary deuterium KIEs at both the α- and β-positions of cinnamic acid in both D_2O and H_2O buffers (the commercially available β-deuterated cinnamic acid was also deuterated on the phenyl ring; the remote isotope was assumed to not influence the KIE at the β-position). KIEs were determined at 25 °C in 100 mM sodium citrate buffer (pL 6.5) by a direct comparison of reaction rates at low substrate concentrations relative to K_M so that the measurements represent KIEs on V_{max}/K_M. The data are presented in Table 2.3.

Table 2.3: Summary of secondary kinetic isotope effects measured for the FDC-catalyzed decarboxylation of deuterated phenylacrylic acids in H_2O and D_2O

deuterium position	2° $^{D}V/K$ (H_2O)	2° $^{D}V/K$ (D_2O)
Cα	0.99 ± 0.02	1.12 ± 0.030
Cβ	1.10 ± 0.016	1.01 ± 0.027
Cα and Cβ	1.15 ± 0.017	1.32 ± 0.035

In H_2O, no apparent 2° KIE was observed at the α-position, whereas at the β-position a large, normal 2° KIE was measured ($2^{\circ D}V/K_{\beta(H2O)}$ = 1.10 ± 0.03; n = 9). In contrast, in D_2O, the apparent 2° KIE at the α-position became significant ($2^{\circ D}V/K_{\alpha(D2O)}$ = 1.12 ± 0.03; n = 9), whereas the 2° KIE at the β-position was suppressed and was at unity within error. When di-deuterated

phenylacrylic acid was the substrate, large 2° KIEs were measured in both H_2O and D_2O. The fact that these KIEs are normal indicates that they both arise from the rehybridization of the α- and β-carbons from tetrahedral to planar geometry during the reaction.

2.3.5 Interpretation of linear free energy analysis and isotope effect

The strong correlation of $\log(k_{cat}/K_M)$ with the Hammett σ^- parameter (Figure 2.4) points to a chemical step in the reaction as rate-determining, rather than a substrate-binding or product release step, in which case ρ would be expected to be close to zero. Interestingly and unexpectedly, for a decarboxylation reaction, ρ is negative ($\rho = -0.39$). Therefore, it seems unlikely, regardless of the precise details of the mechanism, that the decarboxylation step is rate-determining. Otherwise, the buildup of negative charge in the transition state should lead to a positive ρ value, which is generally observed in decarboxylation reactions.

The negative ρ value provides evidence that the 1,3-cycloelimination reaction, which leads to the release of styrene from prFMN, is likely to be rate-determining in the FDC decarboxylation. The correlation of reactivity with σ^- is generally discussed in terms of resonance effects. This formalism derives from the overlap of p-orbitals to form extended π-systems and is thus correlated with the HOMO-LUMO analyses used to rationalize thermal pericyclic reactions. The structure of prFMN suggests that its reactivity toward dipolarophiles (substrates in our case) will resemble that of an azomethine ylide, which have a nucleophilic character and react increasingly rapidly with increasingly electron-withdrawing dipolarophiles (27). Thus, electron-withdrawing substituents on the phenyl ring will slow down the final cyclo-elimination reaction leading to product formation, consistent with our experimental observations.

The 2° KIEs measured for FDC provide further evidence that a chemical step, rather than a substrate binding or product release step, is rate-determining. The observed normal 2° isotope effects are indicative of a change in geometry at the carbon atoms from tetrahedral to planar which points to the rate-determining step involving the formation of the styrene double bond in the final cyclo-elimination reaction. The change in the apparent 2° KIEs observed when the reaction is performed in D_2O is unusual but may be explained by the fact that, when the α-carbon undergoes rehybridization, it contains an additional deuterium from the solvent. This will introduce a cryptic 2° KIE at the α-carbon that could mask the 2° KIE at the β-carbon. When the enzyme is reacted with α-deuterated phenylacrylic acid in D_2O, the α-carbon will contain two deuterium atoms; thus, the observed 2° KIE will be further elevated and will appear as a normal KIE. A similar argument can be brought to explain the further increase in 2° KIEs when α,β-dideuterated substrates are used. The pattern of 2° KIEs further suggests that the 1,3-cyclo-elimination reaction that leads to the formation of the styrene double bond occurs in a concerted but asynchronous reaction in which bond cleavage is advanced at the α-carbon with respect to the β-carbon.

Our results do not definitively rule out a previously considered mechanism in which a Michael addition of prFMN to phenylacrylic acid facilitates decarboxylation as shown in figure 2.2. However, we consider this possibility as less likely. In this mechanism, the 2° KIEs indicates that decarboxylation is rate limiting, concomitant with a change in geometry from tetrahedral to planar at the α- and β-carbons. As discussed above, postulating decarboxylation as the rate-limiting step appears inconsistent with the negative value of ρ associated with the overall reaction observed from linear free energy analysis.

2.4 Conclusions

In conclusion, the results presented here provide evidence supporting the proposed mechanism for FDC which involves a novel cycloaddition reaction of the substrate with the prenylated flavin cofactor. The unusual negative reactivity constant, ρ, and the normal secondary kinetic isotope effects suggest that the rate-determining step in the catalytic cycle is resolution of the product−prFMN adduct through a cyclo-elimination reaction. Further mechanistic studies would be necessary to provide direct evidence for the existence of intermediates of the 1,3-dipolar cycloaddition mechanism.

Subsequently, identification of the key cycloaddition intermediate of FDC decarboxylation has been further pursued by my colleague, Kyle Ferguson. His study utilizes native mass spectroscopy technique to detect different forms of the cofactor bounded to the enzyme FDC (28). Utilizing substrate analog, (Z)-2-Fluoro-2-nitro-vinylbenzene, the decarboxylation step is prevented; and thus, it irreversibly inhibits the catalytic activity of FDC. The m/z values of intermediate prior to decarboxylation step would be different by one proton due to the lack of proton abstraction step in the beginning step of 1,3-dipolar cycloaddition mechanism. The result showed the existence of prenyl-flavin adducted with m/z corresponding to the intermediate from 1,3-dipolar cycloaddition mechanism (Figure 2.7) in agreement with the conclusion of this chapter. Identification of other intermediates is in-progress, utilizing substrate analogs, mutagenesis of active site residues, and native mass spectroscopy.

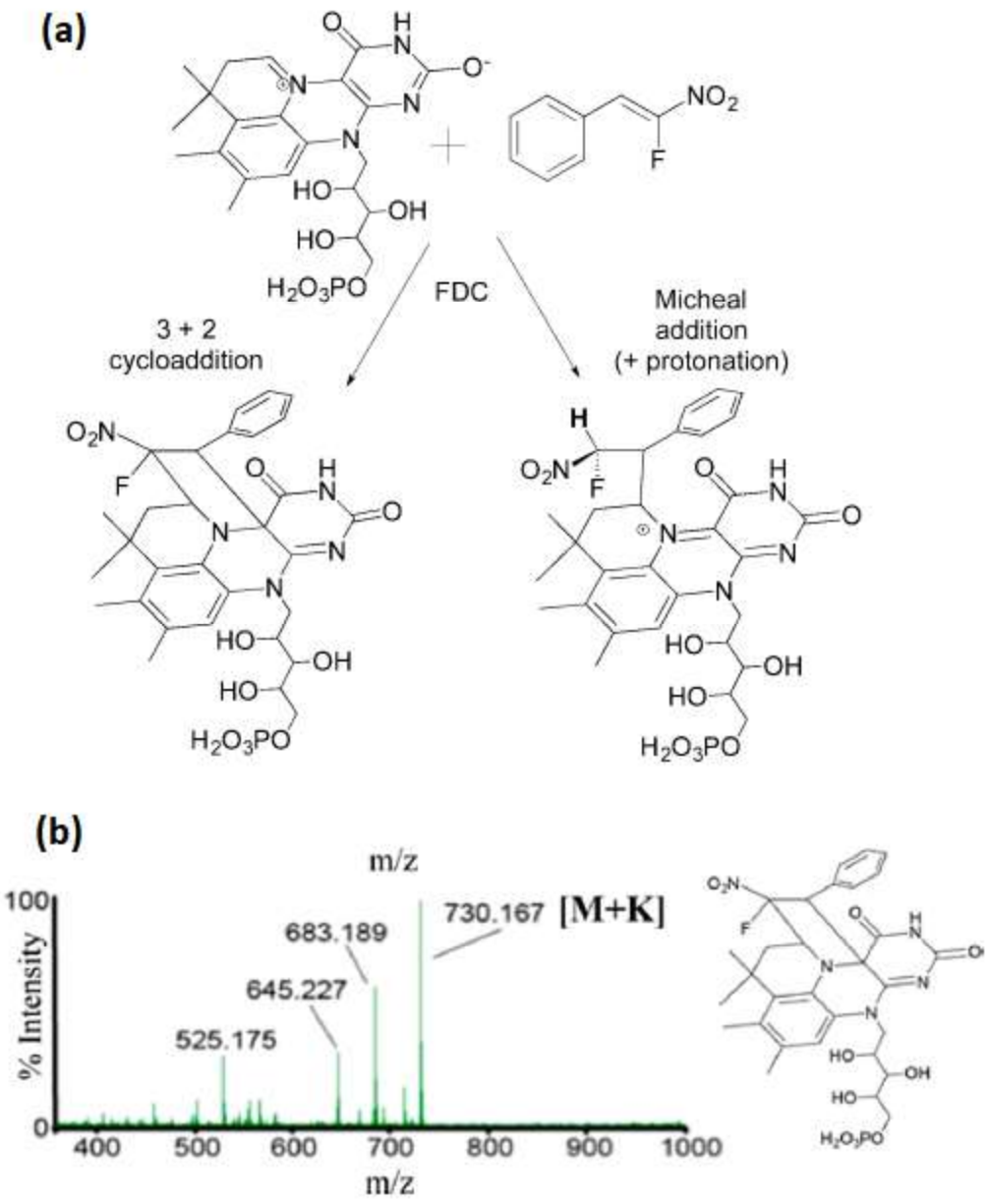

Figure 2.7: (a) Scheme showing the possible reaction products of the substrate mimic, 2-fluoro-2-nitrovinylbenzene, with prFMN by either Michael addition or 1,3-dipolar cyclo-addition pathways. (b) 2-fluoro-2-nitrovinylbenzene -inactivated holoFDC; the peak at 730.167 corresponds to the K+ complex of the cyclo-addition adduct.

2.5 References

1. Jordan F, Patel H. Catalysis in Enzymatic Decarboxylations: Comparison of Selected Cofactor-Dependent and Cofactor-Independent Examples. ACS Catal. 2013 Jul 5;3(7):1601–17.

2. Kourist R, Guterl J-K, Miyamoto K, Sieber V. Enzymatic Decarboxylation—An Emerging Reaction for Chemicals Production from Renewable Resources. ChemCatChem. 2014 Mar 1;6(3):689–701.

3. Cleland WW. Mechanisms of Enzymatic Oxidative Decarboxylation. Acc Chem Res. 1999 Oct 1;32(10):862–8.

4. Belcher J, McLean KJ, Matthews S, Woodward LS, Fisher K, Rigby SEJ, et al. Structure and biochemical properties of the alkene producing cytochrome P450 OleTJE (CYP152L1) from the Jeotgalicoccus sp. 8456 bacterium. J Biol Chem. 2014 Mar 7;289(10):6535–50.

5. Cavin JF, Barthelmebs L, Diviès C. Molecular characterization of an inducible p-coumaric acid decarboxylase from Lactobacillus plantarum: gene cloning, transcriptional analysis, overexpression in Escherichia coli, purification, and characterization. Appl Environ Microbiol. 1997 May;63(5):1939–44.

6. Rodríguez H, Landete JM, Curiel JA, de las Rivas B, Mancheño JM, Muñoz R. Characterization of the p-Coumaric Acid Decarboxylase from Lactobacillus plantarum CECT 748T. J Agric Food Chem. 2008 May 1;56(9):3068–72.

7. Barthelmebs L, Lecomte B, Divies C, Cavin JF. Inducible metabolism of phenolic acids in Pediococcus pentosaceus is encoded by an autoregulated operon which involves a new class of negative transcriptional regulator. J Bacteriol. 2000 Dec;182(23):6724–31.

8. Godoy L, Martínez C, Carrasco N, Ganga MA. Purification and characterization of a p-coumarate decarboxylase and a vinylphenol reductase from Brettanomyces bruxellensis. Int J Food Microbiol. 2008 Sep 30;127(1–2):6–11.

9. Wuensch C, Pavkov-Keller T, Steinkellner G, Gross J, Fuchs M, Hromic A, et al. Regioselective Enzymatic β-Carboxylation of para-Hydroxy- styrene Derivatives Catalyzed by Phenolic Acid Decarboxylases. Adv Synth Catal. 2015 May 26;357(8):1909–18.

10. Clausen M, Lamb CJ, Megnet R, Doerner PW. PAD1 encodes phenylacrylic acid decarboxylase which confers resistance to cinnamic acid in Saccharomyces cerevisiae. Gene. 1994 May;142(1):107–12.

11. Mukai N, Masaki K, Fujii T, Kawamukai M, Iefuji H. . J Biosci Bioeng. 2010 Jun;109(6):564–9.

12. McKenna R, Nielsen DR. Styrene biosynthesis from glucose by engineered E. coli. Metab Eng. 2011 Sep;13(5):544–54.

13. White MD, Payne KAP, Fisher K, Marshall SA, Parker D, Rattray NJW, et al. UbiX is a flavin prenyltransferase required for bacterial ubiquinone biosynthesis. Nature. 2015 Jun 25;522(7557):502–6.

14. Lin F, Ferguson KL, Boyer DR, Lin XN, Marsh ENG. Isofunctional enzymes PAD1 and UbiX catalyze formation of a novel cofactor required by ferulic acid decarboxylase and 4-hydroxy-3-polyprenylbenzoic acid decarboxylase. ACS Chem Biol. 2015 Apr 17;10(4):1137–44.

15. Payne KAP, White MD, Fisher K, Khara B, Bailey SS, Parker D, et al. New cofactor supports α,β-unsaturated acid decarboxylation via 1,3-dipolar cycloaddition. Nature. 2015 Jun 25;522(7557):497–501.

16. Kürti L, Czakó B. Strategic applications of named reactions in organic synthesis: background and detailed mechanisms. Amsterdam ; Boston: Elsevier Academic Press; 2005. 758 p.

17. Waugh MW, Marsh ENG. Solvent Isotope Effects on Alkane Formation by Cyanobacterial Aldehyde Deformylating Oxygenase and Their Mechanistic Implications. Biochemistry (Mosc). 2014 Sep 2;53(34):5537–43.

18. Gadda G, Fitzpatrick PF. Solvent isotope and viscosity effects on the steady-state kinetics of the flavoprotein nitroalkane oxidase. FEBS Lett. 2013 Sep 2;587(17):2785–9.

19. Neims AH, De Luca DC, Hellerman L. Studies on Crystalline D-Amino Acid Oxidase. III. Substrate Specificity and σ-ρ Relationship*. Biochemistry (Mosc). 1966 Jan 1;5(1):203–13.

20. Yorita K, Misaki H, Palfey BA, Massey V. On the interpretation of quantitative structure–function activity relationship data for lactate oxidase. Proc Natl Acad Sci. 2000 Mar 14;97(6):2480–5.

21. Trahanovsky WS, Cramer J, Brixius DW. Oxidation of organic compounds with cerium(IV). XVIII. Oxidative decarboxylation of substituted phenylacetic acids. J Am Chem Soc. 1974 Feb 1;96(4):1077–81.

22. Miyamoto K, Ohta H. Purification and properties of a novel arylmalonate decarboxylase from Alcaligenes bronchisepticus KU 1201. Eur J Biochem. 1992 Dec 1;210(2):475–81.

23. Cleland WW. The Use of Isotope Effects to Determine Enzyme Mechanisms. J Biol Chem. 2003 Dec 26;278(52):51975–84.

24. Cleland WW. The use of isotope effects to determine enzyme mechanisms. Arch Biochem Biophys. 2005 Jan 1;433(1):2–12.

25. Kurtz KA, Fitzpatrick PF. pH and Secondary Kinetic Isotope Effects on the Reaction of D-Amino Acid Oxidase with Nitroalkane Anions: Evidence for Direct Attack on the Flavin by Carbanions. J Am Chem Soc. 1997 Feb;119(5):1155–6.

26. Northrop DB. Steady-state analysis of kinetic isotope effects in enzymic reactions. Biochemistry (Mosc). 1975 Jun 17;14(12):2644–51.

27. Pérez P, Domingo LR, José Aurell M, Contreras R. Quantitative characterization of the global electrophilicity pattern of some reagents involved in 1,3-dipolar cycloaddition reactions. Tetrahedron. 2003 Apr;59(17):3117–25.

28. Ferguson KL, Eschweiler JD, Ruotolo BT, Marsh ENG. Evidence for a 1,3-Dipolar Cycloaddition Mechanism in the Decarboxylation of Phenylacrylic Acids Catalyzed by Ferulic Acid Decarboxylase. J Am Chem Soc. 2017 Aug 16;139(32):10972–5.

Chapter 3: Kinetic Characterization of Prenyl-flavin Synthase from *Saccharomyces cerevisiae*

3.1 Introduction

Ferulic acid decarboxylase (FDC) is found in various strains of yeast where it catalyzes the decarboxylation of various substituted *trans*-phenylacrylic acid derivatives, including ferulic acid (4-hydroxy-3-methoxy-phenylacryilic acid) a breakdown product of lignin, to the corresponding styrene derivatives (1–7). The enzyme serves to detoxify these carboxylic acids that are inhibitory to the growth of the yeast (8–10). FDC has recently been shown to require a novel, modified flavin mononucleotide (FMN) derivative – prenylated-FMN – in which an isopentyl moiety is appended between the C6 and N5 positions of the isoalloxazine flavin nucleus to form an additional 6-membered ring (11,12). This modification converts the flavin from a redox cofactor to one capable of stabilizing the negatively charged intermediates formed during decarboxylation.

PrFMN is synthesized by a specialized prenyl transferase that uses dimethylallyl pyrophosphate to install the additional 6-membered ring on the reduced form of FMN (13,14). This enzyme has been known as PAD1, an abbreviation for phenylacrylic acid decarboxylase, as a result of early genetic studies that linked this gene to decarboxylase activity. In the manuscript currently submitted for Biochemistry in review, the enzyme has been proposed to be referred as prenyl-FMN synthase (PFS) to reflect its enzymatic activity.

Homologs of FDC and PFS are found in many microorganisms, indicating that prFMN-dependent decarboxylases are likely widespread in nature (15–18). In many bacteria, they are represented by UbiD and UbiX proteins that form part of the ubiquinone biosynthesis pathway (19–25). UbiX has been characterized as a PFS and has been the subject of detailed crystallographic studies. UbiD, a homolog of FDC, is believed to catalyze the decarboxylation of ubiquinone biosynthetic intermediate 4-hydroxy-3-octaprenyl-benzoate although this activity has yet to be experimentally demonstrated. Recently, a second prFMN-dependent enzyme has been characterized from *Enterobacter cloacae* and *Klebsiella pneumoniae* that catalyze the reversible decarboxylation of 3,4-dihydroxybenzoic acid (3,4-DHBA) (17,26,27).

A mechanism for prFMN synthesis was proposed based on crystallographic studies of the PFS represented by UbiX from *Pseudomonas aeruginosa* (13). The enzyme catalyzes the reaction of reduced FMN with dimethylallylphosphate (DMAP): the first step is proposed to be nucleophilic attack of N5 on DMAP to form N5-alkylated FMN with the loss of the phosphate group. Formation of the C6 bond occurs next, presumably by a mechanism involving protonation of the dimethylallyl double bond. Finally, oxidation of the flavin nucleus is required to generate the active prFMN cofactor (Figure 3.1a). It is unclear whether, *in vivo*, this step occurs spontaneously or with the assistance of the cognate prFMN-dependent decarboxylase.

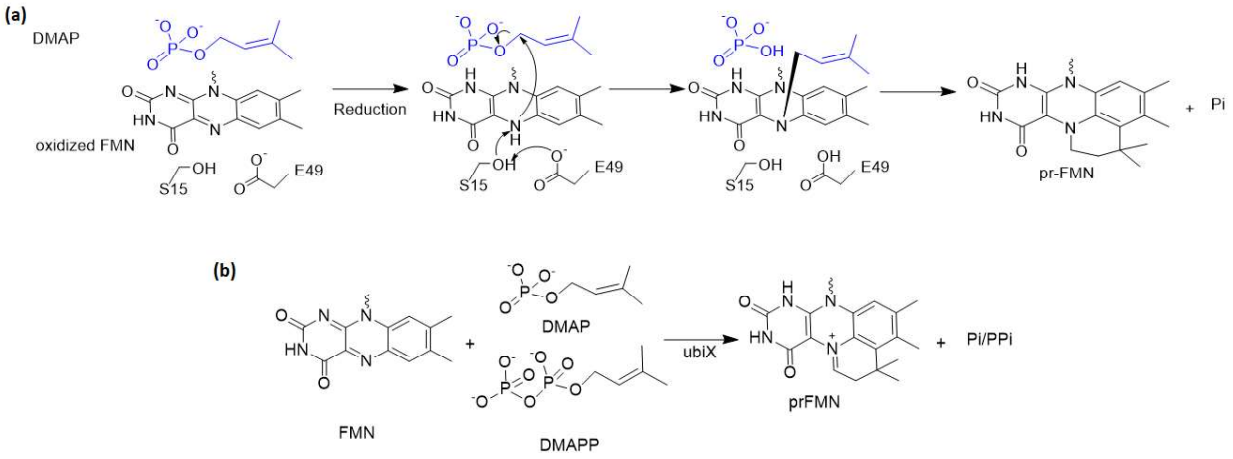

Figure 3.1: (a) Proposed mechanism for the formation of reduced prFMN from reduced FMN and DMAP catalyzed by prenyl-flavin synthase. (b) Overall reaction for the formation of reduced prFMN from reduced FMN and DMAP/DMAPP catalyzed by ubiX/sc-PFS.

This chapter describes studies on the eukaryotic PFS from *Saccharomyces cerevisiae*, scPFS (formerly referred to as PAD1). An assay which couples the production of prFMN to the activation of FDC has been developed and utilized to determine steady state kinetic parameters for enzyme. Moreover, whereas the previously studied bacterial enzymes use DMAP as a substrate, which is not commonly used by prenyl transferase enzymes (28), this chapter finds that scPFS prefers dimethylallylpyrophosphate (DMAPP) as a substrate, which is a common intermediate in isoprenoid biosynthesis.

3.2 Materials and methods

3.2.1 Materials

FMN, and dithiothreitol were purchased from MP biomedicals; dimethylallyl pyrophosphate was purchased from Isoprenoids LC, Tampa FL; potassium ferricyanide was purchased from Acros Organics. All other chemicals were purchased from Sigma-Aldrich.

Malachite green phosphate assay kit was purchased from Cayman Chemical. PiPer™ Pyrophosphate Assay Kit and EnzChek® phosphate assay kit were purchased from ThermoFisher Scientific.

Holo-FDC, apo-FDC and scPFS were recombinantly expressed in *Escherichia coli* and purified as described previously (14).

3.2.2 Malachite Green Phosphate Assay

An end-point assay utilizing malachite green to measure orthophosphate concentration was conduct in 96 well plates. 50 µL reaction mixtures containing 20 µM reduced-FMN, 200 µM DMAP, and 1 µM scPFS were prepared in 100 mM Tris-HCl buffer pH 8. Reduced-FMN stock solutions were prepared by adding excess amount of sodium dithionite. The reactions were quenched every 20 mins over a period of 2 h using 5 µL of commercially provided MG acidic solution. Then, 15 µl of commercially provided MG Blue solution (malachite green stain) were added to each well and mixed by gently tapping. After incubation for 20 mins at room temperature (20^{o}C), the absorbance of each was recorded using a microplate reader set to 620 nm.

3.2.3 EnzChek phosphate Assay

Assay of 730 μL reaction mixture was performed in 1 mL anaerobic cuvette. The reaction mixture contained 100 mM Tris-HCl buffer pH 8, 100 μM FMN and 1 mM DMAP. The mixture was reduced by addition of sodium dithionite in slight excess. Then, 270 μL of EnzChek pyrophosphate assay reagent premix was added to the cuvette to 1 mL. The spectrum from 300 to 500 nm was recorded at various periods of time (20 mins to overnight).

270 μL premix of EnzChek pyrophosphate assay reagent was prepared by 10 mins incubation at 22°C of the mixture containing 50 μL 20X reaction buffer, 200 μL MESG substrate solution, 10 μL purine nucleoside phosphorylase, and 10 μL inorganic pyrophosphatase as described in commercial kit protocol.

3.2.4 Assay for prFMN formation by scPFS

100 mM HEPES buffer supplemented with 100 mM $MgCl_2$ pH 8.5 were prepared and purged with nitrogen gas overnight, and then equilibrated in a Coy anaerobic chamber. Flavin mononucleotide, dimethylallyl pyrophosphate, scPFS, reducing reagents and oxidizing reagents were transferred into anaerobic chamber. The volume of scPFS assay is 0.5 mL. The assay contained substrates at various concentrations from 400 to 600 μM scPFS, 0.75 to 50 μM FMN and 1 to 500 μM DMAPP. The assay also contained 60 μM NADH as additional reducing agent and 4 μM apo-FDC as secondary enzyme for scPFS-FDC dual enzyme assay. Then, sodium dithionite was added to the premix to 1 mM concentration to start the reaction at room temperature (20°C). After time periods varying from 30 seconds to 40 minutes, 5 mM potassium ferricyanide was added to quench the reaction.

3.2.5 GC-MS assay

Routine assays of FDC activity were carried out in diluted quenched scPFS reaction mixture. 125 μL of scPFS reaction mixture, prepared as described in the assay for prFMN formation, was diluted to 500 μL with 1 mM $MgCl_2$ 100 mM HEPES buffer pH 8.5. The mixture was equilibrated for 45 min. Then, FDC assays were allowed to proceed at room temperature using a saturated concentration of cinnamic acid, 2.5 mM, as substrate. After 4 min, the mixtures were quenched with HCl, final concentration 0.27 M and extracted with 400 μL ethyl acetate with 94.7 μM undecane as internal standard. Samples were vortexed and centrifuged in a tabletop microcentrifuge at 10,000 rpm for 10 min to separate organic and aqueous phases. The amount of styrene produced was determined by GC-MS as described previously (14).

3.2.6 HPLC assays

Assays containing 100 μM DMAPP, 2 μM scPFS and 1.5 μM FMN were reacted under the same conditions as optimized GC-MS assay described above with 9 μM of riboflavin as internal standard. After quenching, reaction mixtures were centrifuged in a tabletop microcentrifuge at 10,000 rpm for 10 mins. Then, supernatant was collected for HPLC analysis. Sample analysis was performed using a Shimadzu HPLC system with two LC-20AT pumps, and anSPD-M20A UV-visible diode array detector with monitoring at 450 nm. The stationary phase was a EC 250/4.6 Nucleodur C18 reverse phase column. The column was equilibrated with 5 mM ammonium acetate (A) and analytes eluted with a gradient of increasing acetonitrile (B) under 0.5 mL/min flowrate. The solvent composition was held at 100% (A) for 4 min, and then increased linearly to 15% (B) over 16 min, followed by isocratic elution at 15% (B) for 25 min, then returned to 100% (A) over 5 min and held for 5 min for column equilibration. Under these conditions FMN eluted at 24.46

min and riboflavin eluted at 35.72 min. FMN concentrations were calculated from peak integration and normalized with respect to the riboflavin internal standard.

3.2.7 PiPer™ Pyrophosphate Assay

Assays were performed in 96-well microplates using 50 µL mixture containing 100 mM Tris-HCl pH 8.5 and each component of scPFS reaction: 5 µM FMN, 60 µM NADH, 1 mM sodium dithionite, 5 mM DTT, 500 µM DMAPP and 5mM potassium ferricyanide. Then, 50 µL of the Amplex® Red reagent/inorganic pyrophosphatase/maltose phosphorylase/maltose/glucose oxidase/HRP working solution (WS) prepared as described in commercial protocol was added to the mixture. The absorbance of each well was recorded using a microplate reader set to 565 nm every 5 mins for the total period of 1 h at 37 °C.

3.3 Results and discussion

Initial efforts to develop a quantitative assay for scPFS activity attempted to exploit the fact that phosphate or pyrophosphate (Figure 3.1b) is produced during the reaction. Given that a variety of methods have been developed for phosphate and pyrophosphate detection, this appeared to be a promising strategy to assay PFS activity. Cayman's Malachite Green Phosphate Assay Kit and EnzChek® phosphate Assay Kit have been employed to measure orthophosphate. However, I encountered problems with these colorimetric assays. The malachite green assay yielded a false positive result against DMAP and dithiothreitol (DTT) required in the assay. The EnzChek® phosphate Assay utilizes the secondary enzyme, purine nucleoside phosphorylase (PNP), to convert 2-amino-6-mercapto-7-methylpurine ribonucleoside (MESG) to ribose 1-phosphate and 2-amino-6-merc apto-7-methylpurine in the presence of inorganic phosphate resulting in a spectral

shift from 330 nm to 360 nm. Nevertheless, I could not to obtain a clear signal attributable to the presence of phosphate. Instead, I observed the change of FMN from reduced form to the intermediate spectrum similar to that described previously (14), and finally to the oxidized form. The transient spectrum of FMN interferes with monitored wavelength. Using the assay for end-point measurement yielded no significant increase in absorbance at 360 nm. This could indicate that either there is no reaction on time scale of the preliminary experiment, or the change in spectrum due to phosphate assay is not large enough to be distinguished from FMN. Additionally, PiPer™ Pyrophosphate Assay has been employed to measure pyrophosphate byproduct. The assay utilizes the series of enzymes to amplify phosphate/pyrophosphate signal. Unlike malachite green assay, PiPer™ Pyrophosphate Assay did not react with either DMAPP. However, the assay is susceptible to reducing and oxidizing agents and yielded false positive signals with DTT or ferricyanide at the working concentration of the assay. These experiments are discussed in more detail below.

3.3.1 Malachite green phosphate assay

My initial efforts to develop a quantitative assay for scPFS activity attempted to exploit the fact that phosphate is produced during the reaction. Given that a variety of methods have been developed for phosphate and pyrophosphate detection, this appeared to be a promising strategy to assay PFS activity. This chapter first utilized malachite green colorimetric assay to detect phosphate. The malachite green assay changes color from yellow to green upon complex formation between malachite green molybdate and free orthophosphate under acidic conditions (29). The formation of the green molybdophosphoric acid complex measured at 620-640 nm can be directly correlated to the free phosphate concentration in the solution.

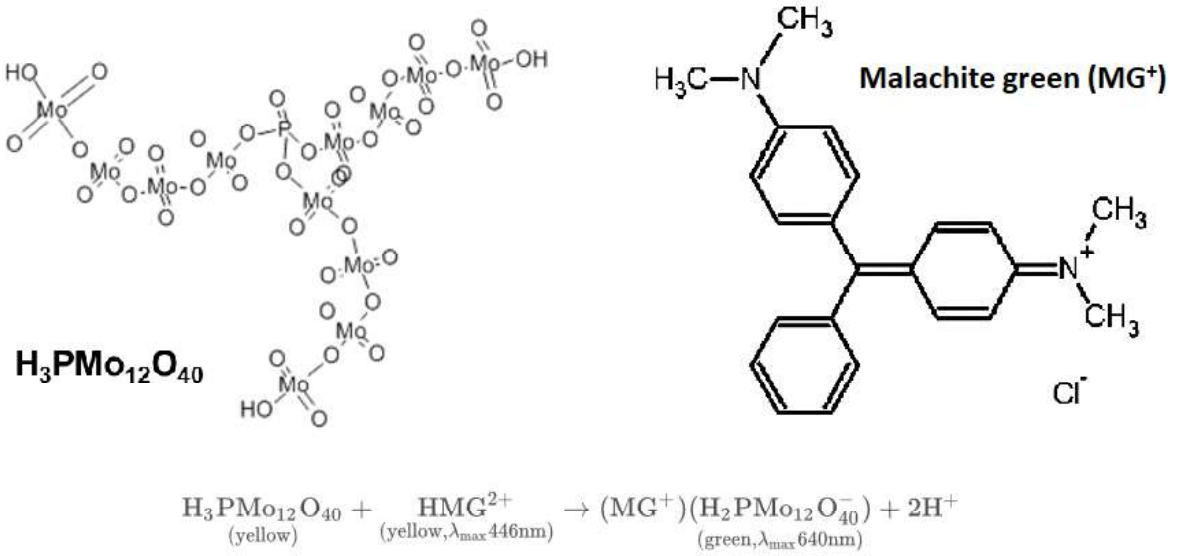

$$\underset{\text{(yellow)}}{H_3PMo_{12}O_{40}} + \underset{(\text{yellow},\lambda_{max}446\text{nm})}{HMG^{2+}} \rightarrow \underset{(\text{green},\lambda_{max}640\text{nm})}{(MG^+)(H_2PMo_{12}O_{40}^-)} + 2H^+$$

Figure 3.2: Chemical reaction describing color change from yellow to green in the malachite green assay

The malachite green end-point assays were conduct in 96 well plates. The reduced FMN is prepared as stock using excess amount of sodium dithionite. The final concentration of reduced FMN in the reaction was 20 μM which was nearly at the limit of the assay according to the provided calibration curve in the commercial protocol. The final concentration of DMAP and scPFS were 200 μM and 1 μM respectively. The reaction mixtures were then quenched at every 20 mins for the period of 120 mins by addition of commercially provided MG acid reagent. The result of this experiment is shown in table 3.1. The absorbance observed from this experiment was much higher than the expected value from the calibration curve and precipitation was observed in the well. Also, it was strange that the absorbance decreased as the reaction was monitored for a longer time. There may be two explanations to this phenomena: first the absorbance is at the very limit of the instrument and thus the number obtained here does not reflect the actual absorbance. Second is that the sample that was quenched early had more time to react with the dye and thus resulted in higher absorbance.

Next, I inspected the base line shift using water and buffer as negative control. The reaction between malachite green assay reagent and water resulted in $\Delta\lambda_{620}$ =0.216 absorbance unit change whereas the reaction with pH 8 100 mM Tris-HCl buffer resulted in $\Delta\lambda_{620}$ =0.275 absorbance unit. Neither of these negative controls had any precipitation. After that, I suspected that the source of precipitation came from side-reaction between FMN and the acid reagent provided from the kit. This turned out to be the case as I saw the precipitation from the reaction with just FMN in Tris-HCl buffer at the quenching step using the provided acid reagent and the final absorbance measurement was 1.45. Thus, I tried using 3 M HCl instead of the provided acid reagent. The pH of the sample was confirmed to be acidic with pH paper, the solution was slightly green, cleared of precipitate and the 620 nm absorbance was dropped to 0.532. However, when I attempted to run the full reaction using 3 M HCl, the precipitate appeared again after adding malachite green dye. Therefore, I decide to test the remaining components of the reaction by observing color and precipitation. It turned out that the malachite green reagent formed a precipitate with dithionite and DMAP. DTT substituted in place of dithionite as a reducing reagent; however, the reduction efficiency of FMN is low and the reduced FMN obtained from DTT was highly susceptible to re-oxidation. In addition, the major issue is the precipitation with DMAP since it is one of the required substrates.

Given the difficulties encountered with malachite green phosphate assay, I decided to look for another high-throughput assay as well as develop assays to study enzymatic activity of scPFS.

Table 3.1: Result from quenching experiment using malachite green assay kit

time to quenching (mins)	A620
20	1.563
40	1.463
60	1.406
80	1.289
100	1.278
120	0.864
Water	0.216
Buffer	0.275

3.3.2 EnzChek phosphate Assay

The next phosphate assay kit employed in this study is Enzcheck phosphate assay kit. This assay utilizes secondary enzyme purine nucleoside phosphorylase which convert 2-amino-6-mercapto-7-methylpurine riboside (MESG) to ribose 1-phosphate and 2-amino-6-mercapto-7-methyl-purine in the presence of free inorganic phosphate (Figure 3.3) (30). The enzymatic conversion of MESG results in a spectrophotometric shift in maximum absorbance from 330 nm for the substrate to 360 nm for the product. The concentration limitation of this assay is at roughly 100 μM phosphate. Thus, the phosphate assays were conducted in 730 μL reaction mixture containing 100 mM Tris-HCl pH 8, 100 μM FMN and 1 mM DMAP with excess amount of sodium dithionite in 1 mL anaerobic cuvette. 270 μL of Enzcheck reagent mastermix, prepared as described in the Methods section, was added to make final volume of 1 mL. The mixture of sodium dithionite and DMAP was used as negative control. By continuously measuring the spectrum over 20 minutes, there was no significant change in absorbance from these DMAP negative controls (Figure 3.4). However, there was constant baseline shift of around 0.4-0.5 absorbance units at 360 nm with reference to pH 8 Tris buffer. In contrast, there is slight signal reduction over time from dithionite negative control (figure 3.5). The result from the control experiment indicated that dithionite does absorb

for a certain amount at this wavelength and could be the source of baseline shift observed earlier. As dithionite was consumed over time from any oxygen that might have leaked into the system, the decreasing absorbance over time was observed. In order to bypass this problem, I came up with two solutions: 1) using a no scPFS reaction as reference to correct for absorbance change 2) measuring the end-point spectrum after letting the reaction completely re-oxidized. I decided to employ both approaches by having two parallel reactions and measuring the end-point spectrum. Figure 3.6 shows the spectrum from the reaction with scPFS and without scPFS at different time points: beginning (time 0), overnight (roughly 20 h which represented the complete conversion), after opening the cap of the cuvette (roughly 10 mins after oxygen was reintroduced to the system), and the final re-oxidized stage (after exposure to O_2 for 2 h). The spectrum after complete re-oxidation stage showed no significant increase in absorbance at 360 nM. The expected result would be the change in 330 nm due to the secondary reaction and the disappearance of 450 nm due to the consumption of FMN. However, no spectral changes were apparent. Replication of the experiment yielded similar results. I note that the re-oxidation rate between reference and reaction cuvette seemed to be different and thus comparing no scPFS and scPFS reaction at specific time point could lead to the wrong conclusion. Thus, the reaction must be completely re-oxidized before valid comparisons can be made.

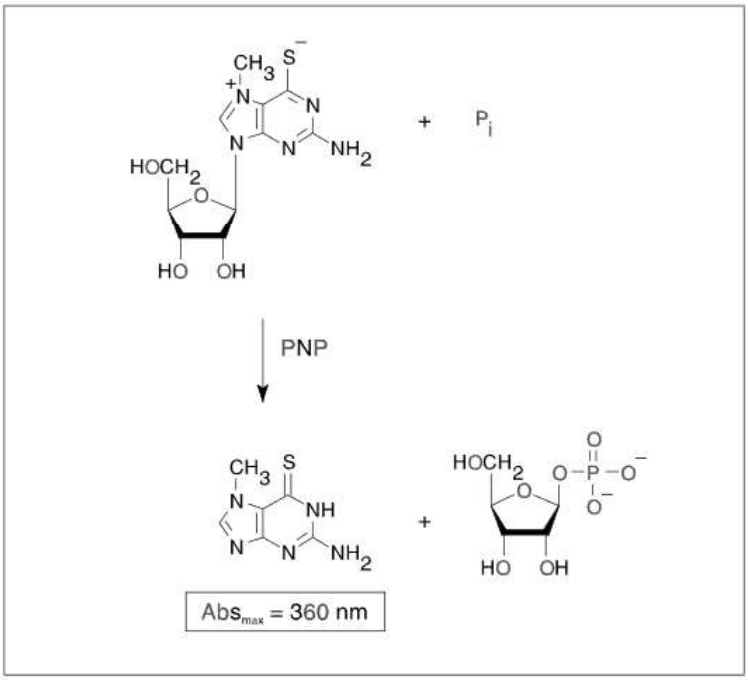

Figure 3.3: Principle of the Enzcheck phosphate assay. In presence of free phosphate, 2-amino-6-mercapto-7-methyl-purine riboside (MESG) is converted to ribose 1-phosphate and 2-amino-6-mercapto-7-methylpurine by purine nucleoside phosphorylase (PNP). The accompanying change in absorption at 360 nm allows quantitation of inorganic phosphate consumed in the reaction. Figure taken from the Enzcheck phosphate assay manual.

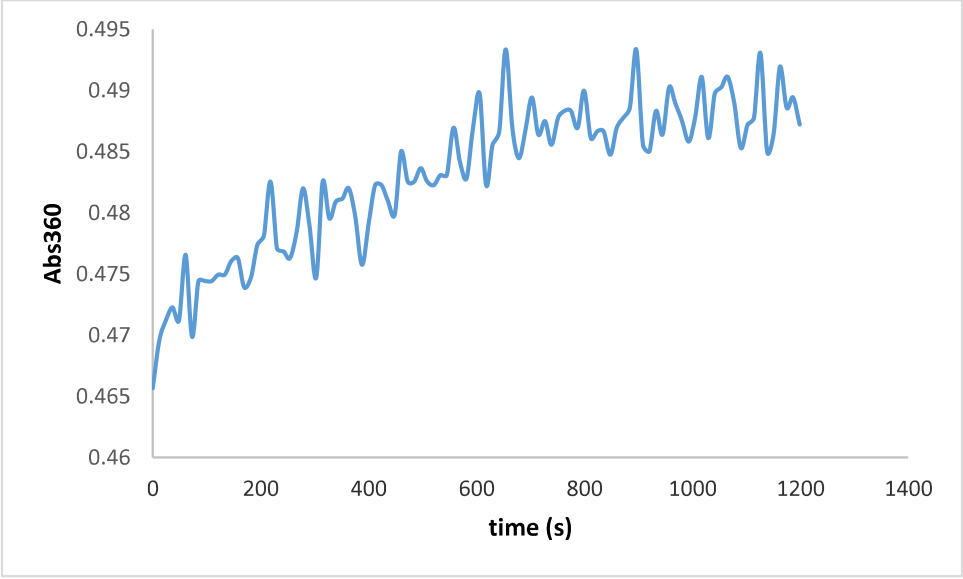

Figure 3.4: Negative control reaction between DMAP and Enzchek phosphate reagent. Absorbance at 360 nm was monitor over a period of 20 mins. The result showed no reaction between DMAP and Enzchek phosphate reagent.

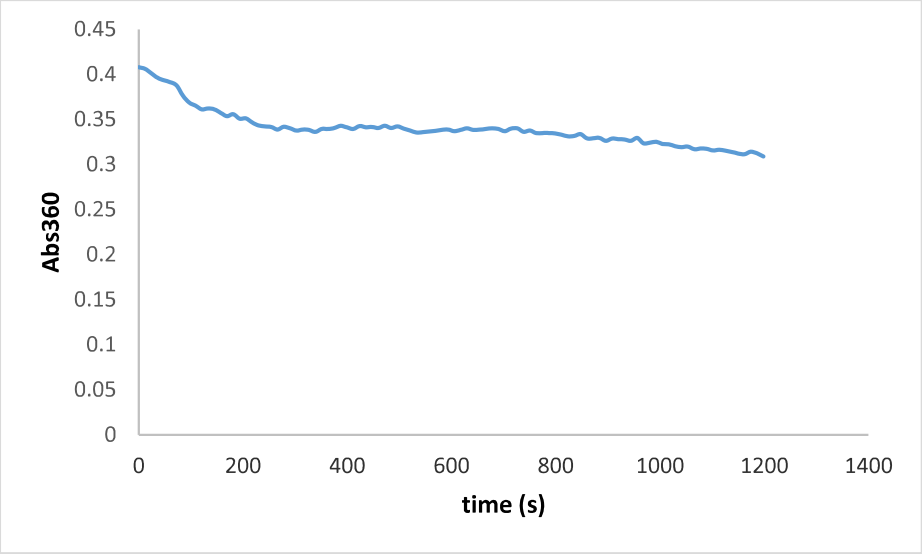

Figure 3.5: Negative control reaction between sodium dithionite and Enzchek phosphate reagent. Absorbance at 360 nm was monitor over a period of 20 mins. The result showed decrease in absorbance by 0.1 arbitrary unit.

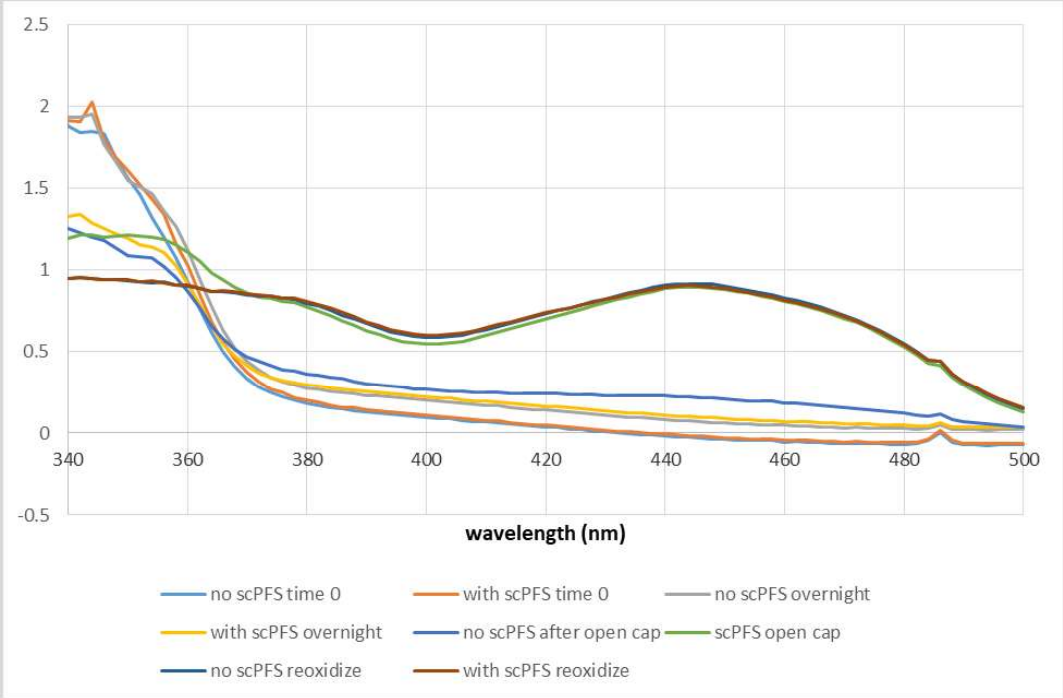

Figure 3.6: Spectra comparing reaction with scPFS and without scPFS and different major events: starting time, overnight reaction, reintroduction of oxygen and completely reoxidation of FMN. Both reactions were prepared from the same batch prior to addition of enzyme. In the "no scPFS reaction" case, the same volume of buffer was added in place of the enzyme. Both reactions contain EnzCheck secondary enzyme set to monitor the presence of phosphate. pH 8 Tris buffer was used as reference spectrum.

Given the difficulties encountered with measuring phosphate production, which seemed to be associated with the very slow turnover rate of scPFS, I next investigated the possibility of coupling the production of prFMN to the activation of FDC. This would allow the formation of one molecule of prFMN to be coupled to the production of many molecules of styrene, thereby affording a considerable amplification of the signal.

3.3.3 Development of a scPFS-FDC coupled assay

In preliminary experiments, 500 μL of the reaction mixture was prepared in 1.5 mL microcentrifuge tube in the Coy anaerobic chamber using 800 nM scPFS. To ensure complete uptake of the generated prFMN cofactor, 17.4 μM apo-FDC was added to the reaction mixture. Other substrates were added in excess amounts: 500 μM DMAP, 50 μM oxidized FMN, and 60 μM NADH. The reaction was initiated upon addition of 1 mM sodium dithionite converting oxidized FMN to its reduced counterpart. After 1 hour of reaction, the mixture was quenched by vigorously shaking in air outside the Coy anaerobic chamber. After equilibrating for 45 mins, 2.5 mM *trans*-cinnamic acid (tCA) was added to the sample to start catalytic activity of FDC. At this concentration of tCA, FDC catalyzes decarboxylation at a velocity that approaches V_{max}. After 4 mins of reaction, assays were quenched with HCl, final concentration 0.27 M and extracted with 400 μL ethyl acetate with 94.7 μM undecane as GC internal standard. Samples were vortexed and centrifuged in a tabletop microcentrifuge at 10,000 rpm for 10 min to separate organic and aqueous phases. The amount of styrene produced is determined by GC-MS.

3.3.3.1 pH optimization

One of the most important aspects when dealing with multiple enzymes in the same reaction mixture is the working pH of the buffer. UbiX activity is reported to be optimized at pH9 (13), whereas the optimal pH for FDC is 6.5 (31). However, the catalytic activity of FDC significantly decreases at pH9 and above. In order to determine suitable pH for analysis of prenylation, 100 mM HEPES buffer pH 7, 8 and 8.5 were selected and tested. In addition, Mn^{2+} was found in the protein structure of FDC and serve to stabilize the protein (15). Therefore, 1 mM of $MgCl_2$, which is similar divalent metal ion, was added to the buffer to help stabilize protein complex. The addition of $MgCl_2$ slightly increased activity of sc-PFS. However, the increase in activity was insignificant, relative to the standard deviation of the data as discussed in more detail in the later section. The results showed that scPFS catalytic activity increased in high pH buffer (figure 3.7). The activity of scPFS at pH 8.5 is almost double the catalytic activity at pH 7. Also, the low activity of FDC at this pH allowed amplification of the signal in GC-MS without oversaturation or a need to overly dilute the sample. Therefore, pH 8.5 was chosen as optimal for the coupling assay.

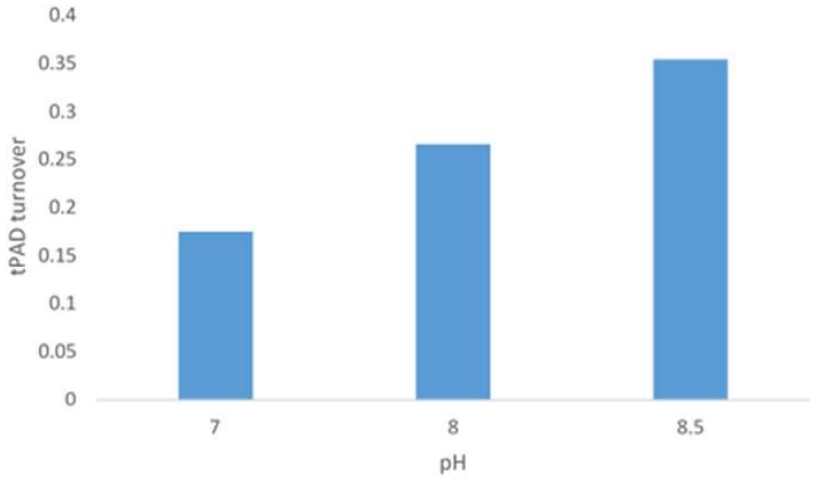

Figure 3.7: Catalytic activity of scPFS at different pH. The assay was conducted in 100 mM HEPES buffer supplemented with 1 mM $MgCl_2$. The reaction mixtures also contained 800 nM scPFS, 500 µM DMAP, 50 µM oxidized FMN, and 60 µM NADH.

3.3.3.2 Investigation of the impact of each substrate with preliminary set up

The impact of each assay component on the catalytic activity of scPFS was further investigated. The experiment was conducted by reducing amount of each substrate and enzyme by half. In addition, dimethylallylpyrophosphate (DMAPP) was tested in place of DMAP. DMAPP is the universal isoprene precursor and is much more common in organisms than DMAP. However, previous studies showed that ubiX could not utilize DMAPP.

The activity of scPFS did not change when the substrate concentrations were lower (table 3.2). This indicates that the catalytic activity of scPFS under these conditions was close to maximal. Interestingly, styrene production, which represents the catalytic activity of the enzyme, was greatly enhanced when DMAPP was used in place of DMAP. The data showed that both DMAPP and DMAP could be used as substrates for scPFS with DMAPP as the preferred substrate.

After optimizing pH and substrate concentrations, an experiment was designed to measure V_{max} and K_m. However, the data were inconsistent and not reproducible. Thus, further investigation was required before applying the assay to measure kinetic parameters.

Table 3.2: Table verified that prenylation by scPFS under preliminary condition was at maximal velocity (V_{max})

Tube#	scPFS (nM)	Apo-FDC (μM)	FMN (μM)	DMAP/DMAPP (μM)	Styrene (μM)
1	800	17.4	50	500	143
2	400	17.4	50	500	65
3	800	17.4	25	500	157
4	800	17.4	50	250	104
5	800	8.7	50	500	122
6	800	17.4	50	250 (DMAPP)	532

3.3.3.3 Investigation of the cause of inconsistency

In order to troubleshoot the inconsistency in activity measurements, I hypothesized two potential causes. First is the delay time due to re-oxidation by oxygen. The other cause of inconsistency could be due to heterogeneity in the assay reagents. In order to investigate the first hypothesis, I switched oxidizing agent from oxygen to potassium ferricyanide. Adding 5 mM ferricyanide to the reaction mixture instantly oxidized FMN, and thus, provided accurate time for the quenching of the prenylation reaction. However, the inconsistency still persisted. Another cause may be the low stability of the enzyme which I observed during purification. I decided to add dithiothreitol (DTT) to reduce any adventitiously formed disulfide bonds on the surface. After pre-incubating scPFS with 5 mM DTT for 10 minutes, I obtained the replicable data. Further investigation on the significance of DTT toward had been conducted by reducing the concentration of DTT in the assay. When the concentration of DTT dropped below 100 μM, the catalytic activity of scPFS was zero and there was no styrene detected in the assay. This result suggested that excess DTT is required to maintain activity of scPFS. Possibly the formation of disulfide bonds prevent substrates binding.

To summarize the protocol for optimal assay conditions, 500 μL of the reaction mixture is prepared in 1 mM $MgCl_2$ 100 mM HEPES buffer pH 8.5 in a Coy anaerobic chamber at 20°C. Initially, 400 nM scPFS is pre-incubated with 5 mM DTT for 10 min to reduce any disulfide bonds on the surface of scPFS. Then, 50 μM oxidized FMN, 4 μM apo-FDC, and 60 μM NADH are added to the mixture. The supplementary NADH is in excess in comparison to enzyme concentration and serves as additional reducing agent. Finally, the reaction is initialized upon addition of 500 μM of DMAP and 1 mM sodium dithionite. After certain amount of time varying from 30 seconds to 40 min, 5 mM potassium ferricyanide is added to the mixture to oxidize FMN and stop scPFS catalytic

activity. After equilibrating the oxidized mixture for 45 min to ensure complete uptake of prFMN by apo-FDC, 2.5 mM trans-cinnamic acid (tCA) is added to 500 μL of mixture to initiate enzymatic decarboxylation. After 4 min, 500 μL assay mixtures are quenched with HCl, final concentration 0.27 M and extracted with 400 μL ethyl acetate with 94.7 μM undecane as GC internal standard. Samples are vortexed and centrifuged in a tabletop microcentrifuge at 10,000 rpm for 10 min to separate organic and aqueous phases. The amount of styrene produced is determined by GC-MS.

3.3.4 DMAPP *vs* DMAP

Guided by reports that the bacterial PFS was specific for DMAP, my initial experiments on the eukaryotic enzyme used DMAP as a substrate. However, the very low levels of activity obtained with DMAP caused me to re-evaluate whether the more common prenyl-donor DMAPP might be a substrate for scPFS. This turned out to be the case. The rate of prFMN formation was compared with either 100 μM DMAPP or 500 μM DMAP present as the prenyl-donor, conditions that represent saturating concentrations of these substrates. Under these conditions, scPFS exhibited ~20 fold higher activity with DMAPP than DMAP (Figure 3.8).

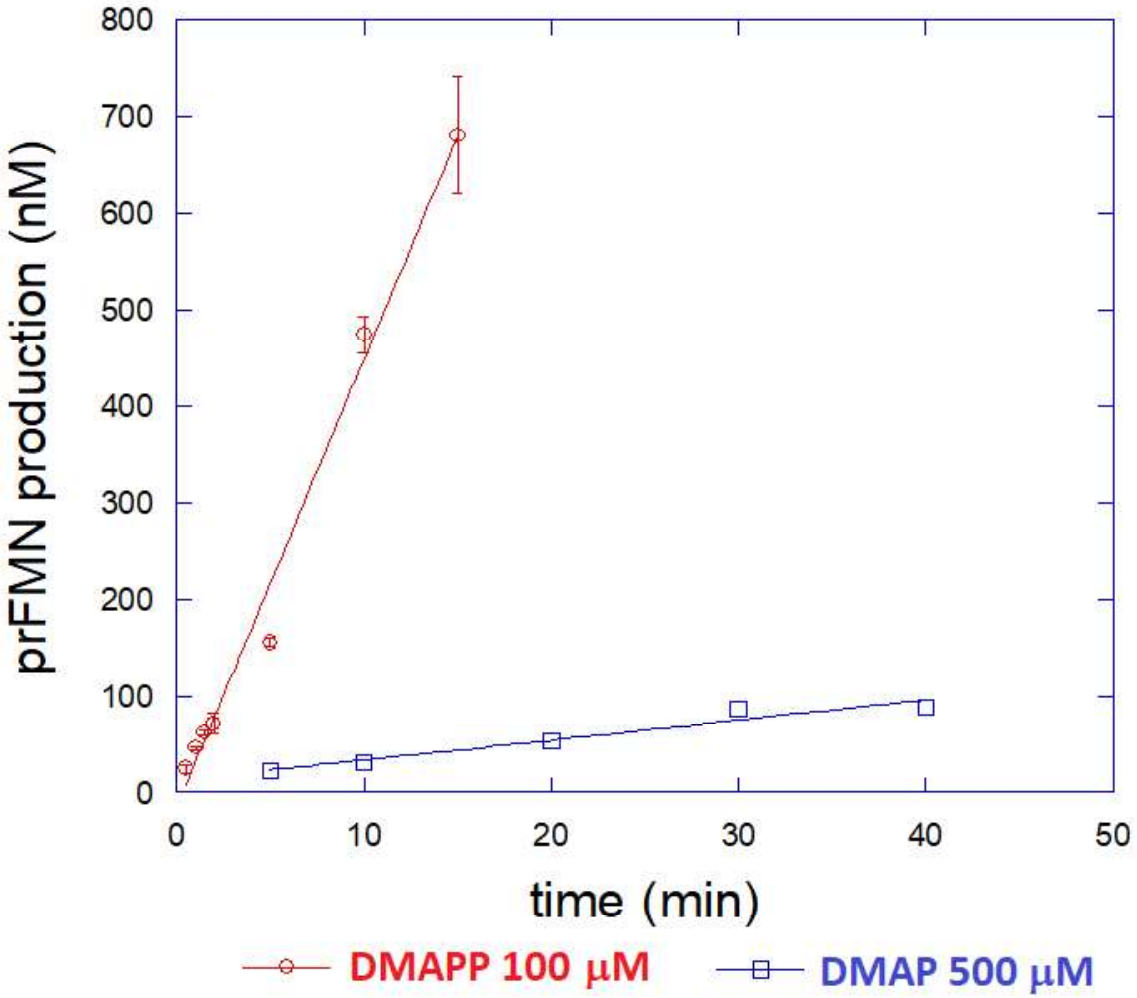

Figure 3.8: Monitoring of catalytic FMN prenylation by scPFS by FDC-coupled assay. The signal for prFMN formation is amplified by coupling with apo-FDC. scPFS reactions were prepared at 20°C under anaerobic condition and had a volume of 500 µL per reaction. The reaction mixture contained 400 nM scPFS pre-incubated with 5 mM DTT for 10 min; 50 µM FMN; 4 µM apo-FDC; and 60 µM NADH. After addition of prenyl-donor, the mixtures were reduced by 1 mM sodium dithionite. In red, the prenyl-donor is 100 µM DMAPP. In blue, the prenyl-donor is 500 µM DMAP. After various amount of time from 30 sec to 40 min, the reactions were quenched with 5 mM potassium ferricyanide. 2.5 mM cinnamic acid was added as the substrate to reactivated FDC. prFMN formation was back-calculated from amount of reactivated FDC.

3.3.5 Steady state kinetic analysis of scPFS

Having demonstrated that the FDC-coupled assay gave linear and reproducible results, I investigated the kinetics of prFMN formation by scPFS. These assays employed 400 nM scPFS that had been pre-reduced with 5 mM DTT for 10 min and a 10-fold molar excess of apo-FDC. To determine the K_M for DMAPP, the concentration of FMN was fixed at 50 μM (assumed saturating) and the concentration of DMAPP varied between 1 and 500 μM. To investigate the K_M for FMN, the concentration of DMAPP was fixed at 500 μM (assumed saturating) and the concentration of FMN varied between 0.75 and 50 μM. The data were fitted to the Michaelis-Menten equation (Figure 3.9) to obtain apparent K_M values for DMAPP, K_M^{app} = 9.8 ± 0.7 μM, and FMN K_M^{app} = 0.61 ± 0.17 μM; k_{cat} measured at saturating concentrations of both substrates was 12.2 ± 0.2 h^{-1}. The lower concentrations of FMN used in these assays the assumptions of the Michaelis-Menten equation are not valid and therefore K_M^{app} determined for FMN should be regarded as an upper bound.

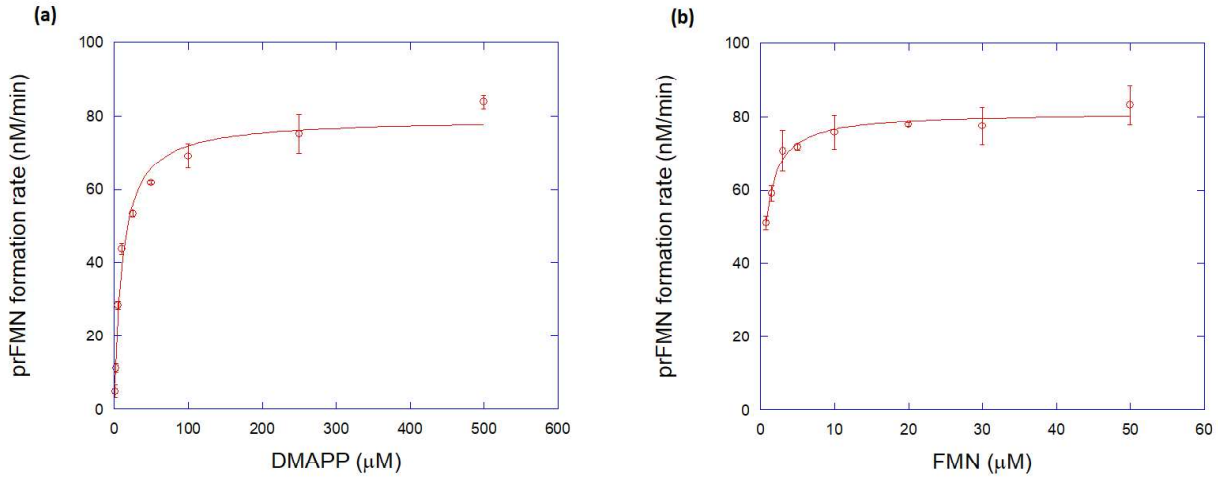

Figure 3.9: Steady state kinetic analysis utilizing FDC coupling assay. The substrate concentrations were variable and the data were fitted into Michaelis-Menten equation. (a) Saturated FMN (50 μM), variable DMAPP from 1 μM to 500 μM. K_M^{app} = 9.8 ± 0.7 μM and k_{cat} = 12.2 ± 0.2 h^{-1}. (b) Saturated DMAPP (500 μM), variable FMN from 0.75 μM to 50 μM. K_M^{app} = 0.61 ± 0.17 μM and k_{cat} = 12.2 ± 0.2 h^{-1}.

3.3.6 Single turnover kinetics of FMN consumption

Taking advantage of the very slow turnover rate exhibited by scPFS, I sought to examine the kinetics in more detail under single turnover conditions. To accomplish these measurements, assays were set up with higher concentrations of scPFS, typically 600 nM, and sub-stoichiometric concentrations of FMN, typically 300 nM. Given the fairly high affinity of scPFS for FMN, most of the FMN in the assay should be bound to the enzyme. The other components of the assay were present at the same concentrations as for the steady-state measurements. The reaction was initiated by the addition of DMAPP (final concentration = 500 μM). At various times aliquots were withdrawn and the quenched by addition of $K_3Fe(CN)_6$. The amount of prFMN formed was then determined from the activity of FDC as described above. The production of prFMN was well described by a first-order kinetic model (Figure 3.10 red) with an apparent first order rate constant of 17.5 ± 1.1 h^{-1}.

The pre-steady state formation of prFMN by scPFS could also be followed more directly by the disappearance of FMN. I initially attempted to detect the formation of prFMN by reverse phase HPLC; however, the small amount of product formed and the absence of a strong long-wavelength chromophore combined with the instability of the cofactor and interference from contaminating analytes prevented me from reliably being able to quantify prFMN by this method. In contrast, consumption of FMN could be followed relatively easily by quantifying the FMN remaining in the assay by HPLC. FMN was detected by chromatography on a C18 reverse phase HPLC column equilibrated in 5 mM ammonium acetate and developed with an increasing gradient of acetonitrile, with peaks monitored at 450 nm, as described in the Methods section. The pre-steady state kinetics of FMN consumption mirrored that formation of prFMN followed by the discontinuous coupled assay described above. The data were well fitted by a single exponential with an observed rate

constant, k_{obs} = 20.3 ±3.8 h^{-1}, a result that is in good agreement with the rate constant for prFMN formation (Figure 3.10 blue).

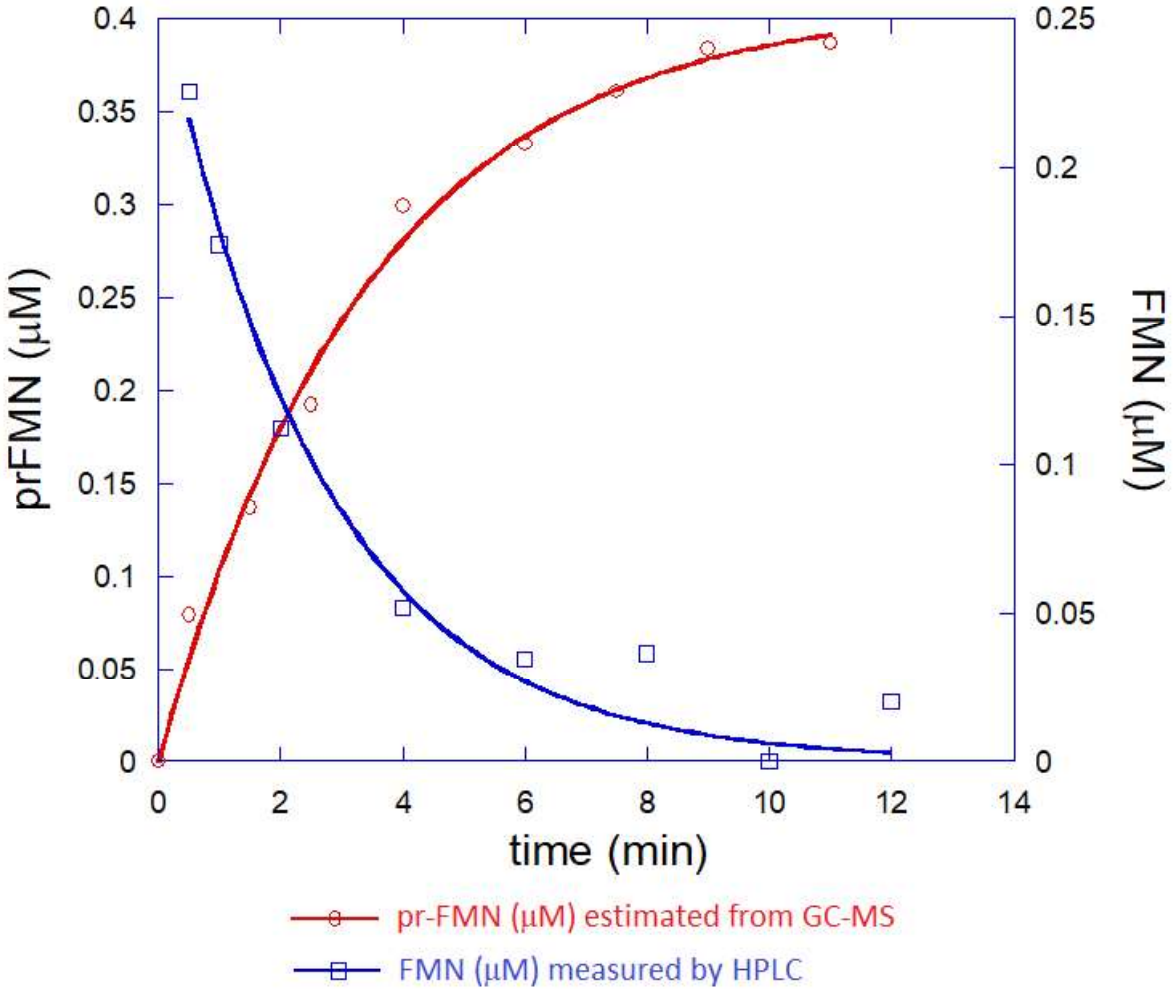

Figure 3.10: Single turnover kinetic analysis of prFMN production by scPFS. (Red) The reaction between 600 nM scPFS and 300 nM FMN was monitored by FDC-coupling assay. k_{obs} = 17.5 ±1.1 h^{-1}. (Blue) The reaction between 2 µM scPFS and 1.5 µM FMN was monitored by HPLC through consumption of FMN. k_{obs} = 20.3 ±3.8 h^{-1}.

3.3.7 PiPer™ Pyrophosphate Assay

It has been clear that the catalytic activity of scPFS is slow. It is even slower when DMAP was used as substrate. This could be one of the reasons causing failure to observe the generation of phosphate by-product in the high throughput phosphate detection assay conducted in the beginning. Therefore, this section describes another attempt to monitor catalytic activity of scPFS given that the preferred DMAPP was used as substrate.

Previous results, described above, suggested that malachite green assay and Enzchek assay may not be suitable phosphate/pyrophosphate detection kit. Here, another commercial available pyrophosphate detection kit, PiPer™ Pyrophosphate Assay, was employed to monitor pyrophosphate generation. In the PiPer™ Pyrophosphate Assay (Figure 3.11) (32,33), inorganic pyrophosphatase hydrolyzes PPi to two molecules of inorganic phosphate (Pi). In the presence of inorganic phosphate, maltose phosphorylase converts maltose to glucose 1-phosphate and glucose. Then glucose oxidase converts the glucose to gluconolactone and H_2O_2. Finally, with horseradish peroxidase (HRP) as a catalyst, the H_2O_2 reacts with the Amplex® Red reagent (10-acetyl-3,7-dihydroxyphenoxazine) to generate resorufin. The formation of resorufin can be monitored through absorbance at 565 nm.

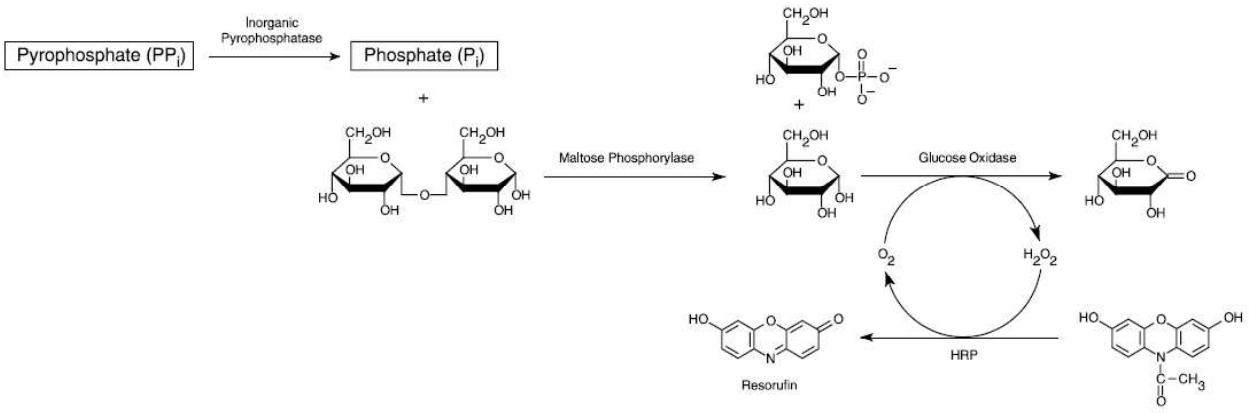

Figure 3.11: Principle of the PiPer™ Pyrophosphate Assay. Inorganic pyrophosphatase converts pyrophosphate to two equivalents of inorganic phosphate. Next, in the presence of the inorganic phosphate, maltose phosphorylase converts maltose to glucose 1-phosphate and glucose. Then, glucose oxidase converts the glucose to gluconolactone and H_2O_2. Finally, with horseradish peroxidase (HRP) as a catalyst, the H_2O_2 reacts with the Amplex Red reagent to generate resorufin, which can be monitored through absorbance at 565 nm. Figure taken from the PiPer™ Pyrophosphate Assay manual.

Pyrophosphate assays were performed in 96-well microplates using 50 µL of pyrophosphate standard (5-100 µM) in 100 mM Tris-HCl pH 8.5. 50 µL of working solution prepared as described in method section was added to each well and the absorbance at 565 nm was recorded in microplate reader at 37 ºC over a period of 1 hr. Each components in scPFS catalytic assay including sodium dithionite, DTT, ferricyanide, FMN, NADH, and DMAPP were tested with the premixed working solution. The experimental results found that some of the reducing agent and oxidizing agent interfered with the signal giving false positive result (Figure 3.12). In order to utilize this assay, several reducing and oxidizing agents are required to be tested prior to the test of pyrophosphate formation from scPFS. Considering the difficulty to optimize the assay that would satisfy both PiPer™ Pyrophosphate Assay and scPFS working condition, the work in this thesis did not continue toward the phosphate/pyrophosphate detection strategy.

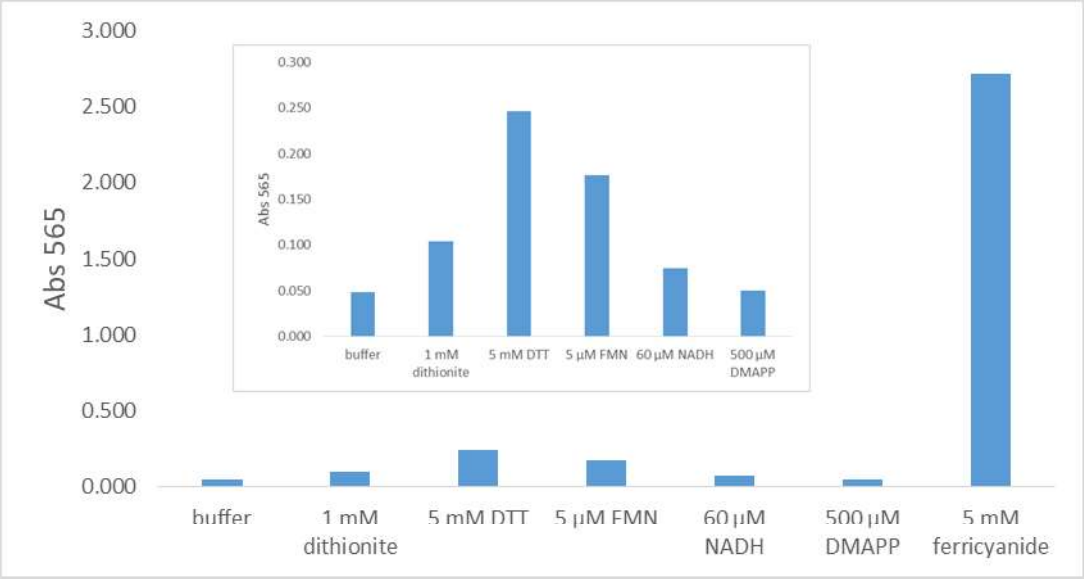

Figure 3.12: Reaction between each components of scPFS prenylation with PiPer™ Pyrophosphate Assay working solution. Results showed strong interference with reducing and oxidizing agents.

3.4 Conclusions

In conclusion, this chapter explored various methods to investigate catalytic activity of scPFS, from commercially available high throughput phosphate/pyrophosphate assay to the scPFS-FDC coupled assay that ultimately proved successful. The complexity of the reaction including the process of reduction and oxidation led to the failure of commercial phosphate/pyrophosphate detection kits. However, it proved possible to study kinetic behavior of scPFS through the coupled enzyme assay. In coupled enzyme assay, each molecule of prFMN generated from scPFS binds to apo-FDC resulting many molecules of styrene. Thus, considerable amplification of the signal is achieved.

The work described here represents the first attempt to explore kinetic parameter of the newly-discovered FMN prenylation reaction. In this work, the source of prenyl donor was re-evaluated. In contrast to the previous publication where the rare prenyl donor DMAP is reported to be prenyl

source of UbiX, the more common prenyl-donor DMAPP is discovered to be a substrate for scPFS. The steady state analysis of scPFS identifies the observed k_{cat}, $K_M^{app\ (DMAPP)}$ to be 12.2 ± 0.2 h^{-1} and 9.8 ± 0.7 μM, respectively. Moreover, the results from single turnover kinetics of FMN consumption yield an apparent first order rate constant of 17.5 ± 1.1 h^{-1} for prFMN formation.

3.5 References

1. Goodey AR, Tubb RS. Genetic and Biochemical Analysis of the Ability of Saccharomyces cerevisiae to Decarboxylate Cinnamic Acids. Microbiology. 1982;128(11):2615–20.

2. Plumridge A, Stratford M, Lowe KC, Archer DB. The Weak-Acid Preservative Sorbic Acid Is Decarboxylated and Detoxified by a Phenylacrylic Acid Decarboxylase, PadA1, in the Spoilage Mold Aspergillus niger. Appl Environ Microbiol. 2008 Jan 15;74(2):550–2.

3. Donaghy JA, Kelly PF, McKay A. Conversion of ferulic acid to 4-vinyl guaiacol by yeasts isolated from unpasteurised apple juice. J Sci Food Agric. 1999 Mar 1;79(3):453–6.

4. Heresztyn T. Metabolism of volatile phenolic compounds from hydroxycinnamic acids byBrettanomyces yeast. Arch Microbiol. 1986 Oct 1;146(1):96–8.

5. Shinohara T, Kubodera S, Yanagida F. Distribution of phenolic yeasts and production of phenolic off-flavors in wine fermentation. J Biosci Bioeng. 2000 Jan 1;90(1):90–7.

6. Chatonnet P, Dubourdieu D, Boidron J, Lavigne V. Synthesis of volatile phenols by Saccharomyces cerevisiae in wines. J Sci Food Agric. 1993 Jan 1;62(2):191–202.

7. Edlin DAN, Narbad A, Gasson MJ, Dickinson JR, Lloyd D. Purification and characterization of hydroxycinnamate decarboxylase from Brettanomyces anomalus. Enzyme Microb Technol. 1998 Mar 1;22(4):232–9.

8. Clausen M, Lamb CJ, Megnet R, Doerner PW. PAD1 encodes phenylacrylic acid decarboxylase which confers resistance to cinnamic acid in Saccharomyces cerevisiae. Gene. 1994 May;142(1):107–12.

9. Baranowski JD, Davidson PM, Nagel CW, Branen AL. INHIBITION OF Saccharomyces cerevisiae BY NATURALLY OCCURRING HYDROXYCINNAMATES. J Food Sci. 1980 May;45(3):592–4.

10. Stratford M, Plumridge A, Archer DB. Decarboxylation of Sorbic Acid by Spoilage Yeasts Is Associated with the PAD1 Gene. Appl Environ Microbiol. 2007 Oct 15;73(20):6534–42.

11. Payne KAP, White MD, Fisher K, Khara B, Bailey SS, Parker D, et al. New cofactor supports α,β-unsaturated acid decarboxylation via 1,3-dipolar cycloaddition. Nature. 2015 Jun 25;522(7557):497–501.

12. Piano V, Palfey BA, Mattevi A. Flavins as Covalent Catalysts: New Mechanisms Emerge. Trends Biochem Sci. 2017 Jun;42(6):457–69.

13. White MD, Payne KAP, Fisher K, Marshall SA, Parker D, Rattray NJW, et al. UbiX is a flavin prenyltransferase required for bacterial ubiquinone biosynthesis. Nature. 2015 Jun 25;522(7557):502–6.

14. Lin F, Ferguson KL, Boyer DR, Lin XN, Marsh ENG. Isofunctional enzymes PAD1 and UbiX catalyze formation of a novel cofactor required by ferulic acid decarboxylase and 4-hydroxy-3-polyprenylbenzoic acid decarboxylase. ACS Chem Biol. 2015 Apr 17;10(4):1137–44.

15. Marshall SA, Payne KAP, Leys D. The UbiX-UbiD system: The biosynthesis and use of prenylated flavin (prFMN). Arch Biochem Biophys. 2017 Oct 15;632(Supplement C):209–21.

16. Marshall SA, Fisher K, Cheallaigh AN, White MD, Payne KAP, Parker DA, et al. Oxidative maturation and Structural Characterization of Prenylated-FMN binding by UbiD, a Decarboxylase Involved in Bacterial Ubiquinone Biosynthesis. J Biol Chem. 2017 Jan 5;jbc.M116.762732.

17. Payer SE, Marshall SA, Bärland N, Sheng X, Reiter T, Dordic A, et al. Regioselective *para* -Carboxylation of Catechols with a Prenylated Flavin Dependent Decarboxylase. Angew Chem Int Ed. 2017 Oct 23;56(44):13893–7.

18. Ebenau-Jehle C, Mergelsberg M, Fischer S, Brüls T, Jehmlich N, von Bergen M, et al. An unusual strategy for the anoxic biodegradation of phthalate. ISME J. 2017 Jan;11(1):224–36.

19. Bentinger M, Tekle M, Dallner G. Coenzyme Q--biosynthesis and functions. Biochem Biophys Res Commun. 2010 May 21;396(1):74–9.

20. Gulmezian M, Hyman KR, Marbois BN, Clarke CF, Javor GT. The role of UbiX in Escherichia coli coenzyme Q biosynthesis. Arch Biochem Biophys. 2007 Nov 15;467(2):144–53.

21. Jacewicz A, Izumi A, Brunner K, Schnell R, Schneider G. Structural insights into the UbiD protein family from the crystal structure of PA0254 from Pseudomonas aeruginosa. PloS One. 2013;8(5):e63161.

22. Meganathan R. Ubiquinone biosynthesis in microorganisms. FEMS Microbiol Lett. 2001 Sep 25;203(2):131–9.

23. Rangarajan ES, Li Y, Iannuzzi P, Tocilj A, Hung L-W, Matte A, et al. Crystal structure of a dodecameric FMN-dependent UbiX-like decarboxylase (Pad1) from Escherichia coli O157: H7. Protein Sci Publ Protein Soc. 2004 Nov;13(11):3006–16.

24. Cox GB, Young IG, McCann LM, Gibson F. Biosynthesis of ubiquinone in Escherichia coli K-12: location of genes affecting the metabolism of 3-octaprenyl-4-hydroxybenzoic acid and 2-octaprenylphenol. J Bacteriol. 1969 Aug;99(2):450–8.

25. Kopec J, Schnell R, Schneider G. Structure of PA4019, a putative aromatic acid decarboxylase from Pseudomonas aeruginosa. Acta Crystallogr Sect F. 2011 Sep 24;67(Pt 10):1184–8.

26. Weber HE, Gottardi M, Brückner C, Oreb M, Boles E, Tripp J. Requirement of a Functional Flavin Mononucleotide Prenyltransferase for the Activity of a Bacterial Decarboxylase in a Heterologous Muconic Acid Pathway in Saccharomyces cerevisiae. Appl Environ Microbiol. 2017 May 15;83(10):e03472-16.

27. Johnson CW, Salvachúa D, Khanna P, Smith H, Peterson DJ, Beckham GT. Enhancing muconic acid production from glucose and lignin-derived aromatic compounds via increased protocatechuate decarboxylase activity. Metab Eng Commun. 2016 Dec 1;3(Supplement C):111–9.

28. Clarke CF, Allan CM. Biochemistry: Unexpected role for vitamin B2. Nature. 2015 Jun 25;522(7557):427–8.

29. O'Toole M, Lau KT, Shepherd R, Slater C, Diamond D. Determination of phosphate using a highly sensitive paired emitter–detector diode photometric flow detector. Anal Chim Acta. 2007 Aug 10;597(2):290–4.

30. Webb MR. A continuous spectrophotometric assay for inorganic phosphate and for measuring phosphate release kinetics in biological systems. Proc Natl Acad Sci U S A. 1992 Jun 1;89(11):4884–7.

31. Ferguson KL, Arunrattanamook N, Marsh ENG. Mechanism of the Novel Prenylated Flavin-Containing Enzyme Ferulic Acid Decarboxylase Probed by Isotope Effects and Linear Free-Energy Relationships. Biochemistry (Mosc). 2016 May 24;55(20):2857–63.

32. Mohanty JG, Jaffe JS, Schulman ES, Raible DG. A highly sensitive fluorescent micro-assay of H2O2 release from activated human leukocytes using a dihydroxyphenoxazine derivative. J Immunol Methods. 1997 Mar 28;202(2):133–41.

33. Zhou M, Diwu Z, Panchuk-Voloshina N, Haugland RP. A stable nonfluorescent derivative of resorufin for the fluorometric determination of trace hydrogen peroxide: applications in detecting the activity of phagocyte NADPH oxidase and other oxidases. Anal Biochem. 1997 Nov 15;253(2):162–8.

Chapter 4 Cofactor analogs

4.1 Introduction

Cofactors are essential for many enzyme activities. Cofactors function in various roles to enhance the activity of an enzyme; such as increasing structural stability, facilitating protein folding, and, most importantly, providing additional chemical functionality essential for the catalysis of many reactions. In the past few years, cofactor engineering has become of great interest. The term "cofactor engineering" includes a large range of cofactor manipulations, from metabolic engineering to increase biosynthesis of cofactor (1–3) to direct modification of cofactor, such as the use of FAD analogs in a Baeyer–Villiger oxygenation reactions (4). This chapter focuses on the generation of cofactor prFMN variants and the analysis of their catalytic activity with FDC.

The decarboxylation reaction catalyzed by FDC requires a novel FMN cofactor generated by scPFS. The pathway by which scPFS synthesizes prenyl-flavin cofactor was unknown until the recent release of a series of crystal structures of the isofunctional enzyme, UbiX (5). Based on these crystal structures, a mechanism for the synthesis of prFMN and the function of prFMN in the FDC reaction have been proposed as discussed in previous chapters (Figure 4.1).

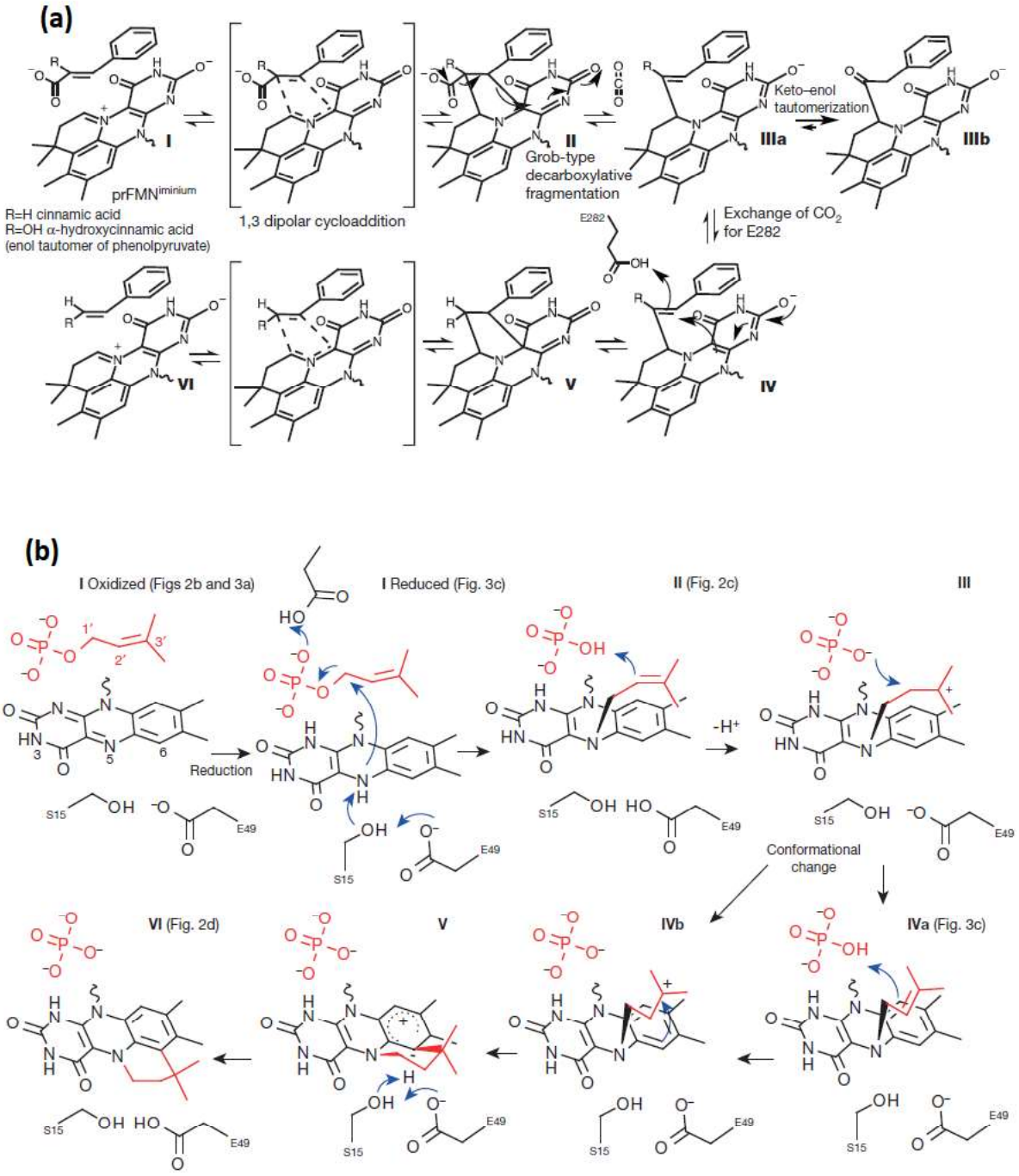

Figure 4.1: (a) Proposed 1,3-dipolar cyclo-addition mechanism for the FDC-catalyzed decarboxylation of phenylacrylic acid (b) Proposed mechanism for the formation of reduced prFMN from reduced FMN and DMAP catalyzed by prenyl-flavin synthase. Figure based on references (5,6).

Cofactor analogs provide a powerful tool to study enzyme specificity as well as identify intermediates in the reaction (7–9). This chapter will examine whether scPFS can use structural analogs of DMAPP to modify FMN, and if so, whether these serve as cofactors for FDC. In addition, given that only C-1' of prFMN is chemically reactive, it is important to determine whether cyclization to the dimethylbenzene ring is required for activity. This could be achieved by examining the reaction of analogs that cannot undergo cyclization. These would be expected to modulate the reactivity of C-1' position in prFMN and might result in the identification of non-natural cofactors for FDC that exhibit superior decarboxylase activity.

Furthermore, modified flavin analogs have proved valuable probes to study the mechanism of flavin- dependent enzymes (10–14). The C-8 methyl group on the isoalloxazine ring can be replaced with a variety of electron-withdrawing or donating substituents to systematically fine tune the reduction potential of the flavin. For example, using 12 FMN analogs with lactate oxidase, it was possible to demonstrate an impressive linear free energy relationship between the Hammett σ-para and σ-ortho parameters and the reduction potential of the free and enzyme-bound FMN analogs (10). This correlation further extended to the rates of lactate oxidation by the reconstituted flavoenzymes.

Flavin analogs can be applied to probe the mechanism by which prFMN is generated. Based on crystallographic data, it was proposed that DMAP reacts with the flavin first at N-5, with the slow step being formation of the C-6–C-3' bond (5,15,16). This is proposed to involve formation of a carbocation intermediate on the dimethylbenzene ring. If this step is rate-determining, electron-donating substituents should stabilize this intermediate and increase the rate of reaction yielding negative reaction constant in Hammett analysis as discussed in chapter 2.

Also, cofactor analogs generated from FMN analogs can be employed to probe the FDC decarboxylation mechanism. C-8 substitutions will alter the electrophilicity of the reactive C-1' carbon in a predictable manner through π-conjugation. 1,3-Dipolar cycloaddition reactions of azomethine ylides (which best represent the chemical characteristics of prFMN) are sensitive to the energy difference between the HOMO of the ylide and the LUMO of the dipolarophile (17–19). Therefore, if the decarboxylation reaction does proceed by cycloaddition, electron-donating substituents would increase the energy of the HOMO, thereby increasing the rate of decarboxylation (assuming this is a kinetically significant step). In contrast, if the cofactor is serving primarily as an electron sink, the opposite trend should be observed and electron-withdrawing substituents should increase the rate of decarboxylation.

This chapter employs kinetic assays developed in the previous chapter to investigate whether prFMN analogs can be synthesized using scPFS. First, scPFS utilizes DMAPP analogs to modify the FMN cofactor. Then, apo-FDC binds the cofactor, allowing it to catalyze decarboxylation. The production of cofactor analogs by scPFS can be monitored through the consumption of substrate, assuming the reactions turnover and scPFS spontaneously releases cofactor analogs. Therefore, the HPLC assay discussed previously in chapter 3 can, in principle, be employed to measure the concentration of the generated cofactor analog as well as kinetic parameters for prenylation. Then, the kinetic parameters for FDC catalyzing decarboxylation using the cofactor analog can be measured by coupling FDC and scPFS as described in the previous chapter.

In addition, the prenylation reaction of modified flavins provided by Prof. Bruce Palfey at University of Michigan will be examined in this chapter.

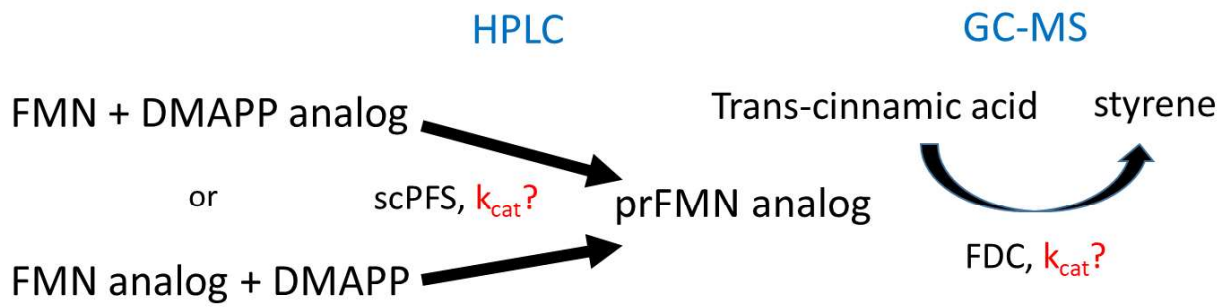

Figure 4.2: Diagram describing the synthesis and the use of cofactor analogs to study phenylacrylic acid decarboxylation

4.2 Materials and methods

4.2.1 Materials

FMN, and dithiothreitol were purchased from MP biomedicals; dimethylallyl pyrophosphate (DMAPP), geranyl pyrophosphate (GPP), and (E)-4-Hydroxy-3-methyl-but-2-enyl pyrophosphate (HMBPP) were purchased from Isoprenoids LC, Tampa FL; potassium ferricyanide was purchased from Acros Organics. 7,8 dichloro flavin mononucleotide was provided by Prof. Bruce Palfey (University of Michigan-Ann Arbor). All other chemicals were purchased from Sigma-Aldrich.

Holo-FDC, apo-FDC and scPFS were recombinantly expressed in Escherichia coli and purified as described previously (20).

4.2.2 Assay for pr-FMN formation by scPFS

100 mM HEPES buffer supplemented with 100 mM $MgCl_2$ pH 8.5 were prepared and purged with nitrogen gas overnight, and then equilibrated in a Coy anaerobic chamber. Flavin mononucleotide, dimethylallyl pyrophosphate, scPFS, reducing reagents and oxidizing reagents were transferred into anaerobic chamber. The volume of scPFS assay is 0.5 mL. The assay contained 2 μM scPFS,

1.5 μM FMN and 200 μM prenyl donor. The assay also contained 60 μM NADH as additional reducing agent and 10 μM apo-FDC as secondary enzyme for GC-MS assay. Then, sodium dithionite was added to the premix to 1 mM concentration to start the reaction at room temperature. After time periods varying from 30 seconds to 30 minutes, 5 mM potassium ferricyanide was added to quench the reaction. In the case of modified Flavin, 200 μM DMAPP and 1.5 μM modified FMN were used as substrates.

4.2.3 HPLC assays

500 μL reaction mixtures were prepared as described in section 4.2.2 with 9 μM of riboflavin as internal standard. After quenching, reaction mixtures were heated at 85^{o}C for 15 mins and centrifuged in a tabletop microcentrifuge at 10,000 rpm for 10 mins. Then, supernatant was collected for HPLC analysis. Sample analysis was performed using a Shimadzu HPLC system with two LC-20AT pumps, and anSPD-M20A UV-visible diode array detector with monitoring at 450 nm. The stationary phase was an EC 250/4.6 Nucleodur C18 reverse phase column. The column was equilibrated with 5 mM ammonium acetate (A) and analytes eluted with a gradient of increasing acetonitrile (B) under 0.5 mL/min flow rate. The solvent composition was held at 100% (A) for 4 min, and then increased linearly to 15% (B) over 16 min, followed by isocratic elution at 15% (B) for 25 min, then returned to 100% (A) over 5 min and held for 5 min for column equilibration. Under these conditions FMN eluted at 24.46 min and riboflavin eluted at 35.72 min. FMN concentrations were calculated from peak integration and normalized with respect to the riboflavin internal standard.

4.2.4 GC-MS assay

Routine assays of FDC activity were carried out in diluted quenched scPFS reaction mixture. 125 µL of scPFS reaction mixture, prepared as described in the assay for pr-FMN formation with 30 mins prenylation, was diluted to 500 µL with 1 mM $MgCl_2$ 100 mM HEPES buffer pH 8.5. The mixture was equilibrated for 45 min. Then, FDC assays were allowed to proceed for 5-40 mins at room temperature using a saturating concentration of cinnamic acid, 2.5 mM, as substrate. The mixtures were quenched with HCl, final concentration 0.27 M and extracted with 400 µL ethyl acetate with 94.7 µM undecane as internal standard. Samples were vortexed and centrifuged in a tabletop microcentrifuge at 10,000 rpm for 10 mins to separate organic and aqueous phases. The amount of styrene produced was determined by GC-MS as described previously (8).

4.2.5 Native mass spectrometry

500 µL of reaction mixtures were prepared as described in section 4.2.2 with 20 µM FMN, 200 µM prenyl donor, 5 µM scPFS and 20 µM apo-FDC. The prenylation reaction was allowed to proceed for 3 hrs in Coy anaerobic chamber and then quenched by exposure to air. Then, samples were ~10 fold concentrated in Vivaspin protein concentrators, MWCO 10000. 50-60 µL of concentrated samples were buffer exchanged into 500 mM ammonium acetate buffer, pH 6.9, using two Micro Bio-Spin P-6 columns (Bio-Rad, Hercules, CA). The final concentration of the buffer exchanged protein was 5-10 µM.

Mass spectrometry of samples was performed by Chunyi Zhao (in Prof. Ruotolo Lab, University of Michigan). Samples were analyzed under native MS conditions using a Synapt G2 ion mobility mass spectrometry platform (Waters Inc, Milford MA) (21). The complexes of FDC with *in vitro* synthesized cofactors were ionized using nanoelectrospray ionization. The initial instrument

settings were set to minimize ion activation; hence, maintaining non-covalent interactions such that no significant signals were observed for free FMN-related peaks. The capillary voltage was set to 1.5 kV, and the sampling and extraction cones were set to 30 V and 0 V, respectively with the trap collision energy at 20 V. For CID experiments, the trap collision energy was raised to 100 V to dissociate cofactors from FDC. Data was processed in Masslynx (Waters Inc, Milford MA) (22).

4.2.6 Molecular docking

Docking was achieved using AutoDock 4 program. Ligand PDB files were generated after energy minimization using Avogadro software. Protein and ligand files were prepared using AutoDock Tools software. Numbers of torsions were set to 3 for dimethylallyl monophosphate (DMAP), 5 for (E)-4-Hydroxy-3-methyl-but-2-enyl phosphate (HMBP) and 6 for geranyl monophosphate (GP).

Grid bow parameters were set as follows:

Number of points in the x-dimension = 60

Number of points in the y-dimension = 58

Number of points in the z-dimension = 56

Spacing = 0.375 Å

Center coordinates x = -5.983, y = 29.720, z = 12.816

This was chosen to encompass the active site at the interface between three monomers.

Atomic map files were generated using the AutoGrid4 program. Docking was then run using the AutoDock4 program with Lamarckian Genetic Algorithm 4.2 parameters set as follows:

Number of GA runs = 100

Population size = 300

Maximum number of evals = 2,500,000 (medium)

Maximum number of generations = 27,000

Maximum number of top individuals that automatically survive = 1

Rate of gene mutation = 0.02

Rate of Crossover = 0.8

GA Crossover mode: twopt

Mean of Cauchy distribution for gene mutation = 0

Variance of Cauchy distribution for gene mutation = 1

Number of generations for picking worst individual = 10

Solutions were analysed using AutoDock Tools, clustering solutions using an rmsd-tolerance of 2.0 Å. Binding energies and Ki were automatically calculated by AutoDock Tools.

4.3 Results and discussion

4.3.1 HPLC Assay

In order to study cofactor specificity of FDC, cofactor analogs must be synthesized. scPFS was employed to catalyze prenylation using substrate analogs. The rate of prenylation and concentration of cofactor analogs were indirectly measured through the consumption of substrate by HPLC.

Due to the saturation limit of FMN detection at 10 μM and scPFS stock concentration of ~40 μM, HPLC assays were performed under single turnover conditions with 2 μM scPFS, 1.5 μM FMN/FMN analogs and 200 μM prenyl donor. Also, kinetic parameters obtained from these experiments can be directly compared with the kinetic parameters obtained in the previous chapter.

First, 7,8-dichloro flavin mononucleotide provided by Prof. Bruce Palfey was selected to perform prenylation. 7,8-dichloro flavin mononucleotide has spectrum similar to FMN; and thus,

disappearance of this analog can be monitored at 450 nm using the same HPLC set up as the protocol developed for original prenylation. The assay with this analog resulted in complete disappearance of the signal representing oxidized FMN at 27.50 min. However, there was a new peak showing up at 26.10 min with much smaller intensity. Thus, I suspected that 7,8-dichloro flavin mononucleotide reacted with the reducing/oxidizing agent to form a different species. This seemed to be the case, since a similar result was observed in a mixture containing 7,8-dichloro flavin mononucleotide and dithiothreitol. Addition of oxidizing agent could not reverse the signal back to that of the original oxidized form. The result suggested that the reactive chloro-substituents react with DTT to form a new FMN analog. Therefore, a different disulfide bond reducing agent must be used to utilize 7,8-dichloro flavin mononucleotide as a FMN analog. Given the limited availability of FMN analogs and the requirement to optimize assay for each analogs and limited amount of time, I decided to focus on study of DMAPP analogs for the rest of this section.

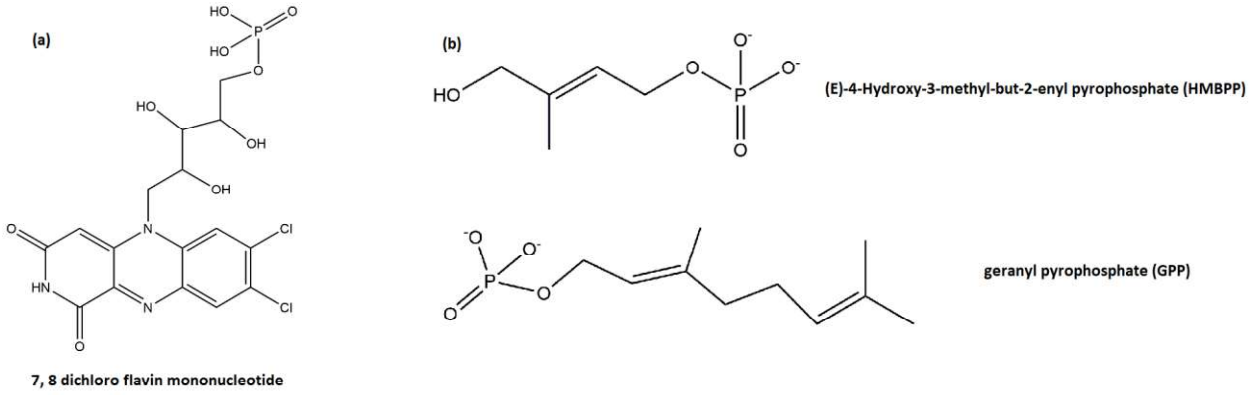

Figure 4.3: Structures of substrate analogs used for synthesis of prFMN analogs by scPFS (a) 7,8-dichloro flavin mononucleotide was selected as a sample of FMN analog in this experiment (b) Structures of (E)-4-Hydroxy-3-methyl-but-2-enyl pyrophosphate (HMBPP) and geranyl pyrophosphate (GPP) represent analogs of prenyl donor dimethylallyl pyrophosphate (DMAPP)

The prenylation of FMN with DMAPP analogs was performed using commercially available (E)-4-Hydroxy-3-methyl-but-2-enyl pyrophosphate (HMBPP) and geranyl pyrophosphate (GPP). The

data were well fitted by a single exponential with an observed rate constant, k_{obs} = 4.45 ± 0.87 h^{-1}, and 3.80 ± 0.34 h^{-1} for HMBPP and GPP respectively (Figure 4.4). As a negative control, the reaction was set up without prenyl donor for 15 mins and the data point was used to represent time zero data point. The reduction in observed rate constant when DMAPP analogs were used as prenyl donor implied specificity toward DMAPP. Note that the reactions did not go to completion. This could indicate that the release of cofactor analog might not be spontaneous.

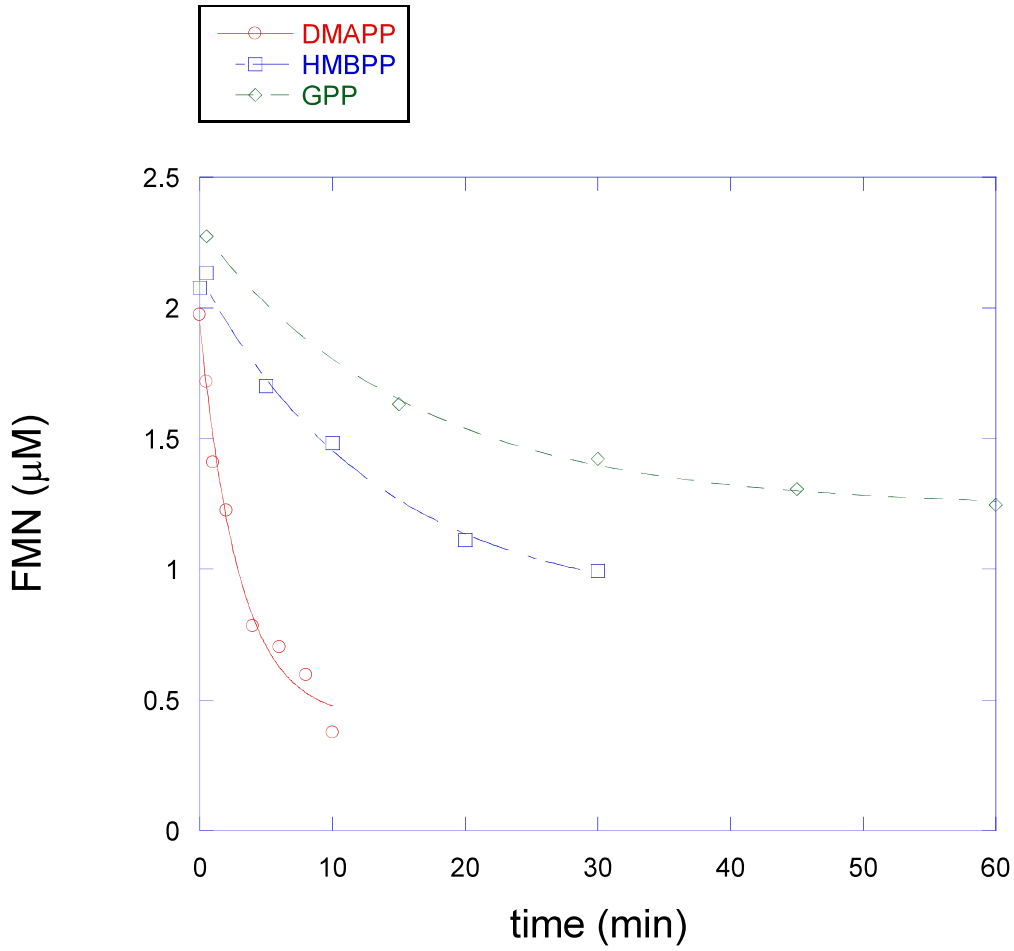

Figure 4.4: HPLC analysis of single turnover kinetic of scPFS prenylation utilized (Red) dimethylallyl pyrophosphate (DMAPP) as substrate (Blue) (E)-4-Hydroxy-3-methyl-but-2-enyl pyrophosphate (HMBPP) as substrate and (green) geranyl pyrophosphate (GPP). Prenylation reactions were monitored through consumption of FMN. Observed rate of prenylation were 20.3 ± 3.8 h^{-1}, 4.45 ± 0.87 h^{-1}, and 3.80 ± 0.34 h^{-1} for DMAPP, HMBPP, and GPP respectively.

4.3.2 GC-MS Assay

The routine FDC-scPFS coupling assays were conducted under single turnover kinetics using the same concentration of substrates as HPLC assay. Prenylation was allowed to proceed for 30 min to achieve maximal generation of cofactor analogs, 1.1 μM for HMBPP and 0.85 μM for GPP. Then, the decarboxylation of *trans*-cinnamic was performed at saturating concentration of substrate. The reaction mixture without prenyl source was used as negative control, representing background activity of apo-FDC. The product of decarboxylation, styrene, was extracted and the concentration was determined by GC-MS. The data were well fitted by a linear regression model. The observed rates of styrene formation were 1.57 ± 0.14 μM/min for background decarboxylation, 7.62 ± 0.26 μM/min for HMBPP cofactor analog, and 1.95 ± 0.17 μM/min for GPP cofactor analog (Figure 4.5). The decarboxylation rate for FDC utilizing cofactor synthesized from GPP was indistinguishable from background level; and thus, implied that FDC could not use this cofactor analog if indeed scPFS was able to synthesize it. In the case of cofactor synthesized from HMBPP, the result yielded observed V_{max} of 5.50 ± 0.37 min^{-1}. This observed V_{max} is ~25 fold slower than original prFMN catalyzed decarboxylation.

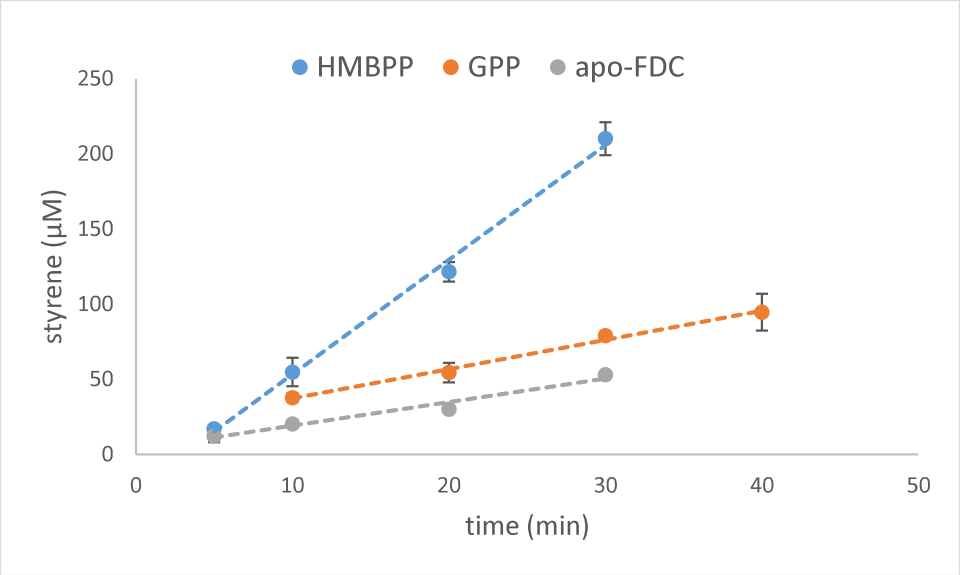

Figure 4.5: Decarboxylation activity of FDC utilized cofactor analog generated from HMBPP (blue) and GPP (red). Background catalytic activity of apoFDC was represented in (grey). The observed rates of styrene formation were 1.57 ± 0.14 µM/min for background decarboxylation, 7.62 ± 0.26 µM/min for HMBPP cofactor analog, and 1.95 ± 0.17 µM/min for GPP cofactor analog.

4.3.3 Native Mass Spectrometry

Native mass spectrometry has proved to be an informative technique to study prFMN. In the recent study of FDC decarboxylation from our lab, the substrate analog (Z)-2-Fluoro-2-nitro-vinylbenzene was utilized to trap intermediate prior to decarboxylation step. Native mass spectrometry was the employed to characterize the intermediate trapped in FDC (22).

Similar native mass spectrometry techniques performed in collaboration with Chunyi Zhao (in Prof. Ruotolo's Lab) were applied to characterize *in vitro* synthesized prFMN cofactors and analogs. 500 µL of scPFS-FDC coupling reactions were conducted in high concentration of substrates and enzymes as described in method section. The prenylation reaction was allowed to proceed for 3 h, quenched by exposure to air and concentrated. Concentrated samples were buffer exchanged into 500 mM ammonium acetate buffer, pH 6.9 and analyzed under native MS

conditions. In the positive control in which DMAPP was used as prenyl source, a peak corresponding to prFMN (m/z = 525.092) was observed (Figure 4.6b). This peak disappeared in negative control where no prenyl donor was added into the reaction mixture (Figure 4.6a). These results verify that the condition used in the *in vitro* assay does not interfere with native MS. However, when HMBPP and GPP were utilized as prenyl donors, no cofactor was observed. This may be due to the low concentration of cofactor analogs generated by scPFS. Unfortunately, this experiment was limited by the amount of enzyme available. Precipitation of scPFS was observed at the end of 3 h reaction. Note that there was no scPFS detected in native MS and cofactors were dissociated from FDC that was added to trap prFMN and analogs. Stable prenyl Flavin synthase will be required in order to improve and raise concentration of cofactor analogs. Furthermore, cofactor analogs had to bind to apoFDC in order to show up in native MS. Cofactor modification might change binding affinity greatly; and thus, lead to low activity and absence of cofactor peaks.

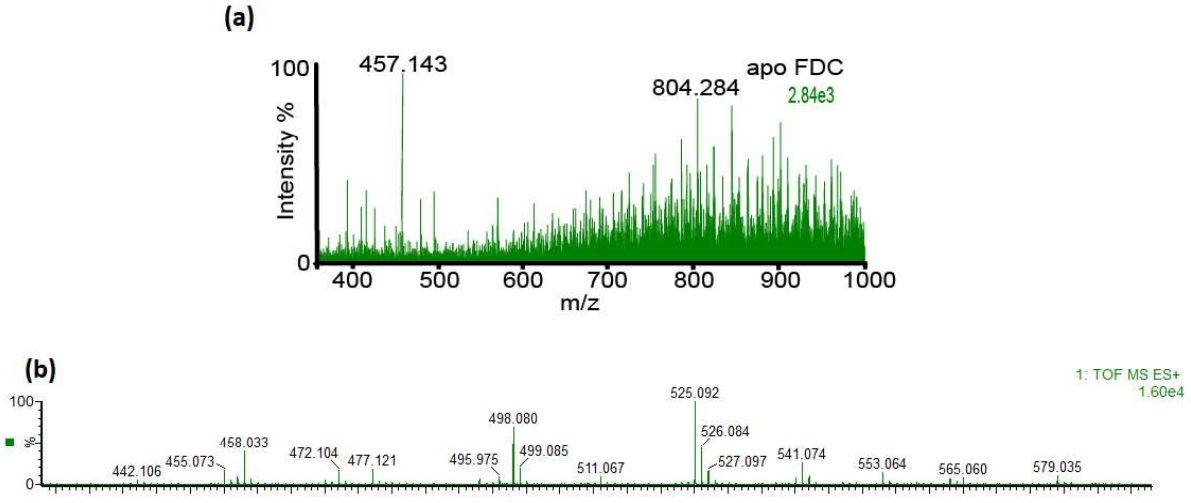

Figure 4.6: Native MS spectrum of scPFS prenylation when (a) no prenyl source was added (b) dimethylallyl pyrophosphate was added as prenyl source. The peak at 525.092 corresponds to prFMN.

4.3.4 Molecular docking

In order to gain better understanding of prenyl donor specificity, molecular docking was employed to computationally fit DMAPP analogs into the active site of prenyl flavin synthase. The UbiX crystal structure (PDB: 4ZAF) (5) was used to represent prenyl flavin synthase since it is currently the only reported crystal structure with substrates intact. UbiX and scPFS are isofunctional and share 50% of amino acid sequence (23–25). However, UbiX was reported to be unable to use pyrophosphate prenyl donor (5). Thus, (E)-4-Hydroxy-3-methyl-but-2-enyl monophosphate (HMBP) and geranyl monophosphate (GP) were used for modeling instead of their pyrophosphate counterparts used in the experiments.

In the molecular docking experiment, DMAP was removed from the crystal structure of UbiX and then DMAP, HMBP and GP were fitted into the active site of UbiX containing oxidized FMN. The result showed that HMBP and GP could be fitted into the active site of UbiX (Figure 4.7). The overlays between original DMAP position and molecular docking prediction were shown in figure 4.8. The relative docking energies were -5.61 kcal/mol, -6.56 kcal/mol and -7.83 kcal/mol for DMAP, HMBP and GP respectively. These results implied that scPFS can bind to DMAPP analogs studied in this chapter. However, in the case of GP, the angle of prenyl transfer π bond was significantly altered while the additional π bond was aligned on top of isoalloxazine ring (Figure 4.8c). This would significantly reduce rate of prenylation, if prenylation did still take place, rather than having the reaction between the additional π bond and isoalloxazine ring. Hydrophobic interactions could stabilize the cofactor analog generated from GPP and prevent it from leaving the active site of scPFS; and thereby provided another possible explanation to why FMN was consumed by scPFS but no decarboxylation activity was observed when HPLC assay and GC-MS dual enzyme assay were conducted using GPP as described above.

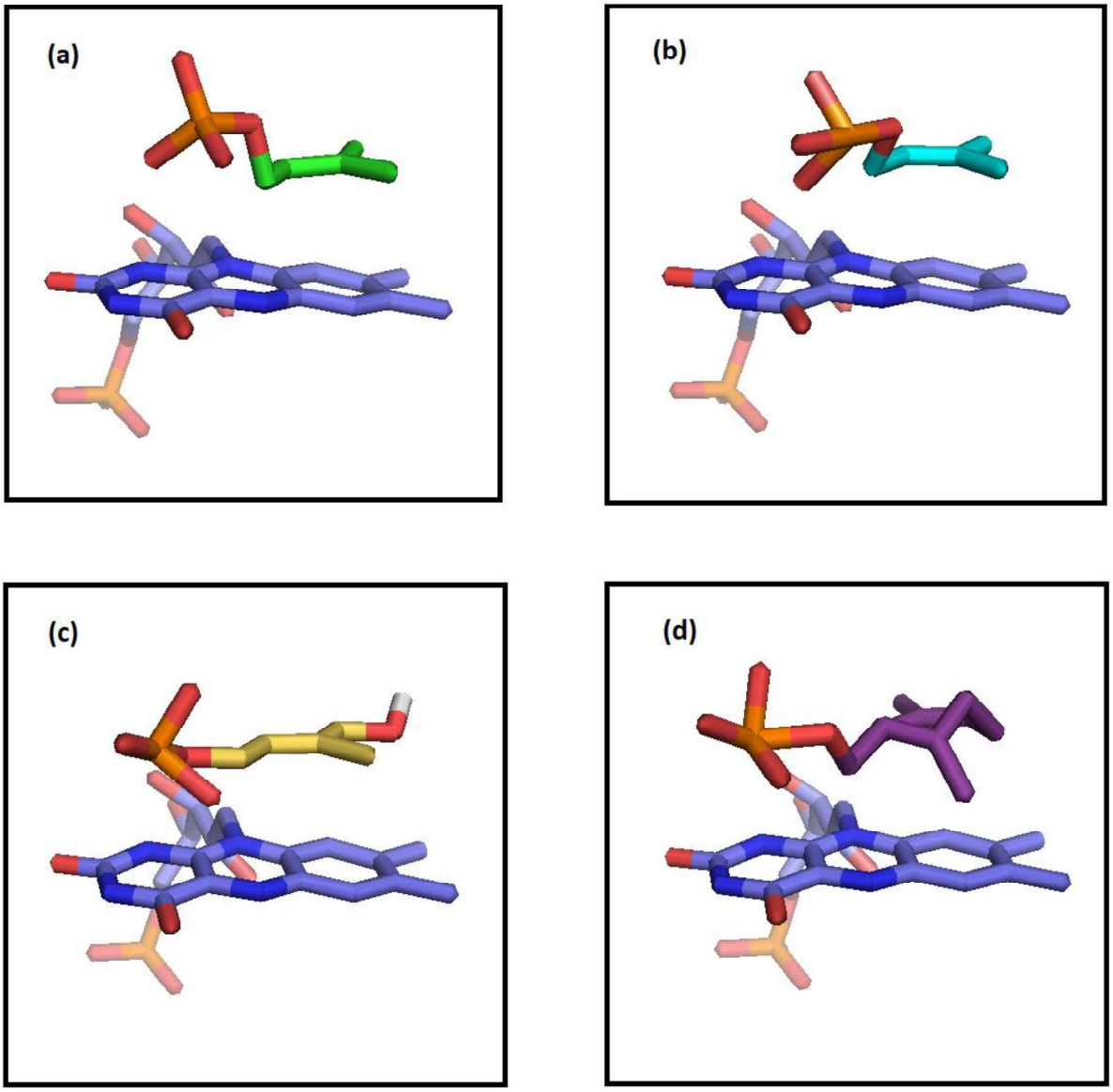

Figure 4.7: Molecular docking simulated the localization and alignment of prenyl source in the active site of UbiX containing FMN (a) original DMAP (b) molecular docking DMAP (c) molecular docking HMBP (d) molecular docking GP

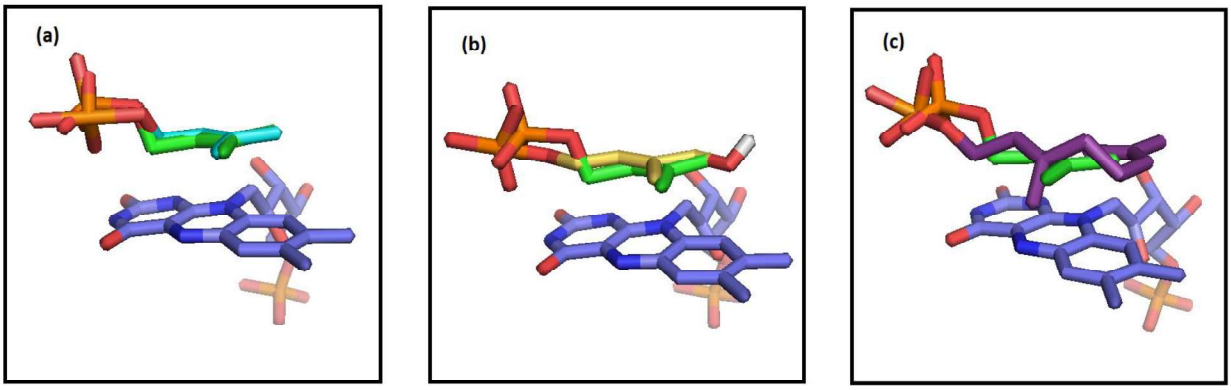

Figure 4.8: Overlay pictures between DMAP from the UbiX crystal structure (PDB: 4ZAF) and prenyl source simulated by molecular docking. (a) Original DMAP and molecular docking DMAP (b) original DMAP and molecular docking HMBP (c) original DMAP and molecular docking GP.

4.4 Conclusions

The work described here represents the first attempt to explore substrate specificity of the newly-discovered FMN prenylation reaction and cofactor flexibility of the phenylacrylic acid decarboxylation. 7,8-dichloro flavin mononucleotide was employed as an FMN analog in an attempt to probe the mechanism through linear free energy analysis. However, susceptibility of the substituent toward DTT resulted in difficulties with this approach. Each analog of FMN will require its own optimizations of HPLC profile and assay condition.

On the other hand, prenylation with commercial DMAPP analogs, HMBPP and GPP, showed promising results. Single turnover kinetics of FMN consumption yields an apparent first order rate constant of $4.45 \pm 0.87\ h^{-1}$, and $3.80 \pm 0.34\ h^{-1}$ for HMBPP and GPP respectively. Under steady state kinetic condition, FDC catalyzed the decarboxylation reaction using cofactor analog generated from HMBPP at V_{max} of $5.50 \pm 0.37\ min^{-1}$. When GPP was used to produce prFMN analog, no significant decarboxylation of *trans*-cinnamic acid was observed. Molecular docking

simulations suggested that the prFMN analog synthesized from GPP might be much more stable than prFMN and could not migrate out of scPFS active site properly. Steric effects could also be another reason to prevent the release of this cofactor. Native mass spectrometry was then employed to directly identify the presence of cofactor analog. The technique was first verified to be successful in its capability to detect *in vitro* synthesized prFMN cofactor. However, no cofactor could be detected when the technique was applied to cofactor analog. The low concentration of cofactor and low binding affinity toward FDC could be the causes. In order to probe the presence of cofactor analogs, the more stable and more active prenyl flavin transferase would be required.

This chapter described preliminary results exploring several options for cofactor engineering of prFMN. Even though many of the experiments led to unsuccessful results, some did show promise such as the case of HMBPP. The insight into GPP could lead to an experiment where GPP is used as the inhibitor to probe the prenylation mechanism, if a more stable prenyl flavin transferase is obtained.

4.5 References

1. Akhtar MK, Jones PR. Cofactor Engineering for Enhancing the Flux of Metabolic Pathways. Front Bioeng Biotechnol [Internet]. 2014 Aug 28 [cited 2017 Nov 19];2. Available from: https://www.ncbi.nlm.nih.gov/pmc/articles/PMC4147997/

2. Heux S, Cachon R, Dequin S. Cofactor engineering in Saccharomyces cerevisiae: Expression of a H2O-forming NADH oxidase and impact on redox metabolism. Metab Eng. 2006 Jul;8(4):303–14.

3. Park J, Choi Y. Cofactor engineering in cyanobacteria to overcome imbalance between NADPH and NADH: A mini review. Front Chem Sci Eng. 2017 Mar 1;11(1):66–71.

4. Martinoli C, Dudek HM, Orru R, Edmondson DE, Fraaije MW, Mattevi A. Beyond the Protein Matrix: Probing Cofactor Variants in a Baeyer–Villiger Oxygenation Reaction. ACS Catal. 2013 Dec 6;3(12):3058–62.

5. White MD, Payne KAP, Fisher K, Marshall SA, Parker D, Rattray NJW, et al. UbiX is a flavin prenyltransferase required for bacterial ubiquinone biosynthesis. Nature. 2015 Jun 25;522(7557):502–6.

6. Payne KAP, White MD, Fisher K, Khara B, Bailey SS, Parker D, et al. New cofactor supports α,β-unsaturated acid decarboxylation via 1,3-dipolar cycloaddition. Nature. 2015 Jun 17;522(7557):497–501.

7. Goedecke K, Pignot M, Goody RS, Scheidig AJ, Weinhold E. Structure of the N6-adenine DNA methyltransferase M.TaqI in complex with DNA and a cofactor analog. Nat Struct Biol. 2001 Feb;8(2):121–5.

8. Maity AN, Lin H-H, Chiang H-S, Lo H-H, Ke S-C. Reaction of Pyridoxal-5′-phosphate-N-oxide with Lysine 5,6-Aminomutase: Enzyme Flexibility toward Cofactor Analog. ACS Catal. 2015 May 1;5(5):3093–9.

9. Banta S, Swanson BA, Wu S, Jarnagin A, Anderson S. Optimizing an Artificial Metabolic Pathway: Engineering the Cofactor Specificity of Corynebacterium 2,5-Diketo-d-gluconic Acid Reductase for Use in Vitamin C Biosynthesis. Biochemistry (Mosc). 2002 May 1;41(20):6226–36.

10. Yorita K, Misaki H, Palfey BA, Massey V. On the interpretation of quantitative structure–function activity relationship data for lactate oxidase. Proc Natl Acad Sci. 2000 Mar 14;97(6):2480–5.

11. Roth JP, Wincek R, Nodet G, Edmondson DE, McIntire WS, Klinman JP. Oxygen Isotope Effects on Electron Transfer to O2 Probed Using Chemically Modified Flavins Bound to Glucose Oxidase. J Am Chem Soc. 2004 Nov 1;126(46):15120–31.

12. Chaiyen P, Sucharitakul J, Svasti J, Entsch B, Massey V, Ballou DP. Use of 8-substituted-FAD analogues to investigate the hydroxylation mechanism of the flavoprotein 2-methyl-3-

hydroxypyridine-5-carboxylic acid oxygenase. Biochemistry (Mosc). 2004 Apr 6;43(13):3933–43.

13. Francisco WA, Abu-Soud HM, Topgi R, Baldwin TO, Raushel FM. Interaction of bacterial luciferase with 8-substituted flavin mononucleotide derivatives. J Biol Chem. 1996 Jan 5;271(1):104–10.

14. Fitzpatrick PF. Insights into the mechanisms of flavoprotein oxidases from kinetic isotope effects. J Label Compd Radiopharm. 2007 Oct;50(11–12):1016–25.

15. Leys D, Scrutton NS. Sweating the assets of flavin cofactors: new insight of chemical versatility from knowledge of structure and mechanism. Curr Opin Struct Biol. 2016 Dec 1;41(Supplement C):19–26.

16. Piano V, Palfey BA, Mattevi A. Flavins as Covalent Catalysts: New Mechanisms Emerge. Trends Biochem Sci. 2017 Jun;42(6):457–69.

17. Pérez P, Domingo LR, José Aurell M, Contreras R. Quantitative characterization of the global electrophilicity pattern of some reagents involved in 1,3-dipolar cycloaddition reactions. Tetrahedron. 2003 Apr;59(17):3117–25.

18. Ferguson KL, Arunrattanamook N, Marsh ENG. Mechanism of the Novel Prenylated Flavin-Containing Enzyme Ferulic Acid Decarboxylase Probed by Isotope Effects and Linear Free-Energy Relationships. Biochemistry (Mosc). 2016 May 24;55(20):2857–63.

19. Coldham I, Hufton R. Intramolecular Dipolar Cycloaddition Reactions of Azomethine Ylides. Chem Rev. 2005 Jul 1;105(7):2765–810.

20. Lin F, Ferguson KL, Boyer DR, Lin XN, Marsh ENG. Isofunctional enzymes PAD1 and UbiX catalyze formation of a novel cofactor required by ferulic acid decarboxylase and 4-hydroxy-3-polyprenylbenzoic acid decarboxylase. ACS Chem Biol. 2015 Apr 17;10(4):1137–44.

21. Ruotolo BT, Benesch JLP, Sandercock AM, Hyung S-J, Robinson CV. Ion mobility-mass spectrometry analysis of large protein complexes. Nat Protoc. 2008;3(7):1139–52.

22. Ferguson KL, Eschweiler JD, Ruotolo BT, Marsh ENG. Evidence for a 1,3-Dipolar Cycloaddition Mechanism in the Decarboxylation of Phenylacrylic Acids Catalyzed by Ferulic Acid Decarboxylase. J Am Chem Soc. 2017 Aug 16;139(32):10972–5.

23. Rangarajan ES, Li Y, Iannuzzi P, Tocilj A, Hung L-W, Matte A, et al. Crystal structure of a dodecameric FMN-dependent UbiX-like decarboxylase (Pad1) from Escherichia coli O157:H7. Protein Sci Publ Protein Soc. 2004 Nov;13(11):3006–16.

24. Gulmezian M, Hyman KR, Marbois BN, Clarke CF, Javor GT. The role of UbiX in Escherichia coli coenzyme Q biosynthesis. Arch Biochem Biophys. 2007 Nov 15;467(2):144–53.

25. Mukai N, Masaki K, Fujii T, Kawamukai M, Iefuji H. PAD1 and FDC1 are essential for the decarboxylation of phenylacrylic acids in Saccharomyces cerevisiae. J Biosci Bioeng. 2010 Jun;109(6):564–9.

Chapter 5: Conclusions and outlooks

5.1 Overview

In the past decade, phenylacrylic acid decarboxylation has become of great interest as a pathway to biosynthesize styrene feedstock for the polymer industry. Originating from investigation into spoilage in the food processing industry, where contamination of styrene was observed (1–3), yeast ferulic acid decarboxylase (FDC1) and phenylacrylic acid decarboxylase (PAD1) were identified as responsible for styrene biosynthesis (4). Both enzymes were originally believed to be decarboxylases (5–7), however, the initial investigations by our lab and others have established the relationship between the two enzymes in which PAD1 generates modified FMN cofactor for FDC1 (8–10). Recent studies of their crystal structures have verified this hypothesis. The novel cofactor is identified as prenylated flavin mononucleotide (prFMN). UbiX, an isofunctional enzyme of PAD1, has been reported to transfer prenyl group from dimethylallyl monophosphate to reduced FMN thereby generating an additional ring on the isoalloxazine moiety of reduced FMN (11). The crystal structure of *Aspergillus Niger* FDC reveals two isomers of oxidized prFMN: a ketamine form and iminium form (12). Therefore, two possible mechanisms, Michael addition mechanism and 1,3 dipolar cycloaddition mechanism, have been proposed to describe how FDC1 incorporates prFMN to catalyze decarboxylation.

Even though the enigmatic presence of styrene in biological systems has been elucidated, a better understanding of how FDC1 converts cinnamic acid to styrene is required in order to apply these enzymes in industry. A low rate of return in comparison to high production costs is one of the most

common limitations in the bio-based product industry. The efficiency and specificity of the enzyme are often targeted for protein engineering to improve the economics of such industrial processes (13). Postulated decarboxylation mechanisms need to be verified in order to study and engineer FDC1 to improve styrene biosynthesis activity. Cofactor engineering of prFMN is another approach to improve the yield of styrene biosynthesis. The work presented here has expanded our current understanding of these enzymes, but just as importantly it has provided new insight for studies that may be fruitful in improving the rate of the reaction.

5.1.1 Probe of decarboxylation mechanism

The initial proposed mechanisms for FDC decarboxylation of phenylacrylic acid proceed through either Michael addition or 1,3 dipolar cycloaddition (12). Through ^{1}H NMR analysis, we found that FDC decarboxylation is stereospecific and the source of proton that replaces the carboxylic group of phenylacrylic acid is freely exchanged with buffer. Proton inventory experiments suggested that this single proton is in motion in the transition state. Linear free energy analysis of FDC decarboxylation resulted in unexpected negative reaction constant, ρ. This result indicated that decarboxylation step, which generally involves a buildup of negative charge in the transition stage and is therefore associated with large positive Hammett reaction constant (14,15), is not the rate limiting step. Instead, the negative Hammett reaction constant provides evidence that the 1,3-cycloelimination reaction in the 1,3 dipolar cycloaddition mechanism is likely to be rate-determining in the FDC decarboxylation. Secondary kinetic isotope measurements showed normal V/K isotope effects on the carbon at β position ($2^{\circ D}V/K_{\beta(H2O)}$ = 1.10 ± 0.03; n = 9). This result indicated that the vinylic carbons undergo a change from sp^3 to sp^2 hybridization during the rate

determining step; and therefore supported the result from linear free energy analysis that the 1,3-cycloelimination step is rate determining step.

In addition, secondary kinetic isotope experiments performed in D_2O show normal V/K isotope effect on α-carbon. This could imply that decarboxylation happens prior to cyclo-elimination as postulated in the proposed 1,3 dipolar cycloaddition mechanism. When the enzyme is reacted with α-deuterated phenylacrylic acid in D_2O, the α-carbon will contain two deuterium atoms; thus, the observed secondary kinetic isotope effect will be further elevated and will appear as a normal kinetic isotope effect. The pattern of secondary kinetic isotope effects further suggests that the 1,3-cyclo-elimination reaction that leads to the formation of the styrene double bond occurs in a concerted but asynchronous reaction in which bond cleavage is advanced at the α-carbon with respect to the β-carbon.

5.1.2 scPFS prenylation assay

Having gained better understanding about FDC decarboxylation and the cofactor used by FDC, we investigate mechanism in which this novel cofactor is synthesized. *Saccharomyces cerevisiae* prenyl flavin synthase (scPFS), formerly known as PAD1 was used as the model enzyme to study prFMN synthesis. Initially, we attempted to exploit the fact that prenylation generates inorganic phosphate or pyrophosphate byproduct. Commercially available high throughput assays such as Malachite green phosphate assay, Enzchek phosphate assay, and PiPer™ Pyrophosphate assay were utilized to monitor scPFS prenylation. Unfortunately, substrate interference led to the failure of commercial phosphate and pyrophosphate detection kits to detect reaction product.

Next, a scPFS-FDC coupled assay was developed and optimized in order to monitor scPFS prenylation through the activation of FDC. This would allow the formation of one molecule of

prFMN to be coupled to the production of many molecules of styrene, thereby affording a considerable amplification of the signal. In the optimized assay, prenylation reaction was performed in 500 μL reaction mixture containing 400 nM scPFS pre-incubated with 5mM DTT, 50 μM oxidized FMN, 4 μM apo-FDC, 60 μM NADH, 500 μM DMAPP and 1 mM sodium dithionite. The reactions were quenched by addition of 5 mM potassium ferricyanide. Then decarboxylation activity of FDC was measure under saturated substrate concentration. Styrene was extracted and concentration was measured by GC-MS. Under this condition, the catalytic activity of scPFS was close to maximal.

With scPFS-FDC coupling assay, we found that scPFS selectively used DMAPP as substrate in contrast to the publication where DMAP was reported to be substrate for UbiX prenylation. Implementing this coupling assay to study steady state kinetic allows us to obtain the observed k_{cat}, $K_M^{app\ (DMAPP)}$ as 12.2 ± 0.2 h^{-1} and 9.8 ± 0.7 μM, respectively. In addition, single turnover kinetic experiments, which were monitored by either scPFS-FDC coupling assay or HPLC assay tracking FMN consumption, yield apparent first order rate constant of 17.5 ± 1.1 h^{-1}.

5.1.3 Cofactor analogs

Following the prenylation assay developed as described above, the assays were employed to investigate whether prFMN analogs can be synthesized using scPFS and whether FDC can utilize prFMN analogs, given that scPFS was able to synthesize them. First, 7,8-dichloro flavin mononucleotide was selected as an FMN analog in an attempt to construct linear free energy correlation with substituted FMN analogs. However, preliminary results showed the susceptibility of the substituent toward the reducing agent used in the assay and suggested that each FMN analog will require its own optimizations of HPLC profile and assay condition.

The synthesis of prFMN analogs was then approached from another direction using DMAPP analogs. Single turnover kinetic assays were conducted using commercially available DMAPP analogs, HMBPP and GPP. These assays allowed apparent first order rate constant to be calculated as $4.45 \pm 0.87\ h^{-1}$, and $3.80 \pm 0.34\ h^{-1}$ for HMBPP and GPP respectively. Assuming consumed FMN was converted to cofactor, steady state kinetic decarboxylation allowed V_{max} to be calculated as $5.50 \pm 0.37\ min^{-1}$ when cofactor analog generated from HMBPP was utilized. In the case of cofactor analog generated from GPP, no decarboxylation activity was observed. Molecular docking simulations suggested that the prFMN analog synthesized from GPP might have problem migrating out of the active site of scPFS.

Furthermore, native mass spectrometry was employed to directly identify the presence of cofactor analog. The technique was first verified to be successful in its capability to detect *in vitro* synthesized prFMN cofactor. However, no modified cofactors could be detected when the technique was applied to detect cofactor analogs. The low concentration of cofactor and low binding affinity toward FDC could be the causes. In order to probe the presence of cofactor analogs, a more stable and more active prenyl flavin transferase would be required.

5.2 Future directions

Even though the investigations described in this thesis and others have elucidated the pathway of styrene biosynthesis in nature, it is still far from ready to be implemented in industry. Further experiments are necessary to provide direct evidence for the decarboxylation mechanism and the FMN prenylation mechanism. Experiments with regard to cofactor analogs described here serve as preliminary results for cofactor engineering. Further investigations are necessary in order to achieve cofactor with superior FDC catalytic activity. The proposed experiments described below could lead to enhancement of styrene biosynthesis activity or application toward biosynthesis of other valuable chemicals.

5.2.1 Substrate analogs (aromatic and aliphatic) and active site mutagenesis to probe mechanism of FDC

Although the 1,3 dipolar cycloaddition mechanism has been suggested in this thesis to be the decarboxylation mechanism employed by FDC1, direct evidence of the formation of the postulated intermediate is required to further verify this mechanism. The substrate inhibitor, 2-fluoro-2-nitrovinylbenzene, has been employed in combination with native mass spectroscopy to probe the existence of pre-decarboxylation intermediate by coworker from our lab (16).

Similarly, native mass spectroscopy could be employed to identify other dicycloaddition intermediates. Mutagenesis of active site residues, particularly at glutamic acid residue 282, could be employed to cause intermediates to accumulate on the enzyme. Furthermore, manipulation of substrate to reduce decarboxylation activity may allow us to detect intermediates in the rate limiting step directly. Hammett analysis showed that a nitro substituent at the *para* position of the substrate benzene ring reduced decarboxylation by an order of magnitude (17). An additional

electron withdrawing group at the *ortho* position could reduce catalytic activity further. Another option would be the addition of a nitro substituent at the β-carbon of cinnamic acid. A nitro group at this position could prevent substrate-cofactor adduct undergoing cycloelimination, and thereby allow us to detect intermediate at the rate determining step.

5.2.2 Cofactor maturation

Oxidative maturation of prFMN is one of the least well-understood steps in the formation of the active prFMN cofactor. It is unclear how or if an enzyme is involved in the conversion of reduced prFMN generated by either UbiX or scPFS to its oxidized form. In the cases of FDC and 3,4-dihydroxybenzoic acid decarboxylases (AroY), prFMN is successfully oxidized by air exposure and thus catalytic activity of FDC and AroY can be reconstituted *in vitro* (12,18,19). However, this is not the case for 3-octaprenyl-4-hydroxybenzoate decarboxylase (UbiD). The crystal structure of UbiD reveals that *in vitro* oxidation to the mature prFMN cofactor stalls at formation of a radical prFMN species (20). These results imply that decarboxylases are required for proper maturation of prFMN cofactor.

Unlike prFMN generated from UbiX, there is no evidence that radical prFMN is formed when scPFS is employed. This observation suggests that there may be more than one pathway to mature prFMN cofactor depending on the enzymes that synthesize this cofactor. It is also possible that there may be another enzyme involved in oxidative maturation of prFMN. It is surprising that cofactor generated from UbiX cannot be matured and utilized *in vitro* by UbiD since both are known to be in the same operon. Understanding how FDC and scPFS work together to mature cofactor and which part of FDC is responsible for this function could prove helpful to further engineer this enzyme to enhance its activity.

5.2.3 Linear free energy analysis, isotope effect and inhibitor complex to probe prenylation mechanism and application of cofactor analogs to probe decarboxylation mechanism

Understanding the prenylation mechanism is no less significant than understanding FDC decarboxylation. Linear free energy analysis and isotope effects can be employed to investigate mechanism by which prFMN is synthesized. If we can solve the problem of the limited availability of substrate analogs for prenylation, linear free energy analysis could provide powerful insight toward both prenylation mechanism, as well as phenylacrylic acid decarboxylation mechanism. By understanding the nature of prFMN cofactor in FDC decarboxylation, the goal of cofactor engineering to achieve cofactor with superior FDC catalytic activity can be advanced.

Furthermore, given that a more stable scPFS homolog can be identified, a substrate mimic inhibitor could be employed in combination with native mass spectroscopy to identify intermediates in the reaction. Results from this thesis indicate that geranyl pyrophosphate could be one potential candidate. The discovery of FMN prenylation intermediate may not only verify the mechanism in which prFMN is synthesized, but may also give insight toward how UbiX and scPFS involve with oxidative maturation of this cofactor.

5.2.4 Active site and cofactor engineering of FDC1 for other functionality

In addition, we can modify the active site of FDC1 and engineer it towards other substrates specifically. FDC is a model enzyme for prFMN-catalyzed decarboxylase. So far, only AroY and FDC are reported to be successfully reconstituted *in vitro*. In contrast to FDC and UbiD, AroY is believed to catalyze decarboxylation through a quinoid intermediate similar to bacterial phenolic acid decarboxylase (PAD) (18). Thus, FDC1 would be a more suitable as a model enzyme to generate UbiD substituted enzyme with ability to reconstitute *in vitro*.

Another target for protein engineering of FDC would be substrate specificity. It has been reported that FDC can convert sorbic acid to 1,3 pentadiene, a monomer for the rubber industry (6,21). However, the catalytic activity is much slower in comparison to cinnamic acid. Degradation of sorbic acid is not the primary role of FDC in nature. However, with active site engineering and cofactor engineering, FDC could be engineered to be selective toward sorbic acid rather than phenylacrylic acid. Thus, further investigation of FDC active site and cofactor could prove valuable in biosynthesis industry.

5.3 References

1. Lickly TD, Lehr KM, Welsh GC. Migration of styrene from polystyrene foam food-contact articles. Food Chem Toxicol. 1995 Jun;33(6):475–81.

2. Tawfik MS, Huyghebaert A. Polystyrene cups and containers: styrene migration. Food Addit Contam. 1998 Jul;15(5):592–9.

3. Steele DH, Thornburg MJ, Stanley JS, Miller RR, Brooke R, Cushman JR, et al. Determination of styrene in selected foods. J Agric Food Chem. 1994 Aug 1;42(8):1661–5.

4. Pagot Y, Belin J-M, Husson F, Spinnler H-E. Metabolism of phenylalanine and biosynthesis of styrene in Penicillium camemberti. J Dairy Res. 2007 May;74(02):180.

5. Vanbeneden N, Gils F, Delvaux F, Delvaux FR. Formation of 4-vinyl and 4-ethyl derivatives from hydroxycinnamic acids: Occurrence of volatile phenolic flavour compounds in beer and distribution of Pad1-activity among brewing yeasts. Food Chem. 2008 Mar 1;107(1):221–30.

6. Stratford M, Plumridge A, Archer DB. Decarboxylation of Sorbic Acid by Spoilage Yeasts Is Associated with the PAD1 Gene. Appl Environ Microbiol. 2007 Oct 15;73(20):6534–42.

7. Clausen M, Lamb CJ, Megnet R, Doerner PW. PAD1 encodes phenylacrylic acid decarboxylase which confers resistance to cinnamic acid in Saccharomyces cerevisiae. Gene. 1994 May;142(1):107–12.

8. Lin F, Ferguson KL, Boyer DR, Lin XN, Marsh ENG. Isofunctional enzymes PAD1 and UbiX catalyze formation of a novel cofactor required by ferulic acid decarboxylase and 4-hydroxy-3-polyprenylbenzoic acid decarboxylase. ACS Chem Biol. 2015 Apr 17;10(4):1137–44.

9. Mukai N, Masaki K, Fujii T, Kawamukai M, Iefuji H. PAD1 and FDC1 are essential for the decarboxylation of phenylacrylic acids in Saccharomyces cerevisiae. J Biosci Bioeng. 2010 Jun;109(6):564–9.

10. McKenna R, Nielsen DR. Styrene biosynthesis from glucose by engineered E. coli. Metab Eng. 2011 Sep;13(5):544–54.

11. White MD, Payne KAP, Fisher K, Marshall SA, Parker D, Rattray NJW, et al. UbiX is a flavin prenyltransferase required for bacterial ubiquinone biosynthesis. Nature. 2015 Jun 25;522(7557):502–6.

12. Payne KAP, White MD, Fisher K, Khara B, Bailey SS, Parker D, et al. New cofactor supports α,β-unsaturated acid decarboxylation via 1,3-dipolar cycloaddition. Nature. 2015 Jun 25;522(7557):497–501.

13. Claypool JT, Raman DR, Jarboe LR, Nielsen DR. Technoeconomic evaluation of bio-based styrene production by engineered Escherichia coli. J Ind Microbiol Biotechnol. 2014 Aug;41(8):1211–6.

14. Miyamoto K, Ohta H. Purification and properties of a novel arylmalonate decarboxylase from Alcaligenes bronchisepticus KU 1201. Eur J Biochem. 1992 Dec 1;210(2):475–81.

15. Straub TS, Bender ML. Cycloamyloses as enzyme models. Decarboxylation of phenylcyanoacetate anions. J Am Chem Soc. 1972 Dec 1;94(25):8875–81.

16. Ferguson KL, Eschweiler JD, Ruotolo BT, Marsh ENG. Evidence for a 1,3-Dipolar Cycloaddition Mechanism in the Decarboxylation of Phenylacrylic Acids Catalyzed by Ferulic Acid Decarboxylase. J Am Chem Soc. 2017 Aug 16;139(32):10972–5.

17. Ferguson KL, Arunrattanamook N, Marsh ENG. Mechanism of the Novel Prenylated Flavin-Containing Enzyme Ferulic Acid Decarboxylase Probed by Isotope Effects and Linear Free-Energy Relationships. Biochemistry (Mosc). 2016 May 24;55(20):2857–63.

18. Payer SE, Marshall SA, Bärland N, Sheng X, Reiter T, Dordic A, et al. Regioselective para-Carboxylation of Catechols with a Prenylated Flavin Dependent Decarboxylase. Angew Chem Int Ed. 2017 Oct 23;56(44):13893–7.

19. Weber HE, Gottardi M, Brückner C, Oreb M, Boles E, Tripp J. Requirement of a Functional Flavin Mononucleotide Prenyltransferase for the Activity of a Bacterial Decarboxylase in a Heterologous Muconic Acid Pathway in Saccharomyces cerevisiae. Appl Environ Microbiol. 2017 May 15;83(10):e03472-16.

20. Marshall SA, Fisher K, Cheallaigh AN, White MD, Payne KAP, Parker DA, et al. Oxidative maturation and Structural Characterization of Prenylated-FMN binding by UbiD, a Decarboxylase Involved in Bacterial Ubiquinone Biosynthesis. J Biol Chem. 2017 Jan 5;jbc.M116.762732.

21. Plumridge A, Stratford M, Lowe KC, Archer DB. The Weak-Acid Preservative Sorbic Acid Is Decarboxylated and Detoxified by a Phenylacrylic Acid Decarboxylase, PadA1, in the Spoilage Mold Aspergillus niger. Appl Environ Microbiol. 2008 Jan 15;74(2):550–2.